

**EXPERIMENTAL INVESTIGATION OF BOILER BLAST LOAD
ON BUILDING STRUCTURES**

TARIKUL ISLAM

MASTER OF SCIENCE IN CIVIL ENGINEERING (STRUCTURAL)



**DEPARTMENT OF CIVIL ENGINEERING
BANGLADESH UNIVERSITY OF ENGINEERING AND TECHNOLOGY,
DHAKA**

Experimental Investigation of Boiler Blast Load on Building Structures

by

TARIKUL ISLAM

Student No.: 1017042312 P

A thesis submitted to Department of Civil Engineering, Bangladesh University of Engineering and Technology, Dhaka in partial fulfillment of the requirement for the degree of Master of Science in Civil Engineering (Structural)

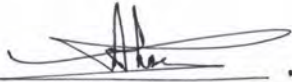


**DEPARTMENT OF CIVIL ENGINEERING
BANGLADESH UNIVERSITY OF ENGINEERING AND TECHNOLOGY,
DHAKA**

FEBRUARY, 2022

The thesis titled “Experimental Investigation of Boiler Blast Load on Building Structures” submitted by Tarikul Islam, Roll No.:1017042312 P, Session: October, 2017 has been accepted as satisfactory in partial fulfillment of the requirement for the degree of Master of Science in Civil Engineering (Structural) on 3rd February, 2022.

BOARD OF EXAMINERS



Dr. Raquib Ahsan
Professor
Department of Civil Engineering
BUET, Dhaka-1000

Chairman
(Supervisor)



Dr. Md. Delwar Hossain
Professor and Head
Department of Civil Engineering,
BUET, Dhaka-1000

Member
(Ex-Officio)



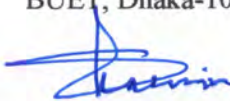
Dr. Syed Ishtiaq Ahmad
Professor
Department of Civil Engineering
BUET, Dhaka-1000

Member



Dr. Tanvir Manzur
Professor
Department of Civil Engineering
BUET, Dhaka-1000

Member

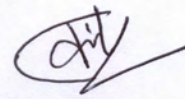


Dr. Sharmin Reza Chowdhury
Professor
Department of Civil Engineering
AUST, Dhaka-1208

Member
(External)

DECLARATION

It is hereby declared that this thesis is a presentation of the original research work of the author under the supervision of Dr. Raquib Ahsan, Professor, Department of Civil Engineering, BUET. Wherever contributions of others are involved, every effort is made to indicate this clearly, with due reference to the literature, and acknowledgement of collaborative research and discussions. Neither the thesis nor any part of it has been submitted elsewhere for any other purposes.



Tarikul Islam
Student ID: 1017042312 P
Date: 03 February 2022

DEDICATED TO

MY

PARENTS, FAMILY, FRIENDS AND TEACHERS

ACKNOWLEDGEMENT

The author expresses his utmost gratitude to Almighty Allah for His graciousness and unlimited kindness, the blessings of Whom is always required for completion of any good work.

First, the author wishes to express his deepest gratitude and sincere appreciation to his supervisor Dr. Raquib Ahsan, Professor, Department of Civil Engineering, BUET, Dhaka for his continuous guidance, invaluable suggestions, encouragement, generous help and unfailing enthusiasm at every stage of this study. His active interest in this topic and valuable advice were the sources of the author's inspiration.

The author would also like to thank Dr. A. F. M. Saiful Amin, Director, BUET-JIDPUS and all the personnel of BUET-JIDPUS for providing their cooperation and support during the experimental works. Additionally, the author would like to thank everyone who helped in different ways and not realize how much they helped.

With his deepest appreciation, the author would like to thank his beloved wife, parents and other family members for their continuous cordial encouragement and inspiration.

Finally, the author would like to thank Mr. Rafjany Yasar. The last stages of the journey were painstaking and would have been impossible without his consistent assistance, encouragement and motivation.

ABSTRACT

Boilers are commonly used in many industries including the RMG sector of Bangladesh to perform numerous industrial processes. Explosion of steam boilers has become a common menace in the last few years in the context of Bangladesh. Moreover, numerous BLEVE (Boiling liquid expanding vapor explosion) incidents have occurred across the world, resulting in fatalities and injuries. Most of the researchers studied the blast due to explosives and extremely flammable fluids and developed different models on blast pressure prediction. Non-flammable fluid (e.g., water) as the filling liquid in steam boilers may behave differently from other explosives and flammable fluids.

The equivalent TNT method is considered for the theoretical prediction of boiler blast load. Initially, the internal energy inside the boiler during the explosion is calculated using the exergy concept (thermodynamic availability) and converted to equivalent TNT mass. Finally, a theoretical pressure-time history of the sample boiler is plotted for the front wall considering different standoff distances and filling degrees.

An experimental investigation of boiler blast is conducted in this study utilizing water heater to have a precise conception of the actual explosion scenario by developing a time-history diagram. A total of nine idealized small-scaled steam boiler samples were prepared for destructive testing, considering standoff distances of 61 cm, 76 cm and 91 cm with filling degrees of 40%, 50% and 60% respectively. The scaled distances of these samples varied from 1.255 m/kg^{0.333} to 2.156 m/kg^{0.333}. For controlled testing a cross shaped groove was cut at the front plate of these boilers. For capturing impact load and internal temperature inside the boiler two load cells, dynamic data logger and temperature sensor were used.

The actual explosion depicts a gradual increase in pressure to the peak positive overpressure, followed by a negative phase. The experimental blast waves have a prolonged blast phase and a lower positive peak overpressure than the theoretical prediction. As the standoff distance increases, the positive peak overpressure rapidly decreases. For a 40% filling degree and at a standoff distance of 61 cm, the positive peak overpressure amounts to 0.6 kPa (approx.). However, it declines rapidly beyond a 76 cm standoff distance and becomes 0.48 kPa (approx.). The behavior is comparable to filling degrees of 50% and 60%.

Moreover, peak overpressure stays near enough for high degrees of filling even with a small standoff distance. However, for a constant standoff distance, minimal increment of peak overpressure is found for the increment of boiler filling degrees.

TABLE OF CONTENT

ACKNOWLEDGEMENT	v
ABSTRACT	vi
TABLE OF CONTENT	vii
LIST OF FIGURES	x
LIST OF TABLES	xiii
NOTATIONS	xv
ABBREVIATIONS	xvii
Chapter 1	
INTRODUCTION	1
1.1 General	1
1.2 Research Objectives	1
1.3 Methodology of Work.....	1
1.4 Scope of the work.....	2
1.5 Organization of the Thesis	2
Chapter 2	
LITERATURE REVIEW	4
2.1 Introduction	4
2.2 Steam Boiler.....	4
2.2.1 Classification of Boiler	4
2.2.2 Boiler explosions	5
2.2.3 Causes of boiler explosion	7
2.3 Air blast Load.....	8
2.4 Previous research on blast load testing of vessel containing flammable and non-flammable fluids	8
2.5 Summary of the previous study.....	10
2.6 Knowledge gaps	11
Chapter 3	
THEORETICAL PREDICTION OF BOILER BLAST LOAD.....	12

3.1	Introduction	12
3.2	Ideal blast wave characteristics	12
3.3	Scaled Distance (Z)	14
3.4	Explosive type and weight	15
3.5	Categories of Blast-loading.....	17
3.5.1	Unconfined explosions	18
3.5.2	Confined explosion	19
3.6	Blast wave reflection.....	20
3.7	Factors affecting blast pressure	22
3.8	Theoretical prediction of boiler blast load	22
3.8.1	Explosion energy calculation.....	22
3.8.2	Structural blast load prediction.....	24
3.8.3	Standoff distance.....	26
3.8.4	Calculation of blast parameters for front wall	27
 Chapter 4		
	MATERIALS AND TEST SETUP	30
4.1	Introduction	30
4.2	Materials Used	30
4.2.1	Mild Steel Pipe.....	30
4.2.2	MS sheet for front and back side of boiler.....	32
4.2.3	Nuts.....	33
4.2.4	Heating Equipment	34
4.2.5	Thermocouple and Digital Display.....	34
4.3	Preparation of Boiler Sample	34
4.4	Test Setup.....	36
4.4.1	Load Cells	36
4.4.2	Data Logger	37
4.4.3	Test Frame	38

4.5	Data acquisition.....	39
Chapter 5		
	RESULTS AND DISCUSSIONS.....	41
5.1	Introduction	41
5.2	Comparison of theoretical pressure time-history with the pressure time-history of sample boiler	41
5.3	Comparison of blast over pressure for different standoff distances.....	52
5.4	Comparison of blast over pressure for different filling degrees	55
5.5	Temperature profile.....	56
Chapter 6		
	CONCLUSION AND RECOMMENDATIONS	59
6.1	Introduction	59
6.2	Conclusions	59
6.3	Recommendations for Future Study.....	60
	REFERENCES	61
	Appendix A.....	a
	A.1 Blast Wave Parameters	a
	A.2 Calculation of Heat of detonation of the actual explosive.....	e
	A.3 Calculation of Peak Incident Overpressure (P_{so})	f
	A.4 Theoretical Calculation of Blast Parameters	f
	Appendix B.....	h
	B.1 Calibration of load cell.....	h
	B.2 Test Data	h
	B.3 Temperature profile:	y

List of Figures

Figure 2.1: Boiler Classification (Agarwal and Suhane, 2017).....	4
Figure 2.2: Pictorial view of boiler explosion (a) Explosion at a sweater factory in Ashulia of Savar, on the outskirts of Dhaka, on the morning of Tuesday, December 10, 2019. Photo: The Daily Star and (b) Factory boiler blast at Tampaco Foils Bangladesh packaging plant kills dozens	6
Figure 3.1: Pressure time history of ideal blast wave (Karlos and Solomon, 2013). ...	12
Figure 3.2: Effect of standoff distance on positive pressure phase of the blast (Karlos and Solomon, 2013).....	14
Figure 3.3: Blast loading categories (U.S. Department of the Army, 1990).	17
Figure 3.4: Types of external explosions and blast loadings; (a) Free-air bursts, (b) Air bursts, and (c) Surface bursts. (Karlos and Solomon, 2013).	19
Figure 3.5: Confinement blast categories (a) Fully vented, (b) Partially vented, and (c) Fully confined (Yandzio and Gough, 1999).	20
Figure 3.6: Propagation of blast pressure (FEMA 426, 2011).	21
Figure 3.7: Incident, reflected and dynamic pressure time histories (Baker, 1973).....	21
Figure 3.8: Triangular assumptions of pressure time history on the front face of the structure (Karlos and Solomon, 2013).....	28
Figure 4.1: Longitudinal flat tension test (a) Dimension of MS pipe specimen, (b) specimens before testing, (c) UTM with test specimen and (d) specimens after testing.	30
Figure 4.2: Stress-strain diagram of mild steel pipes used for sample boiler preparation.	31
Figure 4.3: (a) Cutting of MS pipe, (b) Rear plate (MS Sheet) and (c) Front Plate (MS Sheet).	32
Figure 4.4: Longitudinal flat tension test (a) specimen dimension, (b) prepared specimens before testing (c) specimens after testing.	33
Figure 4.5: (a) Water Heater (b) Thermocouple and (c) Display unit for temperature reading.	34
Figure 4.6: Preparation process of boiler sample.	35
Figure 4.7: Prepared boiler specimens.	36
Figure 4.8: Dimension and Calibration of Load cells.	37

Figure 4.9: DWETRON (DEWE-2600) data logger.	37
Figure 4.10: Dimensions of Test Frame.	38
Figure 4.11: Preparation of setup before the commencement of the test.	39
Figure 4.12: (a) Boiler sample with test frame (b) Scenario during explosion.	40
Figure 5.1: Pressure Time-history of B40S8 (a) Theoretical positive pressure along with reflected impulse and (b) Experimental positive and negative pressure.	43
Figure 5.2: Pressure Time-history of B40S10 (a) Theoretical positive pressure along with reflected impulse and (b) Experimental positive and negative pressure.	44
Figure 5.3: Pressure Time-history of B40S12 (a) Theoretical positive pressure along with reflected impulse and (b) Experimental positive and negative pressure.	45
Figure 5.4: Pressure Time-history of B50S8 (a) Theoretical positive pressure along with reflected impulse and (b) Experimental positive and negative pressure.	46
Figure 5.5: Pressure Time-history of B50S10 (a) Theoretical positive pressure along with reflected impulse and (b) Experimental positive and negative pressure.	47
Figure 5.6: Pressure Time-history of B50S12 (a) Theoretical positive pressure along with reflected impulse and (b) Experimental positive and negative pressure.	48
Figure 5.7: Pressure Time-history of B60S8 (a) Theoretical positive pressure along with reflected impulse and (b) Experimental positive and negative pressure.	49
Figure 5.8: Pressure Time-history of B60S10 (a) Theoretical positive pressure along with reflected impulse and (b) Experimental positive and negative pressure.	50
Figure 5.9: Pressure Time-history of B60S12 (a) Theoretical positive pressure along with reflected impulse and (b) Experimental positive and negative pressure.	51
Figure 5.10: Comparison of maximum positive blast pressure with (a) standoff distance and (b) scaled distance for different filling degrees.	53
Figure 5.11: Comparison of maximum negative blast pressure with (a) standoff distance and (b) scaled distance for different filling degrees.	54
Figure 5.12: Comparison of (a) positive and (b) negative peak overpressure with filling degrees for different standoff distances.	56
Figure 5.13: Internal temperature of the boiler throughout the commencement of the test.	57
Figure 5.14: Comparison of blast temperature with different filling degrees.	58
Figure 5.15: Comparison of Peak positive pressure for different scaled distance and average blast temperatures.....	58

Figure A.1: Variation of peak dynamic pressure q_0 vs P_{so} (Karlos and Solomon, 2013; Unified Facilities Criteria, 2008).	a
Figure A.2: Parameters of positive phase of shock spherical wave of TNT charges from free-air bursts (Karlos and Solomon, 2013; Unified Facilities Criteria, 2008).	b
Figure A.3: Parameters of positive phase of shock hemispherical wave of TNT charges from surface bursts (Karlos and Solomon, 2013; Unified Facilities Criteria, 2008).	c
Figure A.4: Sound velocity in reflected overpressure region (Karlos and Solomon, 2013; Unified Facilities Criteria, 2008).	c
Figure A.5: Parameters of negative phase of shock wave of TNT charges, (a) from spherical free air bursts and (b) from semispherical surface bursts (Karlos and Solomon, 2013; Unified Facilities Criteria, 2008).	d
Figure A.6: Theoretical predicted time history graph for B6010.	g
Figure B.1: Calibration graph for (a) load cell of 75 KN capacity and (b) load cell of 50 KN capacity	h
Figure B.2: Experimental Pressure time-history for B60S10.	y

List of Tables

Table 2.1: List of boiler explosion incidents in Bangladesh (2013 - 2019) (Hossan et al., 2019).....	6
Table 2.2: Tests performed by Johnson et al. with butane and propane (Hemmatian, Planas, et al., 2017).....	9
Table 2.3: Experimental results performed with propane in a 2 m ³ vessel (Birk et al., 2007; Birk and VanderSteen, 2006; Laboureur et al., 2014).....	10
Table 3.1: Heat of detonation of some common explosives (U.S. Department of the Army, 1990).....	16
Table 3.2: Upper limit of charge weight per means of transportation (U.S. Department of the Army, 1990).....	16
Table 3.3: Indicative values of TNT equivalent mass factors (U.S. Department of the Army, 1990).....	17
Table 3.4: Different blast loading categories (U.S. Department of the Army, 1990)....	18
Table 3.5: Summary of various methods of calculating explosion energy of BLEVE.	23
Table 3.6: Explosion energy at different expected temperatures using exergy analysis.	24
Table 3.7: Constants for polynomial equations of Kingery and Bulmash (1984) blast parameters.....	26
Table 3.8: TNT equivalent weight and standoff distance for sample boiler with a constant scaled distance considering an industrial boiler of 1 MT filling capacity.....	27
Table 3.9: Equations used in the calculation of blast parameters for the front wall (U.S. Department of the Army, 1990).....	28
Table 3.10: Theoretical blast pressure and expected experimental blast pressure	29
Table 4.1: Results of longitudinal flat tension test of MS pipe.....	31
Table 4.2: Results of longitudinal flat tension test of MS sheet.....	33
Table 4.3: Description of electric flange heater and thermocouple used in this study..	34
Table 5.1: Comparison of theoretical expected explosion pressure and actual explosion pressure of boiler blast.....	42
Table A.1: Description of the blast wave parameters.....	a
Table A.2: Calculation of released energy using exergy analysis (<i>Ogle et al., 2012</i>).....	e

Table A.3: Calculation of scaled distance from standoff distance and equivalent TNT charge weight.....	e
Table A.4: Calculation of peak incident overpressure from different formulae.....	f
Table A.5: Blast wave parameters for positive phase of the explosion (Figure A.3).....	f
Table A.6: Blast wave parameters for negative phase of the explosion.....	g
Table B.1: Test data from data logger for sample specimen B60S10.	h
Table B.2: Temperature profile of all boiler specimens	y

NOTATION

Symbol	Description
b	Decay coefficient of the waveform
C_D	Drag coefficient (=1 for front wall)
C_r	Sound velocity in reflected medium
C_{ra}	Reflection coefficient
E	Released energy or batch energy
H_{exp}^d	Heat of detonation of the actual explosive
H_{TNT}^d	Heat of detonation of the TNT
i_r	Reflected impulse
i_s	Incident impulse
K	Specific heat ratio
m_T	Overall mass in the vessel
P	Initial pressure
P_a or P_o	Ambient pressure
P_r	Peak reflected pressure
$P_{rupture}$	Rupture peak pressure
P_{so}	Peak overpressure
q	Dynamic pressure
R	Standoff distance
S	Entropy at initial state
S_o	Entropy at final state
T_o	Absolute Temperature at final state
t_o or t_d^+	Positive phase duration
t_A	Time of arrival
t_c	Clearing time
t_d^-	Negative phase duration
t_{of}	Fictitious time for positive phase
t_{rf}	Fictitious duration for the reflected wave
U	Shock front velocity
U or U_i	Overall internal energy of the system just before the explosion
U_o	Internal Energy at final state

Symbol	Description
ΔU	Variation in the internal energy of the vessel content
u_G	Internal energy of the vapor at the final state of the irreversible process
u_L	Internal energy of the liquid at the final state of the irreversible process
V	Initial volume
ΔV	Variation in volume of the whole vessel content
v	Specific Volume at initial state
v_0	Specific Volume at final state
v_G	Specific volume of vapor at the final state of the irreversible process
v_L	specific volume of the liquid at the final state of the irreversible process
W or W_{exp}	Charge mass of explosive
W_{TNT}	Charge mass of TNT
Z	Scaled distance
α_i	Incident angle

LIST OF ABBREVIATIONS

ANFO	Ammonium Nitrate/Fuel Oil
ASTM	American Society for Testing and Materials
BLEVE	Boiling Liquid Expanding Vapor Explosion
FD	Filling Degree
FEMA	Federal Emergency Management Agency
GDP	Gross domestic product
HMX	High Melting Explosive or Her Majesty's Explosive or High-velocity Military Explosive or High-Molecular-weight RDX
JIDPUS	Japan Institute of Disaster Prevention and Urban Safety
MS	Mild Steel
PETN	Pentaerythritol Tetranitrate
RDX	Research Department explosive or Royal Demolition explosive
RMG	Readymade garments
SSD	Safe Standoff / Scaled Distance
TM	Technical Manual
TNT	Trinitrotoluene
UFC	Unified Facilities Code

Chapter 1

INTRODUCTION

1.1 General

The boiler is utilized in many industries, including Bangladesh's RMG, which accounts for up to 84 % of the country's total exports and contributes to GDP (Islam, 2021). The factories use high-capacity steam boilers for dyeing, drying, weaving etc. However, In the last few years, boiler explosions have become a prevalent hazard. A blast wave is caused by the discharge of energy in boiler explosion. The explosion wave can result in injuries and damage, such as building collapse or missile projection. The intensity of an explosion is connected to the extent to which the explosion can conduct mechanical operation.

However, very limited works have been done on the effect of boiler blast load on structures. There are some technical manual and design handbooks available on calculation of blast loads (Brode, 1955; Crowl, 1992a; Hemmatian, Casal, et al., 2017; Kumar et al., 2013; Ogle et al., 2012) , effects of blast loading on Beam and column (Akter, 2019) and blast resistant design (Birajdar and Jawalkar, 2017; Kim et al., 2006; Mills, 1987; Newmark and Hansen, 1961) which are limited to the blast of explosives and extremely flammable fluids. This research aims to uncover a simple analysis method of boiler blast load prediction on structures through destructive testing to minimize the risks, loss of life and properties due to boiler explosions of non-flammable fluids in Bangladesh.

1.2 Research Objectives

The overall objective of the research work is to assess the actual explosion scenario of the boiler blast with the theoretical prediction. The specific objectives are as follows:

1. To predict theoretical pressure on building structures subjected to boiler blast load.
2. To determine boiler blast pressure on structures by destructive test of small sized steam boiler.
3. To compare the results obtained from theoretical prediction with test data.

1.3 Methodology of Work

The theoretical prediction of boiler blast load will be carried out before the experimental test of the boiler sample. The numerical value of the batch energy of boiling liquid expanding vapor explosion (BLEVE) will first be determined using exergy analysis (Brode, 1955; Crowl, 1991; Hemmatian, Casal, et al., 2017; Kumar et al., 2013; Ogle et

al., 2012; Ramirez et al., 2011). Then a theoretical time-history plot for the blast pressure will be determined for the front wall (Karlos and Solomon, 2013). Full-scale blast testing would be the most effective way to learn about the behavior of structures under blast loads. However, due to security concerns, these experiments are limited. For that reason, a destructive test of an idealized small-sized steam boiler (14-15 liters capacity) will be performed. Mild steel pipes and mild steel sheets will be used to make a total of 9 steam boiler samples. A temperature sensor and a water heater will be installed on the boiler's backplate. A cross-signed groove will be formed at the front plate for a controlled test. Two load cells will be attached to a steel sheet in the test arrangement. The load cells will be utilized to record the blast load on the steel sheet in order to generate an experimental time history plot. The empirical equation's results and test data will next be compared to get an understanding of the real explosion scenario.

1.4 Scope of the work

This study was conducted for nine small-sized steam boilers containing nonflammable fluids (water) to have a better understanding of the structural response subjected to boiler blast load. To determine the influence of the standoff distance and filling degrees on the peak overpressure of the boiler explosion, standoff distances of 61, 76 and 91 cm and filling degrees of 40, 50 and 60% were chosen for the 15.44 kg capacity of the sample boiler. For controlled testing a cross shaped groove was cut at the front plate of these boilers. For capturing impact load two load cells were used instead of pressure transducers and attached in the rear mild steel plate (610×635 mm) of the test frame. For water heating purposes a 2000 watts electric immersion heater (tubular flange heater) was utilized and connected to the rear side plate of the sample boiler. The actual steam temperature within the boiler sample was measured using a K-Type temperature sensor of 4 inches length.

1.5 Organization of the Thesis

The thesis is organized into six chapters, each of which focuses on a different aspect of the overall study.

Chapter 1 introduces the background and current state of the problem. This also outlines the research's prospective aims and methods.

Chapter 2 provides a thorough review of the literature on boiling liquid expanding vapor explosions, as well as contemporary research that highlights knowledge gaps.

Chapter 3 provides a short background of boiler blast load, blast-related parameters and methods involved in the theoretical prediction.

Chapter 4 describes the preparation of the sample boiler for the destructive test, equipment used in the test and the preparation of the test frame.

Chapter 5 is dedicated to analyzing the results obtained from theoretical predictions and practical tests. Effect of standoff distance, filling degree and blast temperature was also presented to have a clear idea of the peak overpressure of the blast event.

Chapter 6 presents the conclusions drawn from the observations during this research. This chapter also highlights any suggestion to ensure a better future reproducibility of this research.

Chapter 2 LITERATURE REVIEW

2.1 Introduction

The main goal of this study is to construct a time-history diagram to better understand the structural response due to boiler blast pressures. This chapter summarizes current information about recent boiling liquid expanding vapor explosions (BLEVE), details about boiler explosions and knowledge gaps.

2.2 Steam Boiler

A steel-made closed vessel in which water is heated to generate steam is known as steam boiler. This low-pressure steam is used for a variety of industrial processes as well as to generate hot water for use in heating systems. A steam boiler should logically have the least capacity of 10 liters of water and the least operating pressure of 3.4 kgf/cm². The water inside the tubes is surrounded by hot flue gases. High-pressure boilers have a working pressure of about 165 bar. The rate of steam production in a water tube boiler is high, at 450 tons per hour. For the generation of steam, smaller floor space is necessary i.e., 5 m² per ton per hour.

2.2.1 Classification of Boiler

There are various methods to classify boilers, but the following are the most relevant from the perspective of the subject (Figure 2.1):

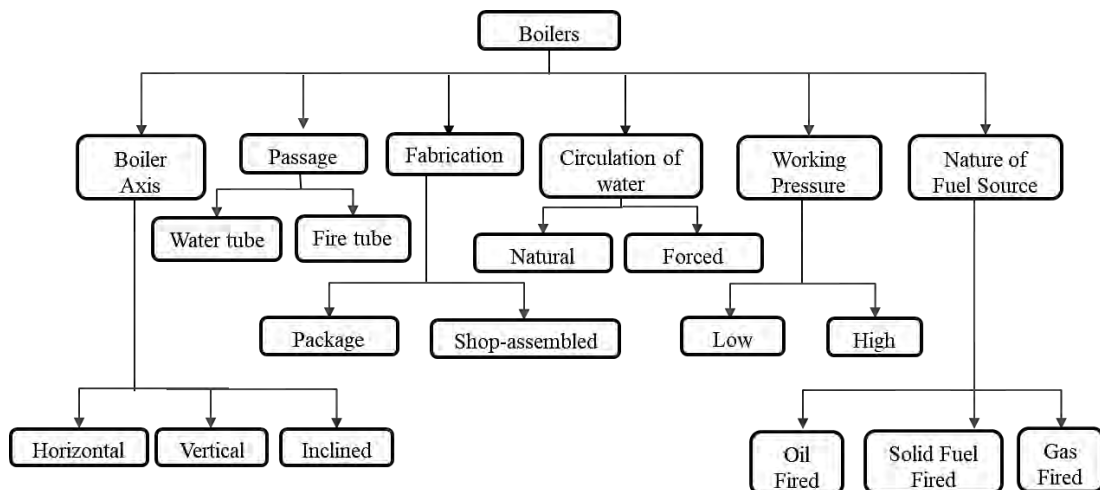


Figure 2.1: Boiler Classification (Agarwal and Suhane, 2017).

2.2.2 Boiler explosions

Steam boilers are widely used in the industries of Bangladesh. Accidents caused by boiler explosions are becoming widespread, resulting in loss of life and properties. Extensive damage of structural components namely adjacent walls, columns etc. are mainly caused by the lack of sufficient knowledge of analysis on this type of explosion loads.

Boilers are a type of pressure equipment that can explode due to heat stress or overpressure. Water level accidents, priming, furnace tube explosions, chamber explosions, and other sorts of mishaps are among the most common. The most severe of them is the damage to a steam drum caused by a boiler operating at excess design pressure, which results in a boiler failure. The boiling liquid expanding vapor explosion (BLEVE) will occur due to the co-existence of boiling water and saturated steam during the boiler operation. In a BLEVE, the explosion occurs when the liquid vaporizes quickly and the vapor expands rapidly in a vessel (Shaluf, 2007). Moreover, due to the combined contribution of overpressure (such as relief valve failure), mechanical damage, thermal stress, and inappropriate working procedure, the strength of the local area's drum wall will be reduced at higher temperatures and pressures, causing fractures (Fang et al., 2013). Therefore, a BLEVE occurs when a liquid is heated over its normal boiling point and its containment breaks down suddenly. Containment losses are generally caused by a catastrophic breakdown of the superheated liquid containing or vessel. The BLEVE blast wave is caused by two factors: compressed vapor inside the vessel and flashing of vapor from the superheated liquid. The blast's size is also determined by the amount of superheat, or the temperature increase over the usual boiling point. The proportion of liquid that flashes rises as the degree of superheat increases, amplifying the severity of the blast (Ogle et al., 2012). The BLEVE from boiler explosion can bring about structural damage and casualties. As a result, quantifying the impact of an explosive incident and taking appropriate safeguards in practice are essential. Safety measures for boiler operation and maintenance is nowhere to be improved and caused great losses in recent years in our country. A number of boiler explosion cases has taken place causing the loss of life and property in Bangladesh. A list of incidents collected from local and international newspapers and news portals is tabulated in Table 2.1.

Table 2.1: List of boiler explosion incidents in Bangladesh (2013 - 2019) (Hossan et al., 2019).

Date	Factory	Place	No. of deaths	No. of injured
2 nd June, 2013	A factory of Nisa Group	Comilla EPZ	2	1
28 th September, 2014	Mega Yarn Dyeing Mills Ltd.	Gazipur	4	1
3 rd June, 2015	Gausia Auto Rice Mill	Sonargaon, Narayanganj	2	18
23 rd January, 2016	Smart Metal and Chemical Industry	Gazipur	7	8
10 th September, 2016	Tampaco Foils Ltd.	Tongi	23	50
4 th July, 2017	Multifabs Ltd.	Gazipur	13	50
19 th April, 2017	Jamuna Auto Rice Mill	Dinajpur	18	10
10 th October, 2017	GPH Ispat Factory Ltd.	Chattogram	1	9
20 th November 2018	Shahjahan Rice Mill	Baliadangi, Thakurgaon	1	2
10 th December, 2019	Natural Village Sweater Ltd.	Khejurbagan, Ashulia	1	1



(a)



(b)

Figure 2.2: Pictorial view of boiler explosion (a) Explosion at a sweater factory in Ashulia of Savar, on the outskirts of Dhaka, on the morning of Tuesday, December 10, 2019. Photo: The Daily Star and (b) Factory boiler blast at Tampaco Foils Bangladesh packaging plant kills dozens

Most of the deaths and injuries were caused due to the failure of walls and columns of the boiler room associated with the structures adjacent subjected to the pressure generated from the explosion. Boiler explosions lead to partial or full collapse of the structure causing deaths and injuries. These losses of life and property is mainly due to the lack of knowledge, analysis methods, response of structure and structural design approach. To minimize the losses, these structures need to be properly designed against the devastating

effect of the boiler explosion. In order to design these structures, extensive research against the pressure generated due to the explosion is of great importance which includes laboratory destructive testing of boilers, intensity, evaluation of blast pressure and explosion radius, effect of pressure on the behavior of reinforced concrete structure and building code development etc.

2.2.3 Causes of boiler explosion

During the industrial revolution, stationary steam engines were widely utilized to power machinery, and there were numerous boiler explosions due to several causes in the early days. William Fairbairn was one of the first people to investigate the subject, and he helped create the first insurance business to cover the damages that such explosions may inflict. He also proved that the hoop stress in a cylindrical pressure vessel, such as a boiler, was double that of the longitudinal stress. These studies assisted him and others in explaining the significance of stress concentrations in deteriorating boilers.

Boiler explosions can be caused by a variety of factors, including inadequate water treatment, which causes scaling and overheating of the plates, a low water level, safety valve blockage, or even a furnace failure, which can lead to a boiler explosion if severe enough. Since the dawn of the industrial revolution, poor operator training has been a common cause of boiler explosions, resulting in neglect or improper mismanagement of the boiler. Boiler rusting was the most common cause of boiler explosions in the late 19th and early 20th centuries, according to inspection data from numerous sources in the United States, the United Kingdom, and Europe. Most of the boiler explosions were outright attributable to inappropriate design, craftsmanship, and hidden defects in low-quality materials, inspection criteria, and quality control failing to keep up with the rapidly expanding boiler manufacturing industry (Kim et al., 2006).

Explosions are caused by a lack of strength in any element of the boilers, as well as over-pressure and over-heating. Original flaws, poor construction, degradation through usage, or mismanagement can all contribute to a lack of strength in steam boilers (Roper and Stephen, 1899). Boiler explosions occur when any component of the boiler is not strong enough to sustain the subjected pressure. One of two things might be causing this: Either the boiler is insufficiently strong to safely sustain its usual working pressure, or the pressure has been allowed to rise over the usual point owing to the safety valves sticking,

or some other such reason. Further analyzes reveal that the immediate cause of the boiler explosion was the gage pressure in the region of combustion produced by a water leakage from the boiler pressure system. The steam boiler was then destroyed by the rapid conversion of water to steam, which was followed by increasing volume and pressure (Švejar et al., 2017).

2.3 Air blast Load

A rapid release of energy causes an explosion. An explosion can occur in a variety of scenarios, including a rapid release of compressed air in a tire, a sudden release of pressured steam in a boiler, or the detonation of powerful explosives. Detonation is caused by a rapid chemical reaction that propagates through the explosive as a supersonic shock wave. A shock wave is characterized as a pressure, temperature, and density discontinuity (Meyers, 1994). The pressures in the explosion just behind the detonation front can be as high as 10–30 GPa (Mays and Smith, 1995). As a result of the immense accumulation of energy pushing back the surrounding environment due to the explosion in the air, a blast wave will produce. The blast wave will spherically expand into the surrounding air after this tremendous discharge of energy. As the blast wave travels through the medium, pressure, temperature, and density increase in an almost constant pattern. Acceleration of the air particles in the direction of the moving front occurs as the shock front propagates, resulting in a net particle velocity.

2.4 Previous research on blast load testing of vessel containing flammable and non-flammable fluids

It is a critical part to estimate the energy of the explosion which is the maximum potential work obtained from the explosive system. Ogle et al., (2012) proposed a method for explosion energy calculation using exergy analysis. In general, the total work found from the exergy method is much higher than other available methods.

Johnson et al., (1991) tested butane and propane in a series of experiments (Table 2.2). Electric immersion heaters were used to heat the containers, which were then coated with a polymeric heat insulator to limit heat loss. The failure of the tanks was caused by the detonation of a short linear-shaped high explosive charge. The experimental fluid was switched from butane to propane in one of the experiments (J6) without affecting vessel capacity. These researchers also conducted a test in which they increased the container

volume (10.8 m³) while maintaining the same amount of butane (2000 kg) as in a previous study (J5). They lowered the quantity of butane in another experiment (J3) to 1000 kg in the same vessel capacity. The overpressures created by the expansion of the vapor phase existent before the burst, as well as the flash vaporization of the liquid, typically coalesced into a single peak in these experiments. Hemmatian et al., (2017) compared the overpressure derived from several theoretical predictions using the TNT equivalent mass approach with the experimental data from Johnson et al. They concluded that theoretical predictions of pressure vessel explosions differ significantly from experimental results.

Table 2.2: Tests performed by Johnson et al. with butane and propane (Hemmatian, Planas, et al., 2017).

Test	Filling degree (%)	Fluid	Amount of fluid (kg)	Volume of vessel (m ³)	P _{rupture} (kPa)	Standoff distance, R (m)	P _{so} (overpressure at a distance R, kPa)
J1	75	Butane	2000	5.66	1460	25/100/150	6.2/1.3/1.1
J2	76	Butane	2000	5.66	1510	25/50/100/150	6.3/3.9/0.9/0.6
J3	38	Butane	1000	5.66	1520	25/50/100/150	5/2.8/1.2/0.8
J4	68	Butane	2000	5.66	770	25/50/100/150	1/0.5/0.17/0.15
J5	40	Butane	2000	10.80	1510	25/50/100/150	8.2/3.4/1.4/0.7
J6	77	Propane	2000	5.66	1520	25/50/100/150	2.3/1.2/0.3/0.3
J7	76	Butane	2000	5.66	1520	25/50/100	7/3.4/1.3

Birk et al., (2006, 2007) utilized 2 m³ liquid propane-filled vessels. The vessels were enveloped by a series of jet fires, and overpressures were monitored at various distances in both the axial and transversal directions.

Table 2.3 summarizes the outcomes of these experiments. The liquid energy has very little impact on the shock overpressure from a BLEVE event. It's possible that the quick liquid flashing that occurs following a tank rupture is too slow to cause a shock wave. The vapor energy is what causes the shock that BLEVEs produce in practice. The findings also demonstrate that failures of cylindrical tanks near the ground have extremely substantial directional impacts. Laboureur et al., (2014) discovered comparable substantial discrepancies with the test results obtained from brick et al. (2006, 2007).

Table 2.3: Experimental results performed with propane in a 2 m³ vessel (Birk et al., 2007; Birk and VanderSteen, 2006; Laboureur et al., 2014)

Test	Filling degree (%)	P _{rupture} (kPa)	Standoff distance, R (m)	P _{so} (overpressure at a distance R, kPa)
B1	17	1863	10/20/30(E)/30(S)/40(E)/40(S)	6.65/3.5/3.11/4.19/2.11/2.73
B2	35	1846	10/20/30/40(E)/40(S)	3.97/3.78/2.29/1.48/2.13
B3	13	1699	10/20/40(E)/40(S)	5.29/2.75/1.72/1.83
B4	21	1894	10/40	5.02/1.675
B5	12	1573	10/20/30/40	4.13/2.58/1.58/1.31
B6	51	1803	10/20/30(E)/30(S)/40(E)/40(S)	13.11/8.95/6.03/2.99/3.37/4.06
B7	52	1563	10/20/30/40	4.563/3.4/1.93/1.58
B8	53	1813	10/20/30(E)/30(S)/40(E)/40(S)	4.15/2.99/2.99/2.29/2.6/0.64
B9	61	1858	10/20/30/40	5.44/5.05/3.59/2.7

Ibrahim et al., (2019) worked on the effect of steam boiler explosion for boiler houses in factories throughout Egypt. They estimated the equivalent TNT charge for different fuels and internal explosion was analyzed using LS-DYNA finite element program. Due the unavailability of the systematic experimental data and complexity of the overpressure boiler explosion was described in terms of TNT equivalency. The numerical models were developed for a standard boiler of 2000 kg capacity with liquid (Diesel) and natural gas (Propane). The average pressure curve on the Boiler wall was compared in different scenarios and with various charges ranging from TNT 100 Kg, 150 Kg, 300 Kg, and 600 Kg. To know numerous consequences and concerns, average pressure values in both scenarios of a single wall and a closed room with air and without air. As a result, the real-life explosion scenario may differ from the theoretical model. The experimental research of the boiler explosion will be explored in this study in order to gain a thorough understanding of the issue by generating a time-history diagram.

2.5 Summary of the previous study

Various uncertainties, some of which are unavoidable, affect the estimation of the explosion created by BLEVEs. For example, the proportion of the overall energy released in the explosion that is engaged in producing the overpressure can be significant and some of this energy is responsible for fracturing the vessel and ejecting the fragments a considerable distance. The value of this percentage will be influenced by a range of factors, including the state of the vessel (corrosion), heating systems, the placement of a welding joint, and so on. As a result, some researchers assume 40%, others 50%, and the

most conservative authors assume 100%. The blast wave's heterogeneity, or directionality, is another source of uncertainty (Birk et al., 2007). The value of overpressure in cylindrical tanks is not the same in the direction of the principal axis. The distance traveled by a fragment of a given weight is linked to the pressure in the vessel right before the explosion. However, the form of the fragment can have a significant impact on this distance. However, this element has not received enough attention in recent years, and therefore cannot be considered in any overpressure estimation.

2.6 Knowledge gaps

As it is seen from the literature review, the following issues need systematic investigations:

1. In BLEVE fire may not ensue if non-flammable fluids are used in the boiler. But previous boiler explosion history indicates substantial damage due to the shock wave overpressure. So, experimental investigation of boiler explosion should be performed to extend the knowledge of actual explosion scenario and peak overpressure.
2. The internal energy of boiling liquid is dependent on the internal temperature of the boiler at the time of the explosion. On the other hand, Peak overpressure will increase with the increase in internal energy. So, the assumption of initial temperature based on the critical temperature of the filling liquid may differ from the actual temperature during the explosion.
3. In previous researches, a time-history plot after the explosion of the steam boiler is not developed yet. So, the total blast duration of the boiler filled with non-flammable fluids needs to be investigated by plotting a pressure time-history graph.

Chapter 3 THEORETICAL PREDICTION OF BOILER BLAST LOAD

3.1 Introduction

This chapter summarizes the characteristics of blast wave, theoretical predictions of blast using the equivalent TNT methods, determination of blast related parameters, batch energy calculation for the sample boiler etc.

3.2 Ideal blast wave characteristics

Figure 3.1 depicts an idealized profile of pressure against time for a free-air blast wave that reaches a location at a fixed distance from the detonation. When the shock front reaches the arrival time t_A , the pressure around the element is initially equal to the ambient pressure P_o , and it increases instantly to a peak pressure P_{so} . The time it takes for the pressure to reach its highest value is relatively short, and it is considered to be zero for design purposes. Side-on overpressure, or peak overpressure, is another name for the peak pressure P_{so} . With increasing distance from the detonation point, the peak overpressure and wave's propagation velocity diminish. The pressure drops at an exponential rate after its peak value until it equals the ambient pressure at t_A+t_o , which is known as the positive phase duration. After the positive phase of the pressure-time diagram, the pressure drops (indicated as negative pressure) and ultimately returns to the ambient value.

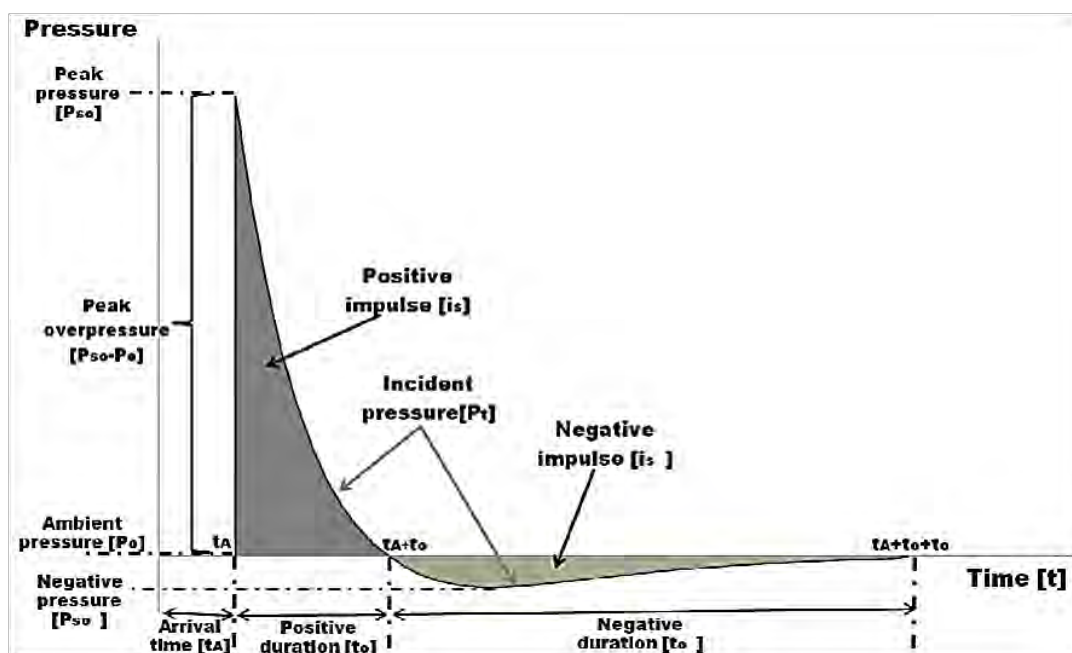


Figure 3.1: Pressure time history of ideal blast wave (Karlos and Solomon, 2013).

The negative phase lasts longer than the positive phase, with a minimum pressure value of P_{so}^- and a duration of t_0 . The structures are susceptible to suction pressure during this phase because, during blast loading, glass pieces from facade failures are occasionally discovered outside rather than within a building. The negative phase of an explosive wave is generally ignored while designing because it has been proven that the positive phase is responsible for the majority of structural damage. Furthermore, because the negative phase of the blast wave produces lower pressures than the positive phase, and because they are in the opposite direction, it is typically reasonable to presume that they have minimal influence on the structural integrity of structures subjected to blast loads. When evaluating a building's total structural performance during an explosion, rather than just its structural integrity, pressures below the ambient pressure value should be considered. Figure 3.1 shows how the positive incident pressure drops rapidly. Friedlander's equation in the following form (Baker, 1973) has been proposed and is commonly used to represent this rate of reduction in pressure values:

$$P_s(t) = P_{so} \left(1 - \frac{t}{t_0} \right) e^{-b \frac{t}{t_0}} \quad (3.1)$$

where, P_{so} = The peak overpressure,

t_0 = The positive phase duration,

b = decay coefficient of the waveform and

t = The time elapsed, measured from the instant of blast arrival.

A non-linear fitting of an experimental pressure-time curve across its positive phase may be used to compute the decay coefficient b . Aside from the peak pressure, the impulse of the blast wave pulse is an even more essential parameter for design requirements. Because it corresponds to the overall force that is delivered to the structure owing to the explosion. It is specified as the shaded region beneath Figure 3.1's overpressure-time curve. The impulse is characterized as positive i_s or negative i_s^- based on the blast wave time history of the corresponding phase. In terms of preventing building collapse, Equation (2) offers the expression in the situation of the positive impulse, which is more significant than its negative counterpart,

$$i_s = \int_{t_A}^{t_A+t_0} P_s(t) dt \quad (3.2)$$

The positive impulse may be determined analytically using the Previously mentioned Friedlander equation (1):

$$i_s = \frac{P_{so} t_o}{b^2} [b - 1 + e^{-b}] \quad (3.3)$$

This equation offers another approach to compute the decay parameter b iteratively using the values of the i_s , P_{so} and t_o .

3.3 Scaled Distance (Z)

The standoff distance between the detonation point and the target structure is a critical parameter in the calculation of blast loading. In Figure 3.2, the velocity and peak pressure of the blast wave are shown as they decrease dramatically as the standoff distance increases.

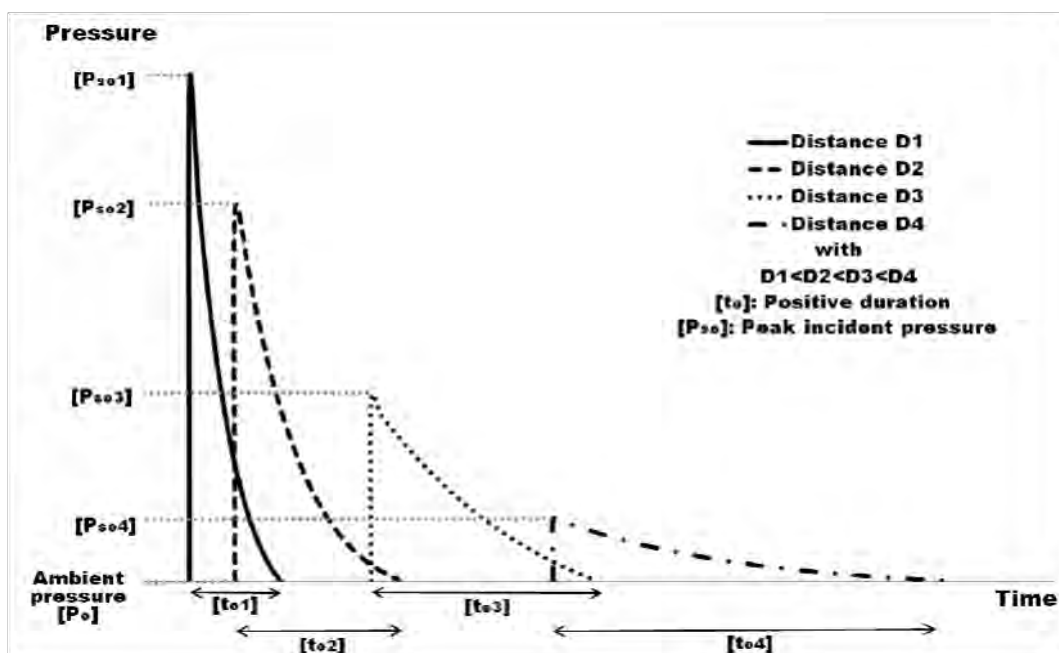


Figure 3.2: Effect of standoff distance on positive pressure phase of the blast (Karlos and Solomon, 2013).

The effects of distance on the detonation characteristics can be measured through the introduction of scaling laws. This procedure allows the engineers to determine the energy release and the distance of the detonation using experiments. The most common type of blast scaling laws are the ones developed by Heinrich Hopkinson-Cranz and Arthur Sachs. These are formulated by assuming that when two charges of the same explosive are detonated at the same distance, the same blast waves will produce. In cases of different

atmospheric conditions, the scaling of Sachs is also possible. A dimensional scaled distance is introduced according to the Hopkinson-Cranz rule, as defined by Equation (4)-

$$Z = \frac{R}{W^{\frac{1}{3}}} \quad (3.4)$$

R denotes the standoff distance between the center of the explosive charge and the target structure. W is the mass of a standard explosive such as TNT (Trinitrotoluene), which is widely used for military purposes.

For assumption, an explosive charge of weight W_1 and typical size d_1 , located at distance R_1 from the point of attention, generates a blast wave of peak overpressure P , impulse i_1 , duration t_{o1} , with arrival time t_{a1} and that $\frac{R_1}{\sqrt[3]{W_1}} = \lambda$. Then, according to this scaling rule, another explosive charge W_2 of characteristic size $d_2 = \lambda d_1$, positioned at a distance $R_2 = \lambda R_1$, would create a blast wave with the same peak overpressure P and identical pattern at this point. Furthermore, due to W_2 , we would get impulse $i_2 = \lambda i_1$, duration $t_{o2} = \lambda t_{o1}$, and arrival time $t_{a2} = \lambda t_{a1}$ at the given point.

3.4 Explosive type and weight

In explosions, several types of explosives are utilized. A datum is required to quantify and estimate blast wave parameters and analyze the detonation properties of each type of explosive material. Trinitrotoluene (TNT) is the widely acknowledged standard; it's a relatively pure, safe-to-handle explosive that is indeed widely available. TNT has been used in a variety of studies and researches.

Because of the broad range of explosives, a universal quantity has been adopted for all blast parameter calculations. TNT (Trinitrotoluene) was chosen because it has similar explosion properties to most solid-type explosives. Equation (5), which uses the ratio of the heat produced during explosion to relate the weight of the specified design explosive to the equivalent weight of TNT:

$$W_e = W_{exp} \frac{H_{exp}^d}{H_{TNT}^d} \quad (3.5)$$

where, W_e = The TNT equivalent weight [kg],

W_{exp} = The weight of the actual explosive [kg],

H_{exp}^d = The heat of detonation of the actual explosive [MJ/kg], and

H_{TNT}^d = The heat of detonation of the TNT [MJ/kg].

Detonation releases around one-third of the explosive's entire chemical energy. The rest is released at a slower pace as the heat from the explosive products' combustion mixes with the ambient air. Several tables describing the heat output of the most commonly used explosives (U.S. Department of the Army, 1990; Unified Facilities Criteria, 2008). Table 3.1 shows estimates of the heat of detonation produced by a variety of popular explosives, as described by (U.S. Department of the Army, 1990). Using Equation (5), these data may be used to calculate the equivalent TNT weight.

Table 3.1: Heat of detonation of some common explosives (U.S. Department of the Army, 1990).

Explosives	Heat of detonation [MJ/kg]
TNT	4.10-4.55
Composition-C4	5.86
RDX	5.13-6.19
PETN	6.69
PENTOLITE 50/50	5.86
NITROGLYCERIN	6.30
NITROMETHANE	6.40
NITROCELLULOSE	10.69
AMON. /NIT (AV)	1.59

A relevant assault scenario using a vehicle-borne or personnel-borne improvised explosive device is generally used to determine the explosive weight. Table 3.2 shows the quantity estimation of explosives that might be transported by different vehicle types.

Table 3.2: Upper limit of charge weight per means of transportation (U.S. Department of the Army, 1990).

Explosives	Explosive's weight (kg)
Suitcase	10
Medium sized Car	200
Large sized Car	300
Pick-up Truck	1400
Van	3000
Truck	5000
Truck with trailer	10000

Table 3.3 illustrates several TNT equivalent weight factors (U.S. Department of the Army, 1990) that may be utilized to calculate the weight of TNT that generates the same blast wave parameters as another explosive of specific weight.

Table 3.3: Indicative values of TNT equivalent mass factors (U.S. Department of the Army, 1990).

Explosives	TNT equivalent mass factors	
	Peak Pressure	Impulse
ANFO	0.82	0.98
TNT	1.00	1.00
Composition-B	1.11	0.98
Composition-C3	1.08	1.01
Composition-C4	1.37	1.19
CYCLOTOL	1.14	1.09
OCTOL 75/25	1.06	1.06
TETRYL	1.07	1.05
HMAX	1.02	1.03
AMATOL	0.99	0.98
RDX	1.14	1.09
PETN	1.27	1.11

3.5 Categories of Blast-loading

Blast loads on structures can be classified into two types depending on the confinement of the explosive charges (unconfined and confined explosions), and further split based on whether the blast loads are created within the donor structure or on acceptor structures. The five probable pressure loads associated with the blast load categories are shown in Figure 3.3 and Table 3.4, which also illustrates the position of the explosive charge that would create these pressure loads, as well as the protective structures subjected to these pressures.

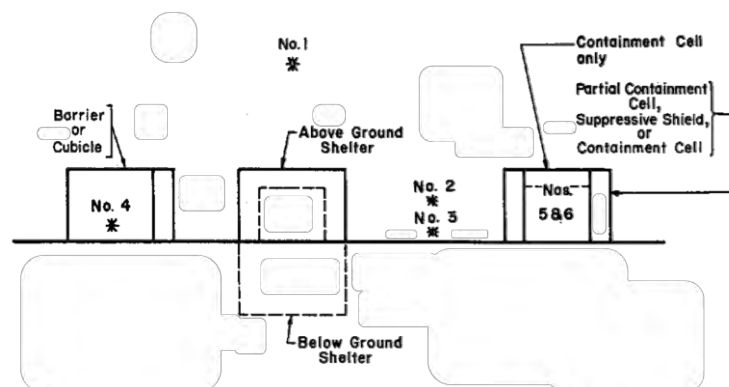


Figure 3.3: Blast loading categories (U.S. Department of the Army, 1990).

Table 3.4: Different blast loading categories (U.S. Department of the Army, 1990).

Blast Loading Categories			
Charge confinement	Category	Pressure load	Protective structures
Unconfined Explosions	a. Free-Air Burst	a. Unreflected	Shelter
	b. Air Burst	b. Reflected	
	c. Surface Burst	c. Reflected	
Confined Explosions	d. Fully Vented	d. Internal Shock e. Leakage	Cubicle
	e. Partially Confined	e. Internal Shock	Partial Containment
		f. Internal gas	Cell or
		g. Leakage	Suppressive Shield
	f. Fully Confined	i. Internal Shock k. Leakage	Full Containment Cell

3.5.1 Unconfined explosions

Explosions that occur outside of a structure might occur in the air, above ground, or on the Earth's surface. All of them will have varying effects on the structure. When dealing with an external blast danger, the designers will prioritize an unconfined explosion.

3.5.1.1 Free air burst explosion

An explosion in free air generates an initial output whose shock wave propagates out from the detonation's center, impacting the structure without any intermediary amplification. The explosive charge is detonated in the air, and the blast waves travel spherically outwards, striking the building instantly without encountering any other barriers or the ground.

3.5.1.2 Air burst explosion

A Mach wave front is formed when an explosive charge is detonated in the air, and the blast waves travel spherically outwards before impinging on the structure after first interacting with the ground.

3.5.1.3 Surface burst explosion

The explosive charge is detonated near the earth's surface, and the blast waves impact the ground locally before spreading hemi-spherically outwards and impinging on the structure.

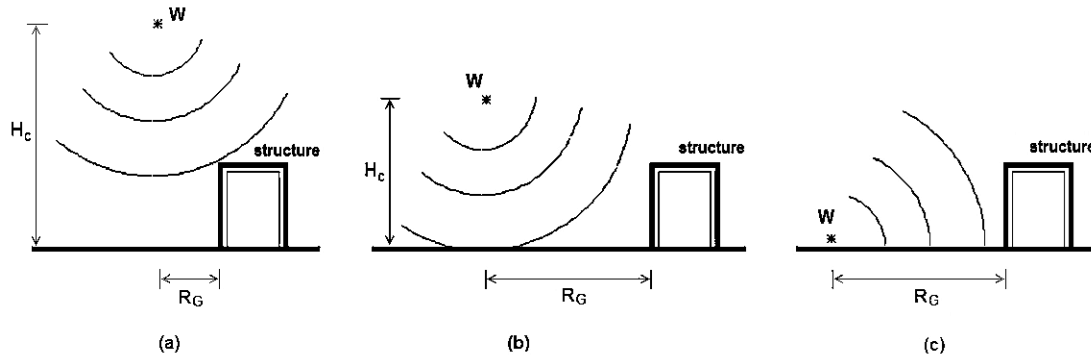


Figure 3.4: Types of external explosions and blast loadings; (a) Free-air bursts, (b) Air bursts, and (c) Surface bursts. (Karlos and Solomon, 2013).

Each of these explosion types is associated with a distinct blast loading of the structure because reflections and interference events along the propagation route can significantly modify the wave strength and hence the loading pressures.

3.5.2 Confined explosion

Internal explosions that are confined and contained usually produce complicated pressure-time histories on the inner surfaces. Although precise loading cannot be predicted, approximations and model relationships can be used to accurately determine blast loads (U.S. Department of the Army, 1990). Procedures for calculating blast loads owing to initial and reflected shocks, quasi-static pressure, directional and uniform venting effects, and vent closure effects are also included. There are two almost separate phases to the loading from a high-explosive explosion within a confined (vented) or contained (unvented) building. The reflected blast loading is the first phase, which generally consists of an initial high-pressure, short duration reflected wave followed by many subsequent reflected pulses. The second phase is referred to as the gas-loading phase.

Effect of Confinement: When an explosion happens within the structures, the pressure associated with the first shock front (free-air pressure) will be extraordinarily high, exacerbated by the structure's reflections. Moreover, depending on the degree of

confinement, the impact of high temperatures and the accumulation of gaseous products created by the chemical process associated with the explosion would apply additional pressures and lengthen the load duration within the structure. Unless the structure is designed to withstand the impacts of internal pressure, the cumulative effects of these pressures may eventually destroy it. With simple individual representations, Figure 3.5 depicts confined blast types.

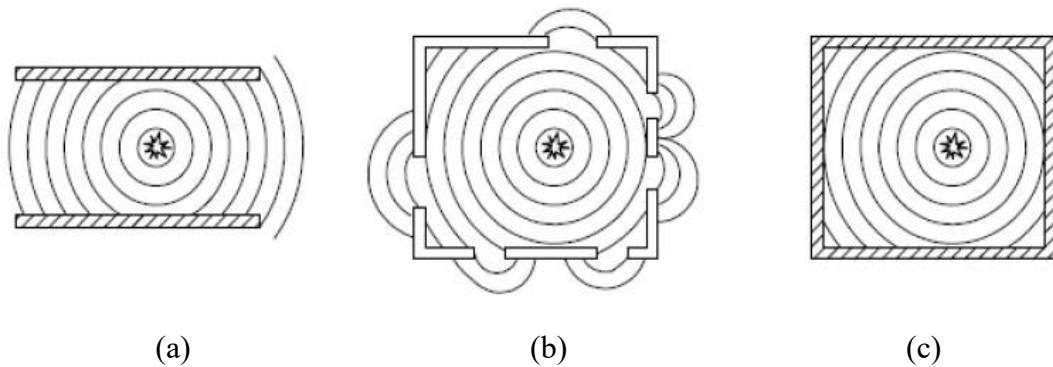


Figure 3.5: Confinement blast categories (a) Fully vented, (b) Partially vented, and (c) Fully confined (Yandzio and Gough, 1999).

3.5.2.1 Fully vented explosion

A completely vented explosion occurs within or near a barrier or cubicle construction that has one or more surfaces exposed to the atmosphere. The initial wave is intensified by the structure's non-frangible parts, and the detonation products are completely vented to the atmosphere, creating a shock wave (leakage pressures) that propagates away from the structure.

3.5.2.2 Partially vented explosion

Within a barrier or cubicle structure with limited size openings and/or frangible (fragile) surfaces, a partially confined explosion will occur. After a finite interval, the original wave, which is amplified by the frangible and non-frangible portions of the structure, and the detonation products are vented to the environment. The accumulation of quasi-static pressure is associated to the confinement of detonation products, which consists of accumulation of high temperatures and gaseous gases.

3.6 Blast wave reflection

Figure 2.11 illustrates the blast wave propagation over a building following the detonation of a truck bomb (FEMA 426, 2011).

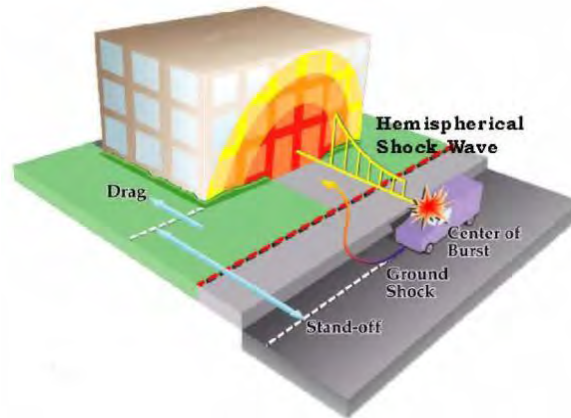


Figure 3.6: Propagation of blast pressure (FEMA 426, 2011).

When a blast wave interferes with a rigid surface, the reflected pressure is greater than the incident peak pressure P_{so} illustrated in Figure 3.1. The nature of the blast wave's propagation through the air is the cause of this increment. The wave travels through air particles, which clash with the surface when it arrives. The particles should be able to bounce back freely in an ideal linear-elastic situation, resulting in a reflected pressure equal to the incident pressure, resulting in a doubling of the acting pressure on the surface. Figure 3.7 depicts the difference between incident and reflected pressures on an infinite surface. Depending on the structural geometry, types, size, weight, the distance of the explosive and the interference of other barriers between the detonation site and the structure, the reflected pressure can be many times more than the incident pressure. A typical dynamic pressure-time history is also shown in Figure 3.7.

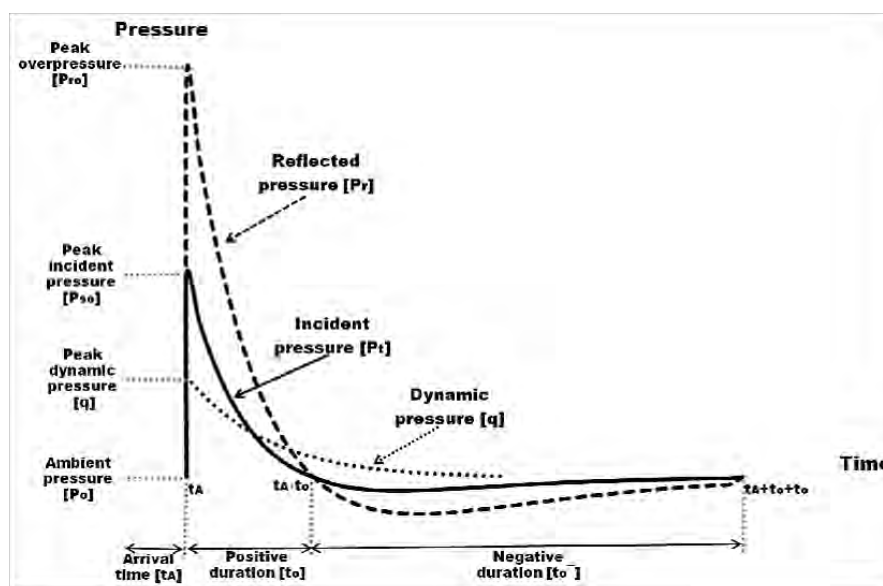


Figure 3.7: Incident, reflected and dynamic pressure time histories (Baker, 1973).

3.7 Factors affecting blast pressure

Once an explosion takes place, the blast waves start travelling in every direction and have direct effect on every object on its path. Several factors contribute to the magnitude and distribution of blast loads. These include:

- a. Shape and type of explosive, detonation speed, and travel distance between the explosive and structure under blast loading.
- b. The clarity of the path that the shock waves travel through (obstacles change shockwave behavior).
- c. The geometrical shape and elevation of the structure.
- d. Open versus closed structures

The above factors can significantly affect the intensity of blast. For instance, buildings with openings allow for incident pressure to propagate inside of the structure and that will create high reflected pressure between the interior walls. Also, the geometrical shape will change the reflection of shock wave line, due to the change in reflection angle (UFC 03-0340-02, 2008). Finally, the distance between the point of blast and the structure will control the intensity of shock wave.

Distant explosions also known as far-field explosions produce uniform pressure on the target structure. Explosion near a structure, which is known as close-in explosion, produces high non-uniform pressures on the target structure.

3.8 Theoretical prediction of boiler blast load

3.8.1 Explosion energy calculation

Several researchers have tried to figure out how to compute the explosive energy of a BLEVE. Prugh (Prugh, 1991) covered a wide range of topics related to BLEVE events and recommended two techniques for estimating the energy of an explosion using the work method. His first technique required computing the isentropic work of expansion for the combined volume of the original head space vapor and the flashed vapor after determining the proportion of liquid flashed. The ideal gas equation of state was believed to apply to the vapor. The energy of the explosion was matched to the expanding work. Prugh's second technique was based on energy. The second technique linked the explosion's work with the superheated liquid's internal energy change. This technique also specifies an isentropic (thermodynamic) route for vapor expansion. The explosion energy is equivalent to the expansion work. The American Institute of Chemical Engineers'

(AIChE) Center for Chemical Process Safety, 2010 (CCPS) proposed this technique. Planas-Cuchi et al (Planas-Cuchi et al., 2004) improved the energy approach by comparing the superheated liquid's internal energy change to the irreversible work done as the expanding vapor pushes against the surrounding atmosphere.

Table 3.5: Summary of various methods of calculating explosion energy of BLEVE.

Author and Year	Equation for Explosion Energy
Prugh (1991)	$E = 10^2 \frac{PV}{k-1} \left[1 - \left(\frac{101}{P} \right)^{\frac{(k-1)}{k}} \right]$
Planas-Cuchi et al., (2004)	$-P_o \times \Delta V = \Delta U$
	$-\Delta U = (u_L - u_G)m_T x - m_T u_L + U_i$
	$P_o \times \Delta V = P_o [(v_G - v_L) m_T x + m_T v_L - V_i]$
	$x = \frac{m_T P_o v_L - V_i P_o + m_T u_L - U_i}{[(u_L - u_G) - (v_G - v_L) P_o] m_T}$
	$W_{TNT} = \beta \times 0.124 \times \Delta U$
Ogle et al., (2012)	$E = (U - U_o) + P_o(v - v_o) - T_o(S - S_o)$

Note: E: Released energy or batch energy (kJ/kg); V: initial volume (m³); P: initial pressure (bar); K: specific heat ratio; P_a or P_o : atmospheric pressure or pressure just after explosion (bar); $-P_o \times \Delta V$: The real expansion works; ΔV : Variation in volume of the whole vessel content (m³); ΔU : variation in the internal energy of the vessel content (kJ kg⁻¹); m_T : overall mass in the vessel (kg); U , U_i : overall internal energy of the system just before the explosion (MJ); u_L : internal energy of the liquid at the final state of the irreversible process (MJ kg⁻¹); u_G : internal energy of the vapour at the final state of the irreversible process (MJ kg⁻¹); v_L : specific volume of the liquid at the final state of the irreversible process (m³ kg⁻¹); v_G : specific volume of vapor at the final state of the irreversible process (m³ kg⁻¹); x : vapor fraction at the final state of the irreversible process (-); β : fraction of the energy released converted into a pressure wave (-); U_o : Internal Energy at final state (KJ kg⁻¹); v_o : Specific Volume at final state (m³ kg⁻¹); P_o : Absolute Pressure at final state (kPa); T_o : Absolute Temperature at final state (K); S_o : Entropy at final state (KJ/K Kg); v : Specific Volume at initial state (m³/kg); S: Entropy at initial state (KJ/K Kg).

Exergy, also known as thermodynamic availability, is the maximum amount of potential work a system can do when it is in thermal, mechanical, or chemical equilibrium with its surroundings. This implies that the superheated liquid flashes from its initial state to its final state, which is defined by the natural environment for a BLEVE (ambient temperature and pressure). Crowl (Crowl, 1992, 1992, 1991) showed how to calculate the maximum potential work from compressed gas or combustible fuel using batch exergy. Though the dispute exists among the investigators about how to calculate the explosion energy for BLEVE, Ogle et al., 2012 (Ogle et al., 2012) examined the explosion energy of BLEVE following the work of Crowl. Table 3.5 demonstrated the summary of available methods which can be adopted for the calculation of explosion energy.

Three trial samples were examined initially to get a sense of the real blasting temperature. Because temperature affects internal energy, specific volume, entropy, and pressure at the moment of the burst. The front plate of the boiler samples was grooved to provide a predetermined failure plane. As a result, the temperature of the explosion was discovered to be between 125 and 132 °C. Exergy analysis was used to compute batch energy or internal energy, which is presented in Table 3.6.

Table 3.6: Explosion energy at different expected temperatures using exergy analysis.

Temperature (K)	Temperature (°C)	Explosion Energy of water using Exergy Analysis (MJ/kg)
393.15	120	0.044
394.15	121	0.044
395.15	122	0.045
396.15	123	0.046
397.15	124	0.047
398.15	125	0.048
399.15	126	0.049
400.15	127	0.05
401.15	128	0.051
402.15	129	0.052
403.15	130	0.053
404.15	131	0.054
405.15	132	0.055

3.8.2 Structural blast load prediction

There are several correlations and ways of estimating the value of incident pressure at a certain distance from an explosion. All the suggested relationships require the value of scaled distance, which can be determined by the explosive mass and the actual distance from the center of the spherical explosion.

(Kinney and Graham, 1985) provide a chemical type explosion-based formula which is shown in Eq. (6). It has been employed widely in computer calculations,

$$P_{so}=P_o \frac{808 \left[1 + \left(\frac{Z}{4.5} \right)^2 \right]}{\left\{ \left[1 + \left(\frac{Z}{0.048} \right)^2 \right] \left[1 + \left(\frac{Z}{0.32} \right)^2 \right] \left[1 + \left(\frac{Z}{1.35} \right)^2 \right] \right\}^{0.5}} \quad (3.6)$$

Where Z (m/kg^{1/3}) is the scaled distance and P_o is the ambient pressure.

Other peak overpressure equations for spherical explosions include those of (Brode, 1955), as indicated in Eq (7). They are proportional to the size of the explosion, with Eq. (7a) true for peak overpressures more than 10 bar (=1 MPa) (near field explosions) and Eq. (7b) valid for pressure values between 0.1 bar and 10 bar (0.01 MPa - 1 MPa) (medium and far-field explosions). The scaled distance is recorded in $m/kg^{1/3}$, whereas the pressure P_{so} is measured in bars,

$$P_{so} = \begin{cases} \frac{6.7}{Z^3} + 1, & \text{for } P_{so} > 10 \text{ bar} \\ \frac{0.975}{Z} + \frac{1.455}{Z^2} + \frac{5.85}{Z^3} - 0.019, & \text{for } 0.1 < P_{so} < 10 \text{ bar} \end{cases} \quad (3.7)$$

Another approach has been suggested (Newmark and Hansen, 1961) that does not include categorization as per the intensity of the detonation and is extensively used for estimating peak overpressure values for ground surface blasts:

$$P_{so} = 6784 \frac{W}{R^3} + 93 \sqrt{\frac{W}{R^3}} \quad (3.8)$$

Where, P_{so} is the peak incident overpressure in bars, W is the weight of equivalent TNT (in metric tons) and R is distance from the center of detonation on the ground to the point of interest (m).

Mills (1987) has also introduced an expression of the peak overpressure in kPa, in which W is expressed in kg of TNT and the scaled distance Z is in $m/kg^{1/3}$, which reads:

$$P_{so} = \frac{1772}{Z^3} - \frac{114}{Z^2} + \frac{108}{Z} \quad (3.9)$$

The strategy recommended by Kingery and Bulmash for determining blast parameters is the most extensively utilized and recognized method. Their work consists of formulas for both spherical (free air bursts) and hemispherical (surface bursts) pressure waves, as well as values for the incident and reflected pressures and all other parameters. The blast parameters given are applicable for distances ranging from 0.05 to 40 meters. Kingery and Bulmash (1984) provide a complete set of mathematical equations that express the aforementioned blast parameters as polynomial functions of the scaled distance logarithm.

$$P_{so} = \exp\{A + B \cdot \ln Z + C \cdot (\ln Z)^2 + D \cdot (\ln Z)^3 + E \cdot (\ln Z)^4 + F \cdot (\ln Z)^5 + G \cdot (\ln Z)^6\} \quad (3.10)$$

Where, P_{so} is the peak incident overpressure in kPa, Z is the scaled distance in $m/kg^{1/3}$ and the value of constant A, B, C, D, E, F and G for peak overpressure (P_{so}), is presented in Table 2.5. Eq. (2.11) can also be used to calculate the other blast parameters like peak reflected pressure P_r , positive phase duration t_o , incident impulse i_s , reflected impulse i_r and shock front velocity U .

Table 3.7: Constants for polynomial equations of Kingery and Bulmash (1984) blast parameters.

Incident pressure, P_{so} (kPa)							
Range	A	B	C	D	E	F	G
0.2-2.9	7.2106	-2.1069	-0.3229	0.1117	0.0685	0	0
2.9-23.8	7.5938	-3.0523	0.40977	0.0261	-	0	0
23.8-	6.0536	-1.4066	0	0	0	0	0
Peak reflected pressure, P_r (kPa)							
0.06-2.0	9.006	-2.6893	-0.6295	0.1011	0.29255	0.13505	0.01973
2.0-40	8.8396	-1.733	-2.64	2.293	-0.8232	0.14247	-0.0099
Positive phase duration, t_o (ms/kg ^{1/3})							
0.02-	0.5426	3.2299	-1.5931	-5.9667	-4.0815	-0.9149	0
1.02-	0.5440	2.7082	-9.7354	14.3425	-9.7791	2.8535	0
2.80-	-2.4608	7.1639	-5.6215	2.2711	-	0.03466	0
Incident impulse, i_s (kPa-ms/kg ^{1/3})							
0.2-0.96	5.522	1.117	0.6	-0.292	-0.087	0	0
0.96-	5.465	-0.308	-1.464	1.362	-0.432	0	0
2.38-	5.2749	-0.4677	-0.2499	0.0588	-	0	0
33.7-	5.9825	-1.062	0	0	0	0	0
Reflected impulse, i_r (kPa-ms/kg ^{1/3})							
0.06-40	6.7853	-1.3466	0.101	-	0	0	0
Shock Front Velocity, U (km/s)							
0.06-	0.1794	-0.956	-0.0866	0.109	0.0699	0.01218	0
1.50-40	0.2597	-1.326	0.3767	0.0396	-0.0351	0.00432	0

Constant for determine other parameters are also presented in Table 3.7. These relationships can be readily programmed and Figs. A.1 through A.5 mentioned in Appendix A show the diagrams for blast parameters for positive and negative phase of the blast wave for both free-air and surface bursts explosions.

3.8.3 Standoff distance

As discussed earlier, scaling law is adopted according to Hopkinson-Cranz law for a boiler of 1 MT filling volume. Finally, for standoff distances 8 ft, 10 ft and 12 ft of 1 MT

boiler, the standoff distances were calculated for the sample boiler of 15.44 Liter capacity. The main purpose for constant scaled distance is to produce the same blast effect from the sample boiler. The time parameters will be changed and pressure and velocity value will remain unchanged at similarly analogous time. Table 3.8 illustrates the values of standoff distance and filling volume of the sample considering the average explosion temperature of 126 °C and an average explosion energy of 0.049 MJ/kg.

Table 3.8: TNT equivalent weight and standoff distance for sample boiler with a constant scaled distance considering an industrial boiler of 1 MT filling capacity.

Sample Designation	FD (%)	Boiler (1 MT volume)		Z (m/kg ^{0.333})	Sample Boiler (15.44 L)		
		R, m (ft)	W _{TNT} (kg)		W _{TNT} (kg)	R (cm)	Filling volume of sample (L)
B60S8	60	2.44 (8)	7.333	1.255	0.113	60.70	9.27
B60S10		3.05 (10)		1.569		75.90	
B60S12		3.66 (12)		1.883		91.0	
B50S8	50	2.44 (8)	6.111	1.334	0.094	60.70	7.72
B50S10		3.05 (10)		1.668		75.80	
B50S12		3.66 (12)		2.001		91.0	
B40S8	40	2.44 (8)	4.889	1.437	0.076	60.90	6.18
B40S10		3.05 (10)		1.796		76.10	
B40S12		3.66 (12)		2.156		91.30	

B: Boiler specimen; FD: filling degree, R: standoff distance (feet or meter or cm); W_{TNT}: TNT equivalent weight of the explosive (water) (kg); Z: scaled distance (m/kg^{0.333}).

3.8.4 Calculation of blast parameters for front wall

For peak incident overpressure calculation of an explosion, various relationships and approaches are discussed in the article 3.7.2. But for simplified calculation modified graphs (Karlos and Solomon, 2013) were used for the determination of positive and negative phase blast parameters. These graphs were adopted from Unified Facilities Criteria (2008). The front face of the structure will be the first to be loaded by the blast wave. A system for calculating the load that must be carried by the front face is proposed in TM5-1300 (U.S. Department of the Army, 1990), although it is assumed that the loaded face is inside the zone of the Mach stem whose height exceeds the overall height of the structure. This indicates that for surface bursts, the detonation point is far enough away from the structure that the blast wave front may be termed planar. The adopted formulae are summarized in Table 3.9 to generate the triangular pressure-time history as illustrated

in Figure 3.8. Table 3.10 shows the expected maximum blast pressure considering the linear relationship of positive impulse.

Table 3.9: Equations used in the calculation of blast parameters for the front wall (U.S. Department of the Army, 1990).

Equation	Notation
$P = P_s + C_D q$	P = combined incident and dynamic pressure after $t_A + t_C$ time. C_D = drag coefficient = 1 for front wall q = dynamic pressure
$t_C = \frac{4S}{(1+R)C_r}$	t_C = clearing time S = smallest of surface's height H or half width $W/2$ C_r = sound velocity in reflected medium (Karlos and Solomon, 2013) R = ratio of S/G , where G is the largest surface's height H or the half width $W/2$.
$t_{of} = \frac{2i_s}{P_{so}}$	t_{of} = fictitious time for positive phase i_s = impulse value of the positive phase of the blast wave P_{so} = peak incident overpressure
$t_{rf} = \frac{2i_r}{P_r}$	t_{rf} = fictitious duration for the reflected wave i_r = total reflected impulse P_r = peak reflected pressure

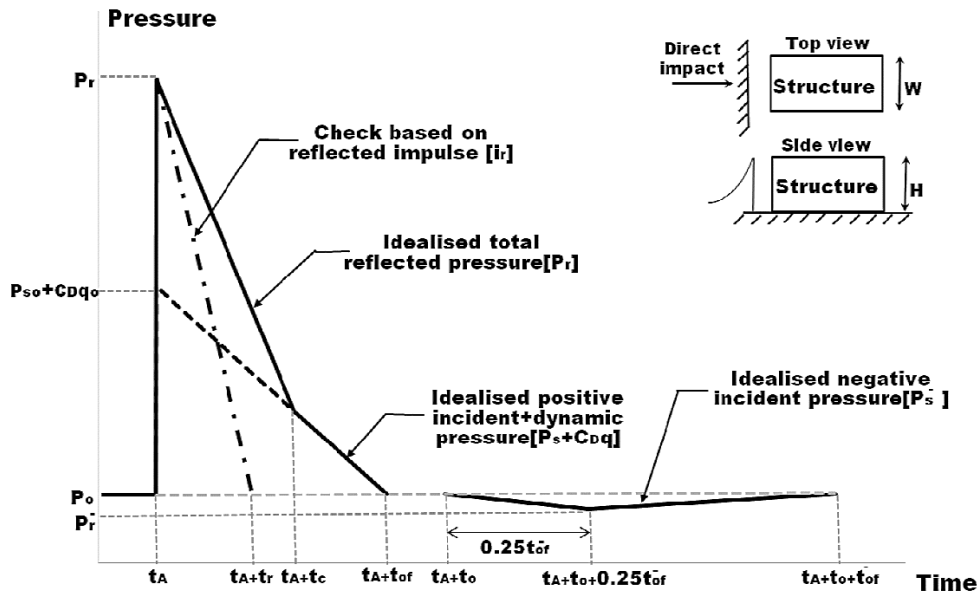


Figure 3.8: Triangular assumptions of pressure time history on the front face of the structure (Karlos and Solomon, 2013).

Table 3.10: Theoretical blast pressure and expected experimental blast pressure

Sample Designation	Idealized positive incident + dynamic pressure P₁ (kPa)	Blast duration of positive phase (theoretical) Δt₁ (sec)	Blast duration of positive phase (Experimental) Δt₂ (sec)	Expected explosion pressure (Experimental) P₂ (kPa)
B40S8	1300	0.00027	24.7	0.014211
B40S10	635	0.00036	11.7	0.019538
B40S12	365	0.00048	20	0.00876
B50S8	1780	0.00024	16.5	0.025891
B50S10	800	0.00037	16.9	0.017515
B50S12	450	0.00047	18.4	0.011495
B60S8	1850	0.00025	13.8	0.033514
B60S10	1000	0.00035	19.1	0.018325
B60S12	550	0.00046	18.3	0.013825

$$P_2 = \frac{P_1 \times \Delta t_1}{\Delta t_2} = \frac{(\text{blast pressure} \times \text{blast duration})_{\text{theoretical}}}{\text{blast duration}_{\text{experimental}}}$$

Chapter 4 MATERIALS AND TEST SETUP

4.1 Introduction

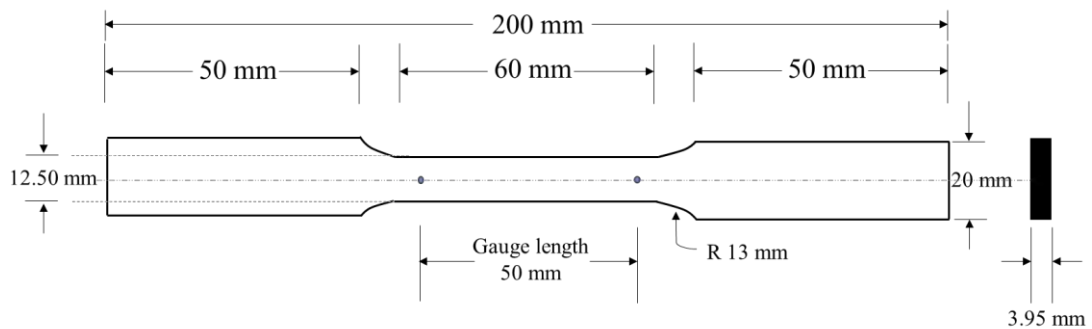
The sample boilers were prepared using mild steel pipes and sheets. Test frame was prepared with MS sheets and angles. Finally, the whole setup with boiler specimen were placed at BUET-JIDPUS for testing. A dynamic data logger along with two load cells was used for data acquisition.

4.2 Materials Used

Boiler is a pressure vessel which is generally made of steel. Therefore, mild steel pipe, Mild steel sheets and mild steel nuts were used to make a sample boiler.

4.2.1 Mild Steel Pipe

A 254 mm (10-inch) diameter MS pipe with a thickness of 3.95 mm was accumulated to construct a cylindrical boiler. For each sample, the pipe's total length was determined to be 305 mm (12 inches). A longitudinal flat tension test was performed on the MS pipe according to ASTM A370-19.



(a)



(b)

(c)

(d)

Figure 4.1: Longitudinal flat tension test (a) Dimension of MS pipe specimen, (b) specimens before testing, (c) UTM with test specimen and (d) specimens after testing.

Figure 4.1 shows the standard dimension and testing of MS pipe and Figure 4.2 illustrates the stress-strain diagram for tensile strength test of MS pipe. The average ultimate tensile strength, yield strength and elongation of MS pipe were found to be 348.05 MPa, 267.09 MPa and 17.50% respectively Table 4.1. Figure 4.3(a) shows the cutting of MS pipe with gas welding.

Table 4.1: Results of longitudinal flat tension test of MS pipe.

SL. No.	Yield strength (MPa)	Average yield strength (MPa)	Ultimate Tensile strength (MPa)	Avg. Ult. tensile strength (MPa)	% Elongation	Average % Elongation
MSP1	267.95		342.28		16	
MSP2	253.37	267.09	340.25	348.05	16	17.50
MSP3	280.51		354.43		14	
MSP4	266.53		355.24		24	

Figure 4.2: Stress-strain diagram of mild steel pipes used for sample boiler preparation.

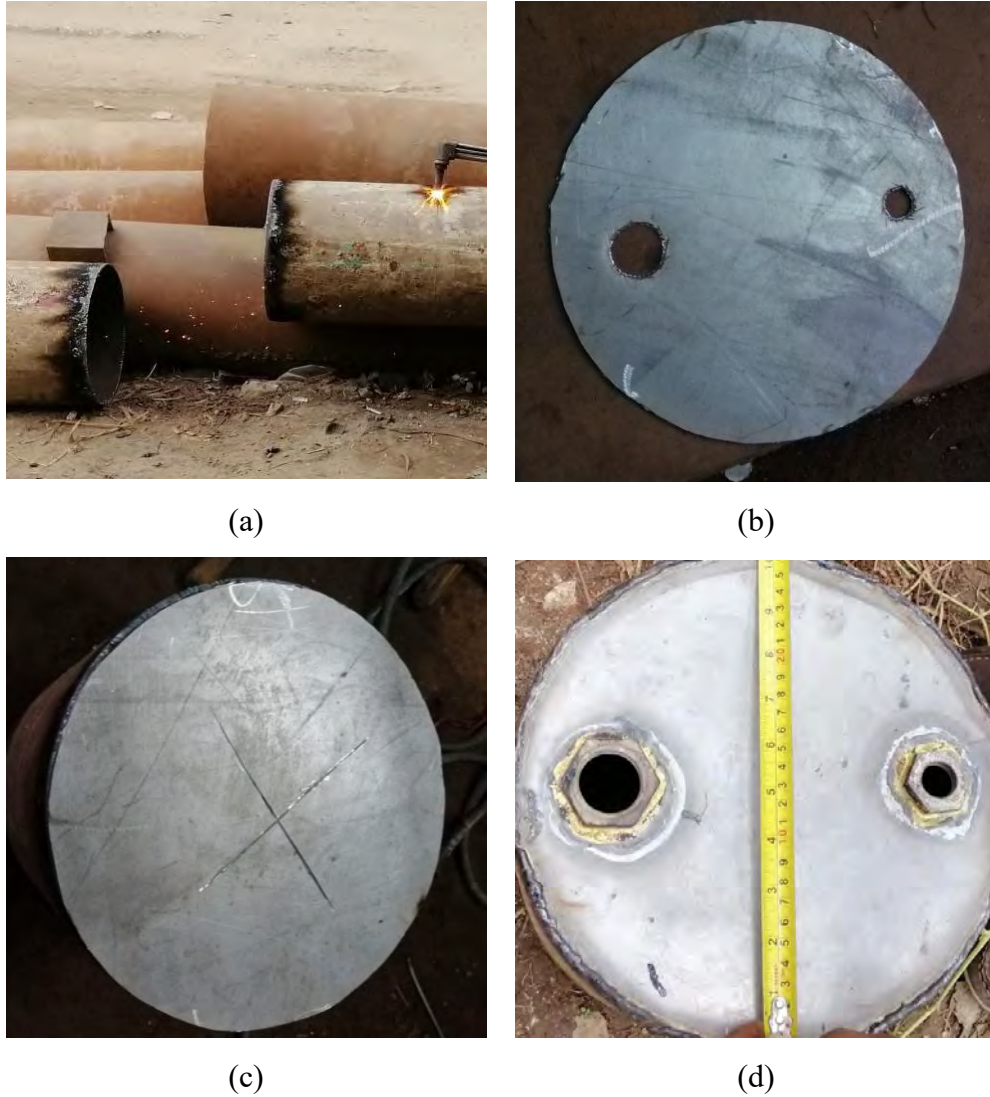


Figure 4.3: (a) Cutting of MS pipe, (b) Rear plate (MS Sheet) and (c) Front Plate (MS Sheet).

4.2.2 MS sheet for front and back side of boiler

The rear and front side plates were made from 1.80 mm (14-gauge) MS sheet. The steel sheet was initially cut into a circular shape with a diameter of 254 mm (10 inches). Two circular holes were drilled into the rear plate for the placement of heating element and thermocouple. The openings may be utilized to fill the boiler with water. To provide a predetermined failure surface, a 1 mm cross-shaped groove was carved in the front plate. The rear and front side plates are shown in Figure 4.3. A longitudinal flat tension test was performed on the MS sheet according to ASTM A370-19. Figure 4.4a shows the dimension and testing of MS sheet. The average ultimate tensile strength and elongation of MS sheet were found to be 611.84 MPa and 16.80% respectively (Table 4.2).

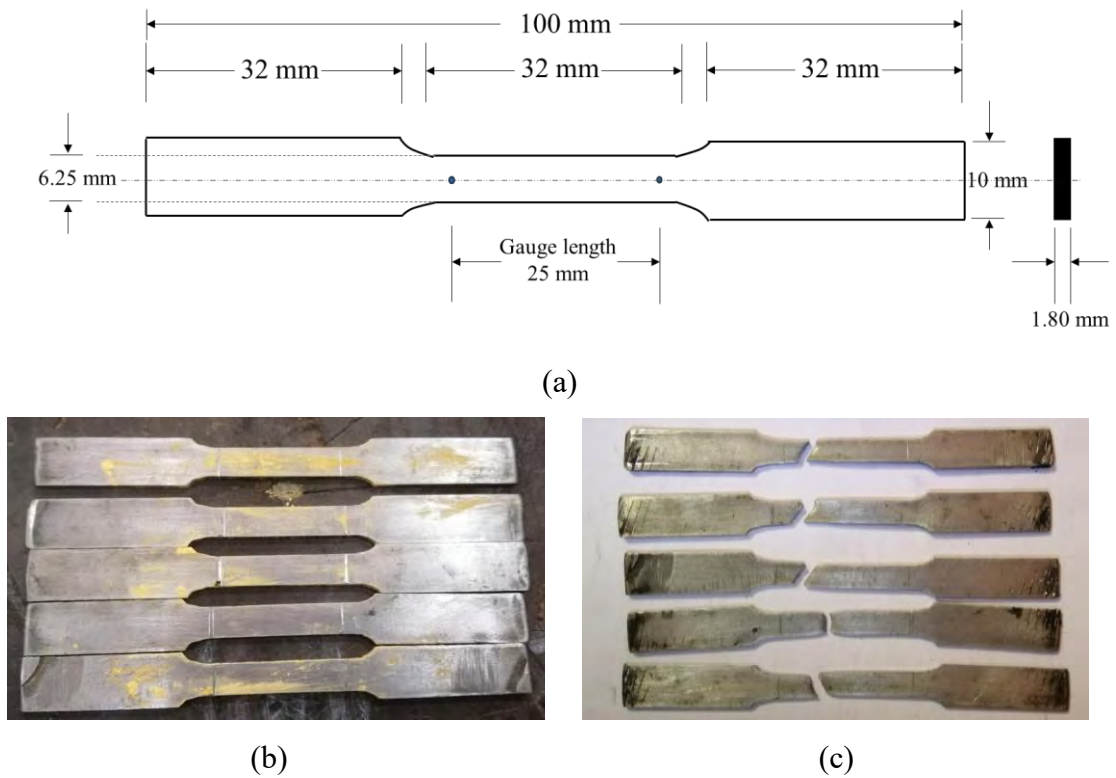


Figure 4.4: Longitudinal flat tension test (a) specimen dimension, (b) prepared specimens before testing (c) specimens after testing.

Table 4.2: Results of longitudinal flat tension test of MS sheet

SL. No.	Calibrated Ultimate Load (N)	Ult. Tensile strength (MPa)	Avg. Ult. Tensile strength (MPa)	% Elongation	Avg. % Elongation
S1	6833.10	607.39		12	
S2	7000.16	622.24		20	
S3	6833.10	607.39	611.84	16	16.80
S4	6916.630	614.812		20	
S5	6833.101	607.387		16	

4.2.3 Nuts

For threaded thermocouples and heaters, two sizes of nuts (12.7 mm and 38.1 mm diameter) were utilized. The use of a threaded thermocouple and heater has the benefit of making the boiler leakproof on the rear side plate.

4.2.4 Heating Equipment

For water heating purposes a 2000 watts electric immersion heater (tubular flange heater) was utilized and connected to the rear side plate of the sample boiler. As it has a threaded portion, it can be easily attached to the boiler using the same size nut. Thread tape was used to make the boiler leakproof at the rear face of the boiler. Figure 4.5 and Table 4.3 demonstrates the pictorial view and the details of the immersion heater.

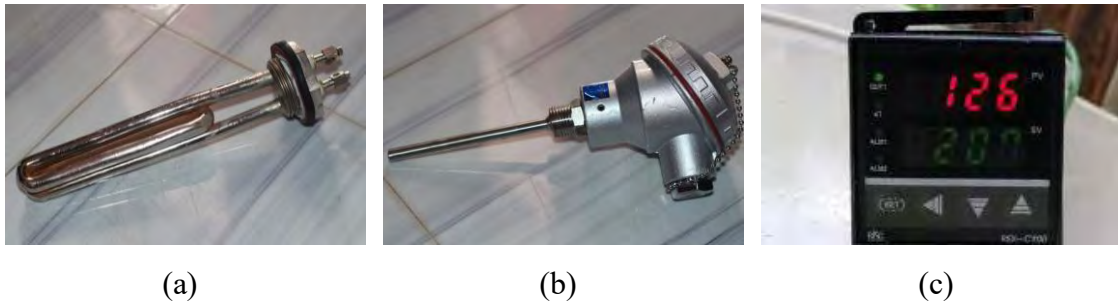


Figure 4.5: (a) Water Heater (b) Thermocouple and (c) Display unit for temperature reading.

4.2.5 Thermocouple and Digital Display

The actual steam temperature within the boiler sample was measured using a K-Type temperature sensor of 4 inches length (Table 4.3). A digital display of output range 0 to 400 °C was used for temperature reading from thermocouple. Figure 4.5 (b and c) depicts the thermocouple and digital display unit.

Table 4.3: Description of electric flange heater and thermocouple used in this study.

Electric Flange Heater		Thermocouple	
Wattage	2000 watts	Temperature range	-200°C to 1260°C
Voltage	230 Volt	Voltage	-6.4 to 9 mV
Total Length	265 mm	Probe length	101.5 mm (4 inches)
Depth of immersion	225 mm	Probe diameter	31.75 mm (1.25 inches)

4.3 Preparation of Boiler Sample

A 1.80 mm thick, 254 mm diameter cross-grooved MS steel sheet was arc welded to the front side of the MS pipe to create the cylindrical boiler sample. Arc welding was also utilized to join rear side. Gas welding was used to join nuts of two different diameters, as described in 4.2.3. The whole working process is shown the Figure 4.6 and the prepared specimens are shown in Figure 4.7.



(a) MS pipes before welding of plates



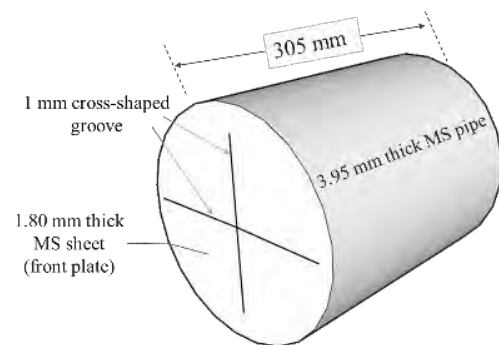
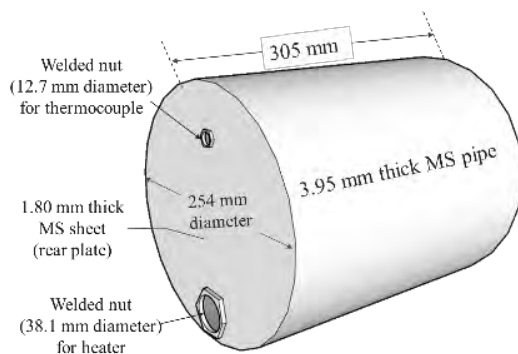
(b) Welding of front MS plate



(c) Welding of rear MS plate



(d) Welded nuts at rear plate



(e) Dimensions of the boiler specimen

Figure 4.6: Preparation process of boiler sample.



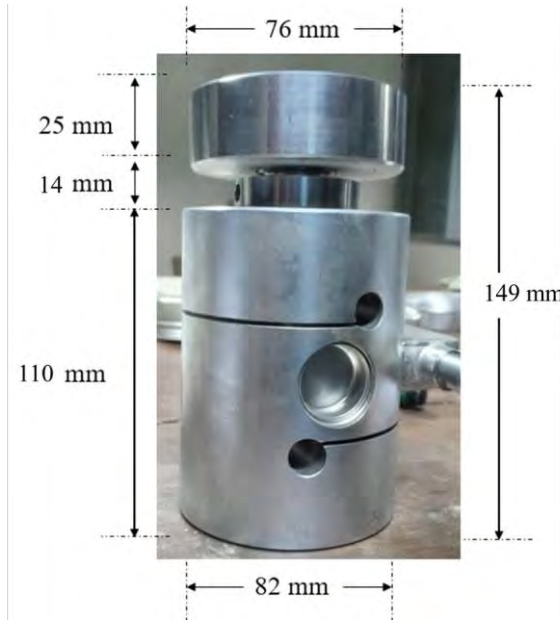
Figure 4.7: Prepared boiler specimens.

4.4 Test Setup

Before the data acquisition process, a test frame was prepared. Two load cells were attached in the frame to get the loads from boiling liquid expanding vapor explosion.

4.4.1 Load Cells

Two load cells made of stainless steel with capacities of 50 KN and 75 KN were used to determine the boiler explosion load. The load cells were calibrated at the Civil Engineering Department's SM Lab before being used. With a 2 mV/V output, these load cells can measure static and dynamic loads in compression and tension. The dimensions of the load cells are shown in Figure 4.8, along with the calibration process.



(a) Dimensions of Load Cell



(b) Calibration of Load Cell

Figure 4.8: Dimension and Calibration of Load cells.

4.4.2 Data Logger

A portable data acquisition system (Figure 4.9) is used which has 16 channels with isolation and up to 64 channels with differential inputs. With low power factors, it enables great accuracy in power calculations. The sensor calibration and correction in the software, in addition to the high precision of DEWETRON's full-isolated input amplifiers, improves measurement accuracy.

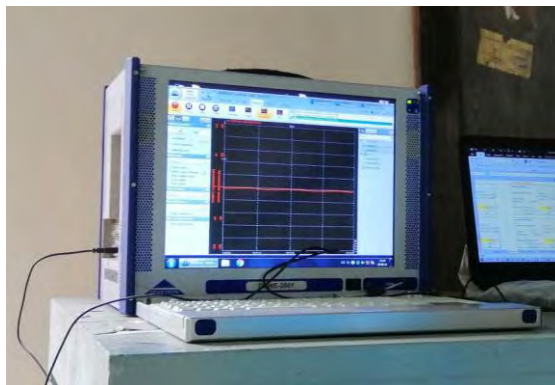


Figure 4.9: DWETRON (DEWE-2600) data logger.

4.4.3 Test Frame

Safety is a key consideration in any blast or explosion test. As a result, a test frame was designed to assure safety. The test frame was made up of three MS sheets and angles (Figure 4.10). The angles are inserted below ground level for more than half of their length. In the rear plate, two 3 cm holes with a center to center spacing of 152.5 mm (6 inches) are drilled for load cell attachment.

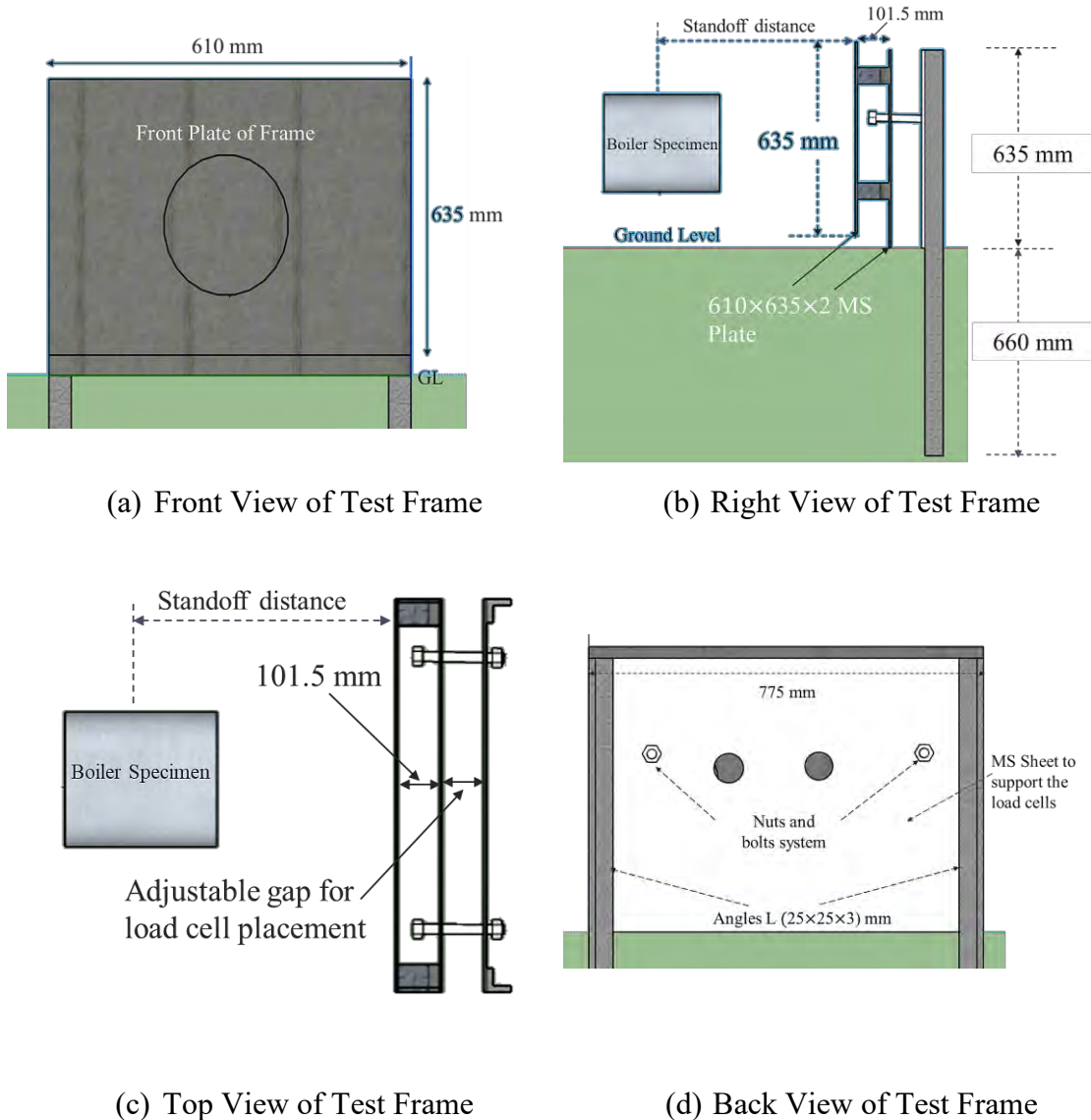


Figure 4.10: Dimensions of Test Frame.

4.5 Data acquisition

The test frame at BUET-JIDPUS was set up following the preparation of the boiler sample. The entire arrangement was set up around 10 meters away from the main building for safety reasons. The testing preparation is demonstrated prior to commencing the test (Figure 4.11).



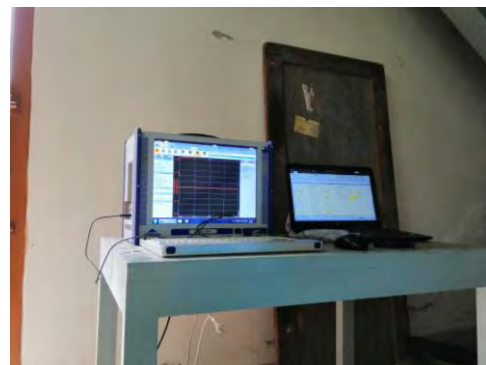
(a) Filling of water



(b) Measuring standoff distance



(c) Additional safety using polythene sheet



(d) Data acquisition room



(e) Placement of camera for recording the video



(f) Placement of temperature display unit

Figure 4.11: Preparation of setup before the commencement of the test.

The thermocouple and heater were welded to the rear portion of the boiler using two threaded bolts. Water was poured into the boiler through the openings as well. Initially, a plastic pipe was used to fill the boiler with the measured amount of water, according to the filling degree. Thread tape was used to seal the connection between the thermocouple and the water heater. The sample was then positioned half the height of the front plate and at a measured standoff distance from the front side of the test frame. Using rebar, the boiler's lateral and backward movement was also restrained. After the placement of the boiler sample, thermocouple and flange heater were connected through the wires to the display unit and the power supply line respectively.

The load cells were attached to the test frame's mid and rear plates. To maintain the stable connection between the plates, a nut-bolt mechanism was used. As a result, loads on the front plate may readily be transmitted to the mid-plate and load cells. The extra wire was then used to connect the load cells and data logger (9-pin serial cable). Temperature readings and load values from the data logger are the primary outputs of the test. Figure 4.12 demonstrated the whole set before and during the explosion.

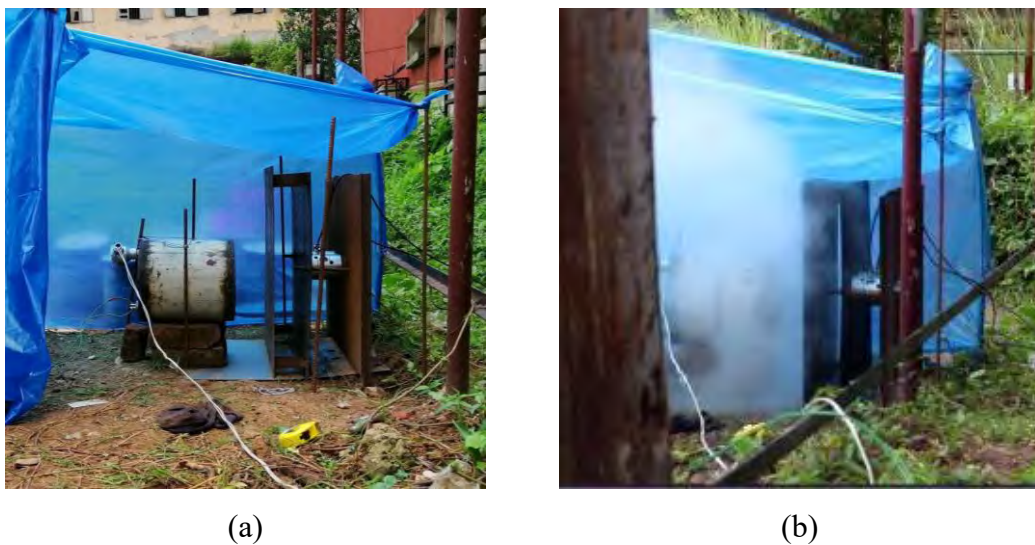


Figure 4.12: (a) Boiler sample with test frame (b) Scenario during explosion.

Chapter 5

RESULTS AND DISCUSSIONS

5.1 Introduction

The findings of theoretical predictions and destructive test data of boiler blast were compared in this chapter in terms of pressure time-history, standoff distance or scaled distance, and boiler filling degree. There are also critical analyses of the results, notable findings, and associated general comments.

5.2 Comparison of theoretical pressure time-history with the pressure time-history of sample boiler

As previously mentioned, the theoretical boiler blast pressure was calculated using the TNT equivalent weight of the explosive (water). TNT equivalent weight was found from the internal energy of the water at the specified blast temperature. The sudden rise of the theoretical positive blast pressure (Figure 5.1 - Figure 5.9) for the various filling degrees of the boiler indicates the shock wave. With certain strongly damped pressure oscillations, the peak overpressure eventually recovers to ambient pressure. Following the positive phase of the blast wave, a negative pressure wave develops. On the other hand, the actual explosion scenario depicts a gradual pressure rise to the peak positive overpressure and the negative phase occurs concurrently. As a result, prolonged blast phase and much lower positive peak overpressure are observed in experimental blast waves compared to the theoretical prediction.

For 40% filling degree (Figure 5.1 - Figure 5.3), the theoretical blast duration of the positive phase ranges between 0.27 ms to 0.48 ms. Whereas the experimental blast duration for the stated filling degree ranges from 11.7 sec to 24.7 sec. When filling degree increases to 50% (Figure 5.4 - Figure 5.6), the predicted blast duration of the positive phase ranges between 0.24 ms to 0.47 ms and the experimental blast duration is decreased. Finally, for 60% filling degree (Figure 5.7 - Figure 5.9), the predicted blast duration of the positive phase ranges between 0.25 ms to 0.46 ms. The ratio between actual blast pressure to expected blast pressure ranges from 20 to 50. So, the theoretical predictions of a boiler explosion do not reflect the actual blast scenario.

Theoretical prediction demonstrates that the positive phase duration of blast wave increases with the increase in standoff distance (Karlos and Solomon, 2013). However, for large standoff distances or scaled distances, the filling degree has minimal effect on

the duration of boiler blast. Table 5.1 shows the expected explosion pressure is significantly lower than the experimental blast pressure of the boiler. Different explosion temperatures, the non-uniform groove on the front plate of the boiler, and the failure surface are all factors that contribute to this behavior.

Table 5.1: Comparison of theoretical expected explosion pressure and actual explosion pressure of boiler blast.

Sample Designation	Idealized positive incident + dynamic pressure P_1 (kPa)	Blast duration of positive phase (theoretical) Δt_1 (sec)	Blast duration of positive phase (Experimental) Δt_2 (sec)	Expected explosion pressure (Experimental) P_2 (kPa)	Actual explosion pressure (Experimental) P_{actual} (kPa)
B40S8	1300	0.00027	24.7	0.014211	0.6142
B40S10	635	0.00036	11.7	0.019538	0.6015
B40S12	365	0.00048	20	0.00876	0.488
B50S8	1780	0.00024	16.5	0.025891	0.6681
B50S10	800	0.00037	16.9	0.017515	0.6049
B50S12	450	0.00047	18.4	0.011495	0.4907
B60S8	1850	0.00025	13.8	0.033514	0.6641
B60S10	1000	0.00035	19.1	0.018325	0.6314
B60S12	550	0.00046	18.3	0.013825	0.5036

$$P_2 = \frac{P_1 \times \Delta t_1}{\Delta t_2} = \frac{(blast\ pressure \times blast\ duration)_{theoretical}}{blast\ duration_{experimental}}$$

(a)

(b)

Figure 5.1: Pressure Time-history of B40S8 (a) Theoretical positive pressure along with reflected impulse and (b) Experimental positive and negative pressure.

ulse [ir]
amic pressure [Ps + CDol]

(a)

(b)

Figure 5.2: Pressure Time-history of B40S10 (a) Theoretical positive pressure along with reflected impulse and (b) Experimental positive and negative pressure.

ulse [ir]
amic pressure [Ps + CDol] 2.1×10^4

(a)

(b)

Figure 5.3: Pressure Time-history of B40S12 (a) Theoretical positive pressure along with reflected impulse and (b) Experimental positive and negative pressure.

ulse [ir]
amic pressure [Ps + CDol] 1.0×10⁵

(a)

(b)

Figure 5.4: Pressure Time-history of B50S8 (a) Theoretical positive pressure along with reflected impulse and (b) Experimental positive and negative pressure.

ulse [ir]
amic pressure [Ps + CDol] 5.2×10^4

(a)

(b)

Figure 5.5: Pressure Time-history of B50S10 (a) Theoretical positive pressure along with reflected impulse and (b) Experimental positive and negative pressure.

ulse [μs]
amic pressure [Pa + CDol] 3.1×10^4

(a)

(b)

Figure 5.6: Pressure Time-history of B50S12 (a) Theoretical positive pressure along with reflected impulse and (b) Experimental positive and negative pressure.

ulse [ir]
amic pressure [Ps + CDol] 1.0×10⁵

(a)

(b)

Figure 5.7: Pressure Time-history of B60S8 (a) Theoretical positive pressure along with reflected impulse and (b) Experimental positive and negative pressure.

ulse [ir]
amic pressure [Ps + CDa] 8.4×10^4

(a)

(b)

Figure 5.8: Pressure Time-history of B60S10 (a) Theoretical positive pressure along with reflected impulse and (b) Experimental positive and negative pressure.

ulse [ir]
amic pressure [Ps + CDol]

(a)

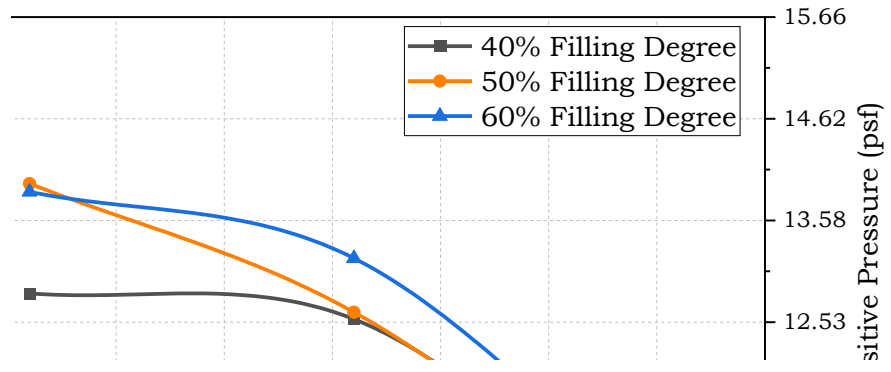
(b)

Figure 5.9: Pressure Time-history of B60S12 (a) Theoretical positive pressure along with reflected impulse and (b) Experimental positive and negative pressure.

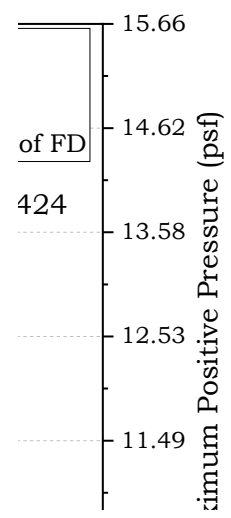
5.3 Comparison of blast over pressure for different standoff distances

The distance between the explosion center and the structure of interest is a key consideration. Blast wave velocity and peak overpressure decrease rapidly with the increase in the distances between the blast center and the destination surface (Karlos and Solomon, 2013). To determine the influence of the standoff distance on the peak overpressure of the boiler explosion, 61, 76, and 91 cm standoff distances were used for the 15.44 kg capacity of the sample boiler, which corresponds to 2.44, 3.05, and 3.66 m standoff distance for a 1 MT industrial boiler. When the standoff distance increases, the positive peak overpressure decreases significantly (Figure 5.10). Positive peak overpressure stays close to 0.6 kPa at a 40% filling degree, although it declines drastically beyond a 76 cm standoff distance. For 50% and 60% filling degrees, similar behavior is seen. Another finding is that peak overpressure stays near enough for high degrees of filling even with a modest standoff distance. The difference in peak overpressure for different filling degrees diminishes as the standoff distance rises.

Scaled distance depends on the weight of the explosive and standoff distance. The scaled distance increases with the increment of standoff distance and results in a small peak overpressure. Again, for same standoff distance, scaled distance differs when filling degree changes. Because weight of explosive is directly related to the filling degree of the steam boiler. Figure 5.10b depicts effect of scaled distance on the positive peak overpressure of the boiler blast. In a conservative sense, the maximum or peak positive overpressure ranges between 0.68 kPa to 0.49 kPa for a scaled distance of $1.255 \text{ m/kg}^{0.333}$ to $2.156 \text{ m/kg}^{0.333}$. Negative peak overpressure should follow the corresponding behavior of the positive pressure. However, the effect of standoff distance or scaled distance is not recognized correctly in the experimental observation of the negative phase (Figure 5.11). The main reason behind this the negative phase of the pressure occurred concurrently with the positive phase.



(a)



(b)

Figure 5.10: Comparison of maximum positive blast pressure with (a) standoff distance and (b) scaled distance for different filling degrees.

(a)

(b)

Figure 5.11: Comparison of maximum negative blast pressure with (a) standoff distance and (b) scaled distance for different filling degrees.

5.4 Comparison of blast over pressure for different filling degrees

The internal energy of the explosive, which is related to the initial temperature of the steam within the boiler, affects the heat of the actual explosion. If the blast temperature varies marginally, the heat of detonation of the actual explosive remains constant, while the weight of the actual explosive changes as the filling degree changes. When the filling degree increases, a small amount of positive peak overpressure increment is noticed for a constant standoff distance (Figure 5.12a). As previously discussed, the maximum positive peak overpressure drastically decreased for the greater standoff distance since the generated pressure wave became nearly plane and uniform pressure can be considered. However, the difference between the positive peak overpressures for the boiler explosion is minor for smaller standoff distances (61 cm and 76 cm). Because of the simultaneous occurrence of positive and negative pressure, an explicit relationship between the filling degree and negative peak pressure could not be established (Figure 5.12b).

(a)

(b)

Figure 5.12: Comparison of (a) positive and (b) negative peak overpressure with filling degrees for different standoff distances.

5.5 Temperature profile

The total duration of the blast test for the steam boiler is directly dependent on the filling degree and the power of the heater. An electric flange heater of 2000 watt was used in this study and the overall test duration ranges from 45 to 55 minutes for 40% filling degree of the boiler (Figure 5.13). Whereas the test duration for 50% and 60% filling degrees ranges from 35 to 50 minutes. Since the weight of the explosive is higher for high filling degrees resulting in a high-pressure increment. Thus, the internal pressure of the boiler increases within a short duration of time. Figure 5.14 demonstrates that the average initial temperature during the blast increases with the increase in filling degrees. However, the temperature incremental rate is small. Figure 5.15 demonstrates that, when the initial temperature inside the boiler increases from 389.82 K to 400.50 K, the peak positive overpressure also increases from 0.57 kPa to 0.60 kPa respectively. This increment occurs due to the high internal energy for higher temperatures. However, the peak positive overpressure drastically decreases with the increase in scaled distance.

Figure 5.13: Internal temperature of the boiler throughout the commencement of the test.

Figure 5.14: Comparison of blast temperature with different filling degrees.

Figure 5.15: Comparison of Peak positive pressure for different scaled distance and average blast temperatures

Chapter 6 CONCLUSION AND RECOMMENDATIONS

6.1 Introduction

The main objective of this research was to predict theoretical pressure on building structures subjected to boiler blast load and to determine the boiler blast pressure on structures by the destructive test of steam boiler. To achieve that objective, small-sized steam boilers were prepared from MS pipes, MS sheets and heaters.

6.2 Conclusions

Based on the experimental investigations done on prepared boiler specimens, the following conclusions can be drawn:

- i. The real explosion scenario illustrates a progressive rise in pressure to a peak positive overpressure, followed by a negative phase. As a result, experimental blast waves show a longer blast phase and substantially lower positive peak overpressure than theoretical predictions.
- ii. The explosion duration was theoretically predicted to be between 0.24 and 0.48 milliseconds. On the other hand, the experimental blast duration ranges from 11.7 to 24.7 seconds. Therefore, theoretical boiler explosion predictions differ from the actual blast scenario. The non-uniform groove on the front plate of the boiler, as well as the failure surface, all contribute to this behavior.
- iii. The positive peak overpressure drops rapidly as the standoff distance rises. At a 40% filling degree, positive peak overpressure remains close to 0.6 kPa, but it drops precipitously beyond a 76 cm standoff distance. The behavior is comparable with 50% and 60% filling degrees. Moreover, even with a small standoff distance, peak overpressure remains close enough for high degrees of filling. The difference in peak overpressure for various filling degrees reduces when the standoff distance increases. In a conservative sense, the maximum or peak positive overpressure ranges between 0.68 kPa to 0.49 kPa for a scaled distance of 1.255 m/kg^{0.333} to 2.156 m/kg^{0.333}.
- iv. If the blast temperature fluctuates slightly, the actual explosive's heat of detonation remains constant. However, the weight of the actual explosive changes as the filling degree changes. For a constant standoff distance, a small amount of positive peak overpressure increment is detected as the filling degree increases.

For short standoff distances (61 cm and 76 cm), the difference between the positive peak overpressures for the boiler explosion is negligible. An explicit connection between the filling degree and negative peak pressure could not be established due to the simultaneous occurrence of positive and negative pressure.

- v. The internal pressure of the boiler increases within a short duration of time due to the high-pressure increment for higher filling degrees. When the initial temperature inside the boiler increases from 389.82 K to 400.50 K, the peak positive overpressure also increases from 0.57 kPa to 0.60 kPa respectively. This increment occurs due to the high internal energy for higher temperatures.

6.3 Recommendations for Future Study

Experimental investigations conducted in this research indicate that the actual boiler explosion scenario differs from the theoretical prediction of blast pressure. Based on the findings of the present research work, the following recommendations are made for future studies:

- i. This study was conducted for small-sized steam boilers containing nonflammable fluids (water). However, a large-scale boiler blast test containing various flammable and non-flammable fluids may be performed for a more satisfactory understanding of the blast pressure.
- ii. The degree of filling of the boiler has minimal effect on the blast pressure. On the other hand, standoff distance has a remarkable influence on boiler blast pressure. As a result, to gain a better insight into boiler blast pressure, the test may be conducted for filling degrees ranging from 20% to 80% and a broad range of standoff distance.
- iii. The initial temperature at the time of the blast was found much lower compared to the critical temperature of the water which mainly depends on the internal pressure of the boiler, how the boiler is heated, the influence of welding, condition of the boiler and the strength of the boiler material. Most of the boiler blast pressure is absorbed during the breaking of the boiler (ductile failure) and only a fraction of the mechanical energy is released. So, further investigation is needed to determine the percentage of released energy.

REFERENCES

- Agarwal, S., and Suhane, A. (2017). Study of Boiler Maintenance for Enhanced Reliability of System A Review. *Materials Today: Proceedings*, 4(2), 1542–1549. <https://doi.org/10.1016/j.matpr.2017.01.177>
- Akter, S. (2019). *Response of RC Beam and Column Subjected To Blast Loading*. Bangladesh University of Engineering and Technology.
- ASTM A370-19. (2019). Standard Test Methods and Definitions for Mechanical Testing of Steel Products. *ASTM International*, West Conshohocken, PA, USA., 1–50. <https://doi.org/10.1520/A0370-19E01>
- Baker, W. E. (1973). *Explosions in Air*. University of Texas Press.
- Birajdar, S. S., and Jawalkar, G. C. (2017). Analysis of Blast Loading on Structural Components. *International Journal of Scientific Engineering and Research (IJSER) ISSN (Online): 2347-3878*, 5(48096), 7–12.
- Birk, A. M., Davison, C., and Cunningham, M. (2007). Blast overpressures from medium scale BLEVE tests. *Journal of Loss Prevention in the Process Industries*, 20(3), 194–206. <https://doi.org/10.1016/j.jlp.2007.03.001>
- Birk, A. M., and VanderSteen, J. D. J. (2006). On the transition from non-BLEVE to BLEVE failure for a 1.8 M3 propane tank. *Journal of Pressure Vessel Technology, Transactions of the ASME*, 128(4), 648–655. <https://doi.org/10.1115/1.2349579>
- Brode, H. L. (1955). Numerical solutions of spherical blast waves. *Journal of Applied Physics*, 26(6), 766–775. <https://doi.org/10.1063/1.1722085>
- Center for Chemical Process Safety. (2010). *Guidelines for Vapor Cloud Explosion, Pressure Vessel Burst, BLEVE and Flash Fire Hazards*. American Institute of Chemical Engineers, New York. <https://www.aiche.org/resources/publications/books/guidelines-vapor-cloud-explosion-pressure-vessel-burst-bleve-and-flash-fire-hazards-2nd-edition>
- Crowl, D. A. (1991). Using Thermodynamic Availability to Determine the Energy of Explosion. *Plant/Operations Progress*, 10(3), 136–142. <https://doi.org/10.1002/prsb.720100306>
- Crowl, D. A. (1992a). Calculating the energy of explosion using thermodynamic availability. *Journal of Loss Prevention in the Process Industries*, 5(2), 109–118. [https://doi.org/10.1016/0950-4230\(92\)80007-U](https://doi.org/10.1016/0950-4230(92)80007-U)
- Crowl, D. A. (1992b). Using Thermodynamic Availability to Determine the Energy of Explosion for Compressed Gases. *Plant/Operations Progress*, 11(2), 47–49. <https://doi.org/10.1002/prsb.720110206>
- Fang, Q., Zhe, Z., and Qingmin, S. (2013). Application of phast in the quantitative consequence analysis for the boiler BLEVE. *Proceedings of the 2013 3rd International Conference on Intelligent System Design and Engineering Applications, ISDEA 2013*, 369–372. <https://doi.org/10.1109/ISDEA.2012.92>

- FEMA 426. (2011). *Reference Manual to Mitigate Potential Terrorist Attacks Against Buildings* (2nd ed., Issue October). Homeland Security Science and Technology. <https://www.dhs.gov/xlibrary/assets/st/st-bips-06.pdf>
- Hemmatian, B., Casal, J., and Planas, E. (2017). A new procedure to estimate BLEVE overpressure. *Process Safety and Environmental Protection*, *111*, 320–325. <https://doi.org/10.1016/j.psep.2017.07.016>
- Hemmatian, B., Planas, E., and Casal, J. (2017). Comparative analysis of BLEVE mechanical energy and overpressure modelling. *Process Safety and Environmental Protection*, *106*, 138–149. <https://doi.org/10.1016/j.psep.2017.01.007>
- Hossan, M. Z., Islam, S., Khan, M. F., Shammi, S., and Amin, M. A. (2019). Boiler explosion in Bangladesh: Causes, consequences and precautions. *ACM International Conference Proceeding Series*, 297–301. <https://doi.org/10.1145/3335550.3335592>
- Ibrahim, M. F., El-Arabaty, H. A., and Moharram, I. S. (2019). Effect of steam boiler explosion on boiler room and adjacent buildings structure. *International Journal of Engineering Science Invention (IJESI)*, *8*(02), 17–37.
- Islam, M. S. (2021). Ready-made garments exports earning and its contribution to economic growth in Bangladesh. *GeoJournal*, *86*(3), 1301–1309. <https://doi.org/10.1007/s10708-019-10131-0>
- Johnson, D. M., Pritchard, J. M., and Wickens, M. J. (1991). *Large scale experimental study of Boiling Liquid expanding Vapour Explosions (BLEVEs)*. British Gas plc, Research and Technology Division.
- Karlos, V., and Solomon, G. (2013). Calculation of Blast Loads for Applications to Structural Components. *Publications Office of the European Union (JRC Technical Reports)*, 1–58. <https://doi.org/10.2788/61866>
- Kim, T., Lee, D., Ko, H., and Cho, S. (2006). *Design of Blast-Resistant Buildings in Petrochemical Facilities* (2nd ed.). Task Committee on Blast-Resistant Design of the Petrochemical Committee of the Energy Division of the American Society of Civil Engineers.
- Kingery, C. N., and Bulmash, G. (1984). *Technical report ARBRL-TR-02555: Air blast parameters from TNT spherical air burst and hemispherical surface burst*. AD-B082 713, US Army Ballistic Research Laboratory, Aberdeen Proving Ground, MD.
- Kinney, G. F., and Graham, K. J. (1985). *Explosive Shocks in Air* (2nd ed.). Springer-Verlag Berlin Heidelberg. <https://doi.org/10.1007/978-3-642-86682-1>
- Kumar, K., Patel, D., Sehravat, V., and Gupta, T. (2013). Performance and Exergy Analysis of the Boiler. *International Journal of Science and Research (IJSR)*, *14*(6), 2319–7064.
- Laboureur, D., Heymes, F., Lapebie, E., Buchlin, J. M., and Rambaud, P. (2014). BLEVE Overpressure: Multiscale Comparison of Blast Wave Modeling. *Process Safety Progress*, *33*(3), 274–284. <https://doi.org/10.1002/prs.11626>

- Mays, G. C., and Smith, P. D. (1995). *Blast Effects on Buildings: Design of Buildings to Optimize Resistance to Blast Loading*. Thomas Telford Publications.
- Meyers, M. A. (1994). *Dynamic Behavior of Materials*. John Wiley and Sons, Inc. <https://doi.org/10.1002/9780470172278>
- Mills, C. A. (1987). The design of concrete structures to resist explosions and weapon effects. *Proceedings of the 1st Int. Conference on Concrete for Hazard Protections*.
- Newmark, N. M., and Hansen, R. J. (1961). Design of blast resistant structures. In Harris and Crede (Ed.), *Shock and Vibration Handbook* (3rd ed.). McGraw-Hill.
- Ogle, R. A., Ramirez, J. C., and Smyth, S. A. (2012). Calculating the explosion energy of a boiling liquid expanding vapor explosion using exergy analysis. *American Institute of Chemical Engineers*, 31(1), 51–54. <https://doi.org/10.1002/prs.10465>
- Planas-Cuchi, E., Salla, J. M., and Casal, J. (2004). Calculating overpressure from BLEVE explosions. *Journal of Loss Prevention in the Process Industries*, 17(6), 431–436. <https://doi.org/10.1016/j.jlp.2004.08.002>
- Prugh, R. W. (1991). Quantitative evaluation of “BLEVE” hazards. *Journal of Fire Protection Engineering*, 3(1), 9–24. <https://doi.org/10.1177/104239159100300102>
- Ramirez, J. C., Ph, D., Smyth, S. A., Ph, D., Rd, W., Ogle, R. A., and Ph, D. (2011). TOWARDS AN EXERGY-BASED EXPLOSION ENERGY MODEL FOR BOILING- LIQUID EXPANDING-VAPOR EXPLOSIONS. *Proceedings of the ASME 2011 International Mechanical Engineering Congress and Exposition*, 1–6.
- Roper, and Stephen. (1899). *Roper’s Engineer’s Handy Book* (15th ed.). Philadelphia: David McKay.
- Shaluf, I. M. (2007). An overview on BLEVE. *Disaster Prevention and Management: An International Journal*, 16(5), 740–754. <https://doi.org/http://dx.doi.org/10.1108/09653560710837037>
- Švejar, J., Klakurková, L., and Skála, Z. (2017). Analysis of the causes of boiler explosion. *Materials Science Forum*, 891 MSF(April), 263–268. <https://doi.org/10.4028/www.scientific.net/MSF.891.263>
- U.S. Department of the Army. (1990). *Structures to Resist the Effects of Accidental Explosions*.
- Unified Facilities Criteria. (2008). Structures to Resist the Effects of the Accidental Explosions. In *UFC 3-340-02 Structures to Resist the Effects of Accidental Explosions*. U.S. Army Corps of Engineers, Naval Facilities Engineering Command, Air Force Civil Engineer Support Agency.
- Yandzio, E., and Gough, M. (1999). *Protection of Buildings Against Explosions*. Steel Construction Institute, Ascot. <https://www.worldcat.org/title/protection-of-buildings-against-explosions/oclc/47874123>

Appendix A

A.1 Blast Wave Parameters

Table A.1 presents the blast wave parameters that are needed to plot the theoretical pressure-time history diagram. Scaled distance should be calculated before determining these parameters.

Table A.1: Description of the blast wave parameters

P_{so}	Peak positive incident pressure, kPa	$t_o/W^{1/3}$	Scaled duration of positive phase, ms/kg ^{1/3}
P_{so}^-	Peak negative pressure, kPa	$t_o^-/W^{1/3}$	Scaled duration of negative phase, ms/kg ^{1/3}
P_r	Peak positive normal reflected pressure, kPa	$L_w/ W^{1/3}$	Scaled wavelength of positive phase, m/kg ^{1/3}
$i_s/ W^{1/3}$	Scaled unit positive incident impulse, kPa-ms/kg ^{1/3}	$L_w^-/ W^{1/3}$	Scaled wavelength of negative phase, m/kg ^{1/3}
$i_r/ W^{1/3}$	Scaled unit positive reflected impulse, kPa-ms/kg ^{1/3}	U	Shock front velocity, m/ms
$i_r^-/ W^{1/3}$	Scaled unit negative reflected impulse, kPa-ms/kg ^{1/3}	u	Particle velocity, m/ms
$t_A/ W^{1/3}$	Scaled time of arrival of blast wave, ms/kg ^{1/3}	W	Charge weight, kg
R_h	Standoff distance, m	Z	Scaled distance, m/kg ^{1/3}

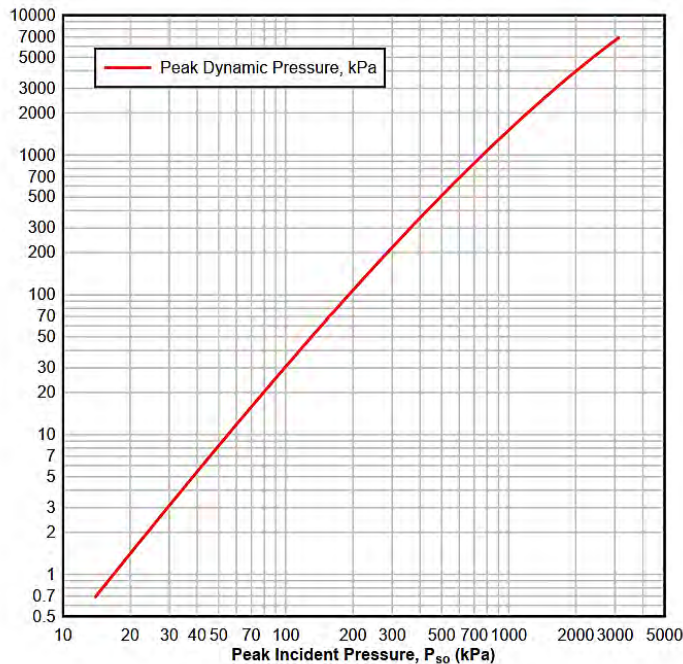


Figure A.1: Variation of peak dynamic pressure q_o vs P_{so} (Karlos and Solomon, 2013; Unified Facilities Criteria, 2008).

Figure A.1 depicts the variance of peak dynamic pressure as a function of peak incident pressure. Figure A.2 and Figure A.3 display graphs for the calculation of the positive blast parameters for spherical and semispherical blast waves. Whereas Figure A.5 can be used to calculate the negative blast wave parameters. Sound velocity of reflected overpressure can be easily found in Figure A.4.

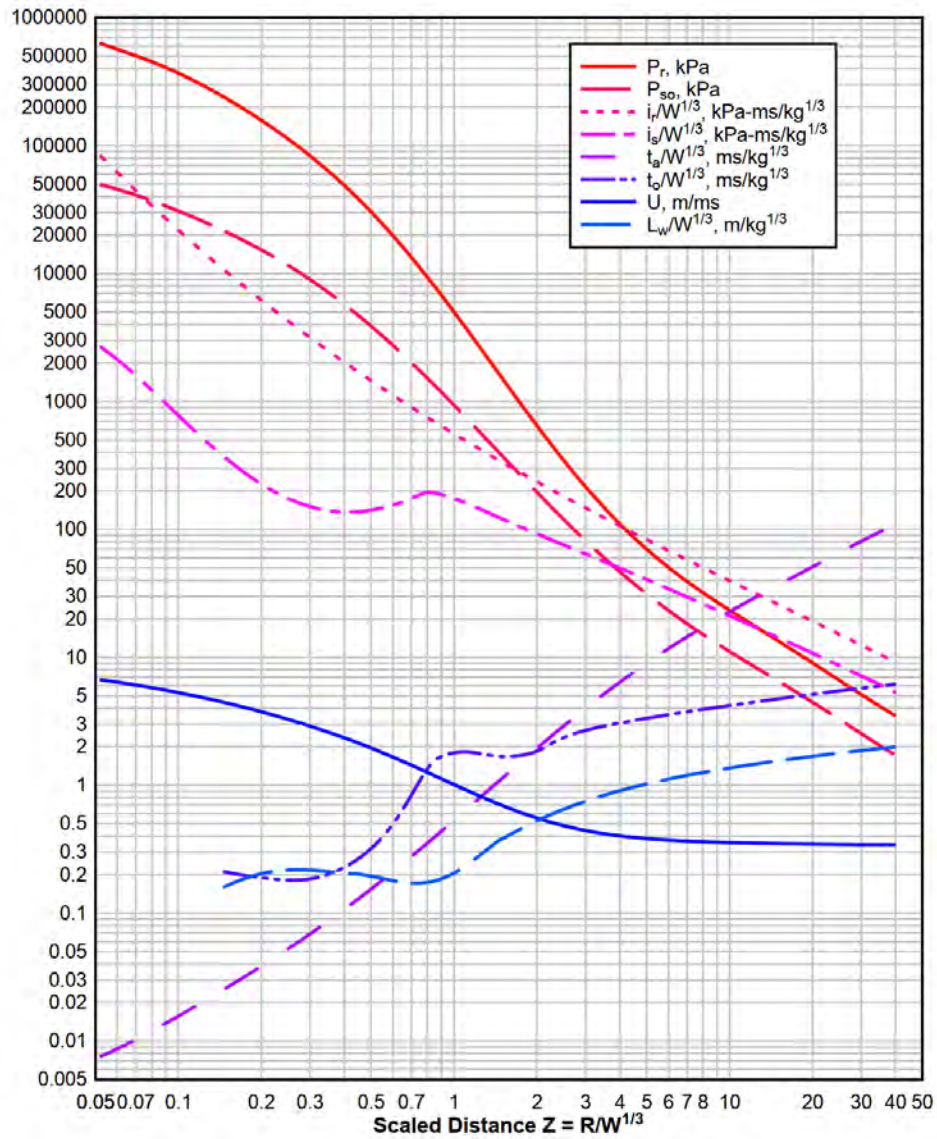


Figure A.2: Parameters of positive phase of shock spherical wave of TNT charges from free-air bursts (Karlos and Solomon, 2013; Unified Facilities Criteria, 2008).

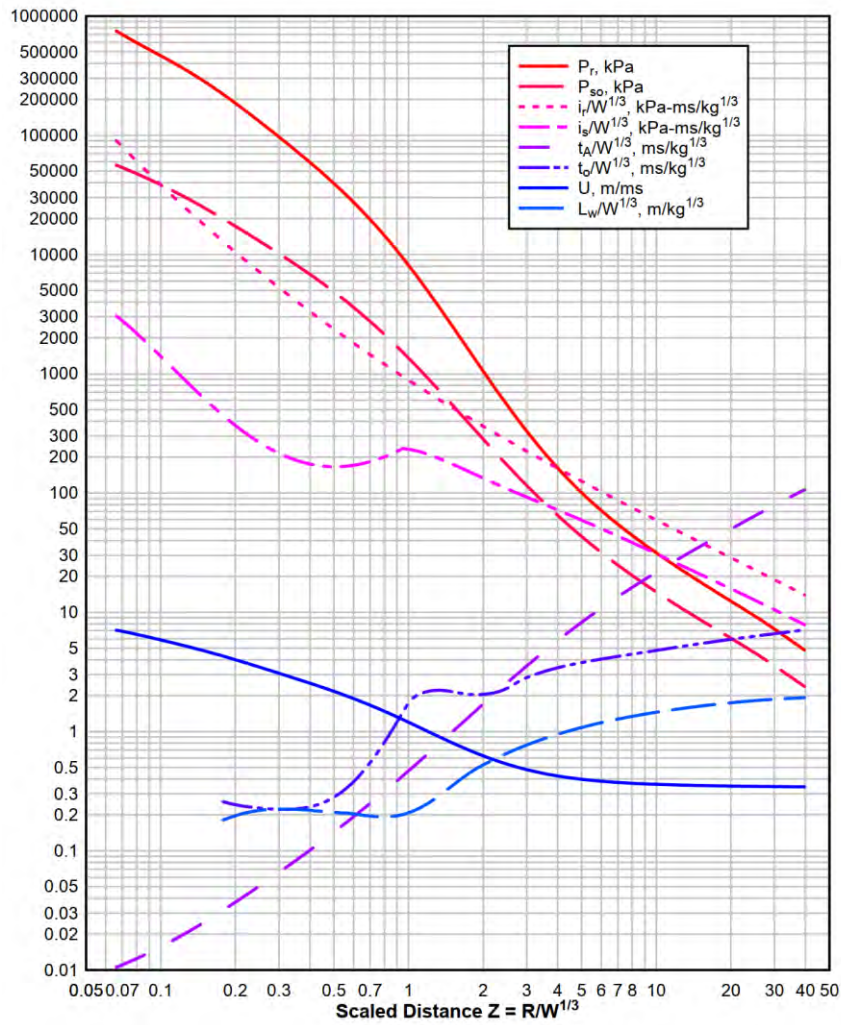


Figure A.3: Parameters of positive phase of shock hemispherical wave of TNT charges from surface bursts (Karlos and Solomon, 2013; Unified Facilities Criteria, 2008).

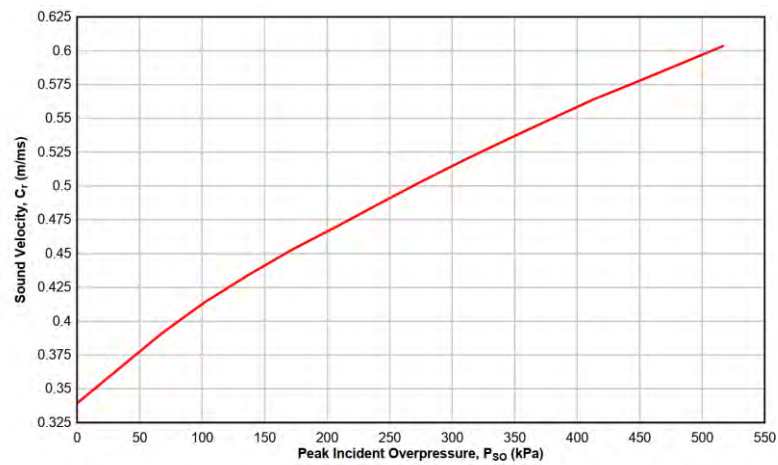
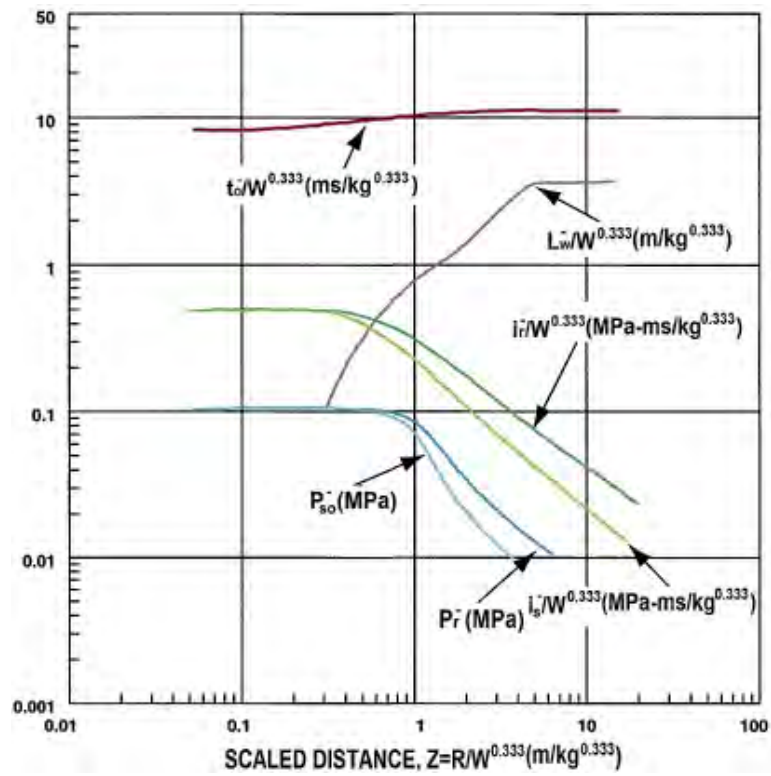
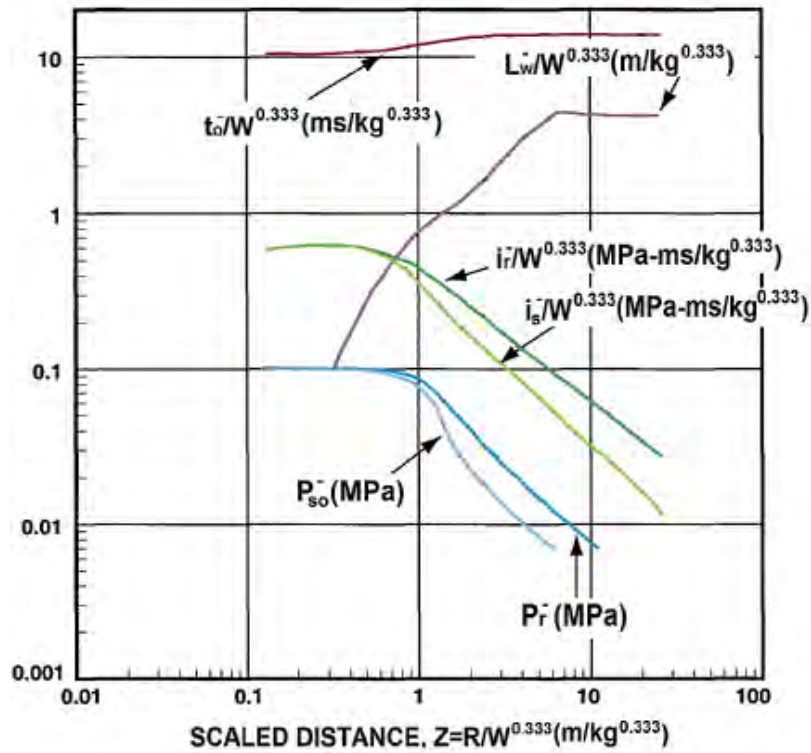


Figure A.4: Sound velocity in reflected overpressure region (Karlos and Solomon, 2013; Unified Facilities Criteria, 2008).



(a)



(b)

Figure A.5: Parameters of negative phase of shock wave of TNT charges, (a) from spherical free air bursts and (b) from semispherical surface bursts (Karlos and Solomon, 2013; Unified Facilities Criteria, 2008).

A.2 Calculation of Heat of detonation of the actual explosive

As from preliminary test samples showed the initial temperature inside the boiler at the time of blast ranges between 120 °C to 135°C. The average internal energy during the blast was taken as 0.049 MJ/kg. For Boiler sample B60S10 the internal energy calculation using exergy analysis and scaled distance from equivalent TNT weight are tabulated (Table A.2 and Table A.3) below-

Table A.2: Calculation of released energy using exergy analysis (*Ogle et al., 2012*)

Description	Values
U_o : Internal Energy at final state (KJ kg ⁻¹)	142.44
v_o : Specific Volume at final state (m ³ kg ⁻¹)	0.0010057
P_o : Absolute Pressure at final state (kPa)	104.385
T_o : Absolute Temperature at final state (K)	307
S_o : Entropy at final state (KJ/K Kg)	0.49155
U : Overall internal energy of the system at initial state (KJ kg ⁻¹)	550.35
v : Specific Volume at initial state (m ³ /kg)	0.0010707
S : Entropy at initial state (KJ/K Kg)	1.6452

$$\begin{aligned} \text{The released energy/ batch energy, } E &= (U - U_o) + P_o(v - v_o) - T_o(S - S_o) \\ &= (550.35-142.44)+104.385 \times (0.0010707-0.0010057)-307 \times (1.6452-0.49155) \\ &= 54 \text{ KJ/kg} \end{aligned}$$

So, the heat of detonation of the actual explosive (water), $H_{exp} = E = 0.054 \text{ MJ/kg}$

Table A.3: Calculation of scaled distance from standoff distance and equivalent TNT charge weight.

Description	Values
Capacity of the sample boiler (kg or Liter)	15.44
Filling degree (%)	60
W_{exp} : Weight of the explosive (Kg)	$0.60 \times 15.44 = 9.27$
R_h : Standoff distance (m)	0.76
W : TNT equivalent Change (Kg)	$W = W_{exp} \frac{H_{exp}}{H_{TNT}} = 9.27 \frac{0.054}{4.50} = 0.112$
Z : Scaled distance (m/kg ^{0.333})	$\frac{R_h}{\sqrt[3]{W}} = \frac{0.76}{\sqrt[3]{0.112}} = 1.58$

A.3 Calculation of Peak Incident Overpressure (P_{so})

Various formula for the calculation of the peak incident overpressure is discussed in the section 3.7.2. Table A.4 shows the calculated value of the peak incident overpressure using the formula and from Figure A.3.

Table A.4: Calculation of peak incident overpressure from different formulae.

Reference	P_{so} (kPa)
Kinney and Graham (1985)	365.43
Brode (1955)	270.40
Newmark and Hansen (1961)	324.83
Mills (1987)	480.43
Graph (Karlos and Solomon, 2013)	500

A.4 Theoretical Calculation of Blast Parameters

Table A.5 below shows how to calculate the blast parameters for $z = 1.58 \text{ m/kg}^{1/3}$. Multiplication by $W^{1/3}$ has been used to produce absolute values where necessary.

Table A.5: Blast wave parameters for positive phase of the explosion (Figure A.3).

Front face	Positive incident impulse, i_s	Reflected pressure, P_r [kPa]	Positive reflected impulse, i_r	Arrival time, t_A	Positive duration, t_o	Shock wave speed, U [m/ms]	Wave length, L_w
Diagram read scaled values	180	3000	500	1	2.10	0.80	0.38
Absolute values	87.10	3000	241.80	0.5	1.10	0.80	0.20

Velocity of sound, Figure A.4: $C_r = 0.58 \text{ m/ms}$

$$\text{Clearing Time: } t_c = \frac{4S}{(1+R)C_r} = \frac{4 \times 0.30487}{(1+0.5) \times 0.58} = 1.41 \text{ ms}$$

$$\text{Fictitious time for positive phase: } t_{of} = \frac{2i_s}{P_{so}} = \frac{2 \times 87.10}{500} = 0.35 \text{ ms}$$

$$\text{Fictitious duration for the reflected wave, } t_{rf} = \frac{2i_r}{P_r} = \frac{2 \times 241.80}{3000} = 0.17 \text{ ms}$$

Peak dynamic pressure, (Figure A.1): $q_o = 500 \text{ kPa}$

Drag coefficient for front wall: $C_D = 1$

$$\text{Combined incident and dynamic pressure: } P_{so} + C_D q_o = 500 + 1 \times 500 = 1000 \text{ kPa}$$

If the whole response of the structure to blast loading is required, the negative phase parameters of the blast load should also be evaluated. The schematics in Figure A.5 (b) are utilized, and the values of the parameters are presented in the following table.

Table A.6: Blast wave parameters for negative phase of the explosion.

Front face	Incident negative pressure, P_{so}^- [kPa]	Negative incident impulse, i_s^-	Reflected pressure, P_r^- [kPa]	Negative reflected impulse, i_r^-	Negative duration, t_o^-	Negative wave length, L_w^-
Diagram read scaled values	35	0.21	58	0.31	14.50	1.15
Absolute values	35	200	58	200	7.10	0.6

$$\text{Fictitious time for negative phase: } t_{of}^- = \frac{2i_s^-}{P_{so}^-} = \frac{2 \times 200}{35} = 11.43 \text{ ms}$$

$$\text{Fictitious duration for the negative reflected wave, } t_{rf}^- = \frac{2i_r^-}{P_r^-} = \frac{2 \times 200}{58} = 6.9 \text{ ms}$$

Finally, the theoretical predicted time history graph for B6010 is shown in Figure A.6

Figure A.6: Theoretical predicted time history graph for B6010.

Appendix B

B.1 Calibration of load cell

Load cells along with the dynamic data logger was calibrated (Figure 4.8) using universal test machine and a calibrated load cell. Figure B.1 shows the calibrated graphs for both load cells.

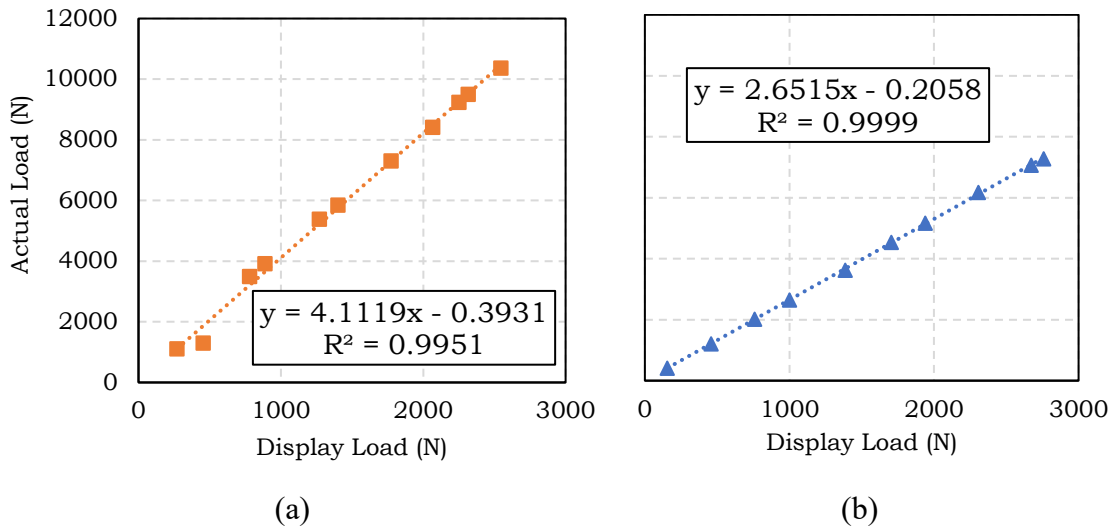


Figure B.1: Calibration graph for (a) load cell of 75 KN capacity and (b) load cell of 50 KN capacity

B.2 Test Data

Test data found from the two load cells were calibrated using the calibration equation and average blast pressure was calculated using the average load and area ($4 \text{ ft}^2 = 371612.16 \text{ mm}^2$) of the front plate of the test frame. Table B.1 summarizes the test results and the estimation of blast pressure for the boiler sample B60S10. The completed pressure time-history graphs are shown in Figure B.2.

Table B.1: Test data from data logger for sample specimen B60S10.

Time (s)	Data from load cell 1	Data from load cell 2	Calibrated Load of load cell 1 (N)	Calibrated Load of load cell 2 (N)	Average Load (N)	Average pressure (kPa)
0	0.3415	0.2335	1.0041	0.4192	0.7117	0.0019
0.1	-0.0618	-0.3438	-0.6541	-1.1115	-0.8828	-0.0024
0.2	-0.5015	-0.9732	-2.4620	-2.7803	-2.6212	-0.0071
0.3	-0.8877	-1.5260	-4.0502	-4.2463	-4.1482	-0.0112

Time (s)	Data from load cell 1	Data from load cell 2	Calibrated Load of load cell 1 (N)	Calibrated Load of load cell 2 (N)	Average Load (N)	Average pressure (kPa)
0.4	-1.1007	-1.8309	-4.9258	-5.0546	-4.9902	-0.0134
0.5	-1.4718	-2.3622	-6.4519	-6.4632	-6.4575	-0.0174
0.6	-1.8937	-2.9662	-8.1869	-8.0648	-8.1259	-0.0219
0.7	-2.3245	-3.5828	-9.9582	-9.6999	-9.8291	-0.0264
0.8	-2.3461	-3.6137	-10.0468	-9.7816	-9.9142	-0.0267
0.9	-2.4005	-3.6917	-10.2708	-9.9884	-10.1296	-0.0273
1	-2.1967	-3.3999	-9.4327	-9.2148	-9.3237	-0.0251
1.1	-2.0711	-3.2201	-8.9163	-8.7381	-8.8272	-0.0238
1.2	-2.0402	-3.1758	-8.7891	-8.6207	-8.7049	-0.0234
1.3	-2.4925	-3.8233	-10.6491	-10.3376	-10.4933	-0.0282
1.4	-2.4880	-3.8169	-10.6306	-10.3205	-10.4755	-0.0282
1.5	-2.3813	-3.6642	-10.1919	-9.9156	-10.0537	-0.0271
1.6	-2.1277	-3.3011	-9.1488	-8.9527	-9.0508	-0.0244
1.7	-1.8497	-2.9031	-8.0056	-7.8975	-7.9515	-0.0214
1.8	-1.8041	-2.8379	-7.8184	-7.7247	-7.7716	-0.0209
1.9	-1.5807	-2.5181	-6.8999	-6.8768	-6.8883	-0.0185
2	-1.4953	-2.3957	-6.5483	-6.5523	-6.5503	-0.0176
2.1	-1.3920	-2.2480	-6.1240	-6.1606	-6.1423	-0.0165
2.2	-1.1569	-1.9114	-5.1570	-5.2680	-5.2125	-0.0140
2.3	-1.0538	-1.7638	-4.7330	-4.8766	-4.8048	-0.0129
2.4	-1.1033	-1.8347	-4.9368	-5.0647	-5.0007	-0.0135
2.5	-0.9491	-1.6139	-4.3024	-4.4792	-4.3908	-0.0118
2.6	-0.8998	-1.5433	-4.0997	-4.2920	-4.1959	-0.0113
2.7	-0.6486	-1.1838	-3.0670	-3.3388	-3.2029	-0.0086
2.8	-0.5149	-0.9923	-2.5171	-2.8312	-2.6742	-0.0072
2.9	-0.3738	-0.7904	-1.9370	-2.2957	-2.1163	-0.0057
3	-0.2603	-0.6279	-1.4704	-1.8649	-1.6676	-0.0045
3.1	-0.3913	-0.8154	-2.0089	-2.3620	-2.1854	-0.0059
3.2	-0.0899	-0.3840	-0.7698	-1.2183	-0.9941	-0.0027
3.3	-0.0021	-0.2584	-0.4088	-0.8850	-0.6469	-0.0017
3.4	-0.0606	-0.3421	-0.6493	-1.1070	-0.8782	-0.0024
3.5	0.2007	0.0319	0.4251	-0.1153	0.1549	0.0004
3.6	0.3769	0.2842	1.1497	0.5536	0.8516	0.0023
3.7	0.8529	0.9657	3.1072	2.3605	2.7338	0.0074
3.8	1.3471	1.6730	5.1390	4.2360	4.6875	0.0126
3.9	1.5807	2.0074	6.0996	5.1227	5.6111	0.0151
4	1.6357	2.0862	6.3259	5.3316	5.8288	0.0157
4.1	1.3764	1.7150	5.2596	4.3473	4.8034	0.0129
4.2	1.5178	1.9174	5.8411	4.8841	5.3626	0.0144
4.3	1.6925	2.1675	6.5593	5.5470	6.0532	0.0163
4.4	1.8500	2.3930	7.2071	6.1450	6.6761	0.0180
4.5	2.2282	2.9343	8.7620	7.5803	8.1712	0.0220

Time (s)	Data from load cell 1	Data from load cell 2	Calibrated Load of load cell 1 (N)	Calibrated Load of load cell 2 (N)	Average Load (N)	Average pressure (kPa)
4.6	1.9765	2.5740	7.7270	6.6249	7.1760	0.0193
4.7	2.1347	2.8005	8.3777	7.2255	7.8016	0.0210
4.8	2.3918	3.1686	9.4350	8.2015	8.8183	0.0237
4.9	1.9368	2.5172	7.5638	6.4743	7.0191	0.0189
5	1.7493	2.2488	6.7930	5.7628	6.2779	0.0169
5.1	1.7584	2.2619	6.8304	5.7973	6.3139	0.0170
5.2	1.5020	1.8949	5.7763	4.8243	5.3003	0.0143
5.3	1.1216	1.3503	4.2120	3.3803	3.7962	0.0102
5.4	0.7158	0.7694	2.5433	1.8400	2.1916	0.0059
5.5	0.5550	0.5392	1.8821	1.2296	1.5558	0.0042
5.6	0.1790	0.0010	0.3361	-0.1974	0.0693	0.0002
5.7	0.0222	-0.2236	-0.3088	-0.7928	-0.5508	-0.0015
5.8	-0.3994	-0.8270	-2.0422	-2.3928	-2.2175	-0.0060
5.9	-0.8095	-1.4141	-3.7287	-3.9496	-3.8392	-0.0103
6	-1.3780	-2.2278	-6.0660	-6.1071	-6.0866	-0.0164
6.1	-1.9801	-3.0899	-8.5422	-8.3928	-8.4675	-0.0228
6.2	-2.9534	-4.4831	-12.5441	-12.0868	-12.3155	-0.0331
6.3	-3.2381	-4.8906	-13.7147	-13.1675	-13.4411	-0.0362
6.4	-3.2995	-4.9784	-13.9670	-13.4004	-13.6837	-0.0368
6.5	-3.1820	-4.8103	-13.4840	-12.9545	-13.2192	-0.0356
6.6	-2.9570	-4.4882	-12.5587	-12.1003	-12.3295	-0.0332
6.7	-3.1145	-4.7137	-13.2066	-12.6984	-12.9525	-0.0349
6.8	-3.3398	-5.0362	-14.1328	-13.5534	-13.8431	-0.0373
6.9	-3.2096	-4.8499	-13.5977	-13.0594	-13.3285	-0.0359
7	-2.6399	-4.0343	-11.2549	-10.8968	-11.0759	-0.0298
7.1	-2.1665	-3.3566	-9.3083	-9.1000	-9.2042	-0.0248
7.2	-1.9656	-3.0690	-8.4822	-8.3374	-8.4098	-0.0226
7.3	-1.9650	-3.0682	-8.4799	-8.3353	-8.4076	-0.0226
7.4	-1.8554	-2.9114	-8.0294	-7.9195	-7.9744	-0.0215
7.5	-1.6731	-2.6503	-7.2795	-7.2273	-7.2534	-0.0195
7.6	-1.4570	-2.3409	-6.3909	-6.4069	-6.3989	-0.0172
7.7	-0.9617	-1.6319	-4.3543	-4.5270	-4.4406	-0.0119
7.8	-0.6237	-1.1481	-2.9644	-3.2441	-3.1043	-0.0084
7.9	-0.4820	-0.9453	-2.3820	-2.7064	-2.5442	-0.0068
8	0.2251	0.0670	0.5257	-0.0224	0.2517	0.0007
8.1	0.6104	0.6185	2.1099	1.4399	1.7749	0.0048
8.2	1.1130	1.3379	4.1764	3.3474	3.7619	0.0101
8.3	1.4094	1.7622	5.3953	4.4726	4.9339	0.0133
8.4	1.4853	1.8708	5.7072	4.7605	5.2339	0.0141
8.5	1.4759	1.8574	5.6686	4.7249	5.1967	0.0140
8.6	1.6510	2.1081	6.3889	5.3897	5.8893	0.0158
8.7	1.9264	2.5023	7.5211	6.4348	6.9780	0.0188

Time (s)	Data from load cell 1	Data from load cell 2	Calibrated Load of load cell 1 (N)	Calibrated Load of load cell 2 (N)	Average Load (N)	Average pressure (kPa)
8.8	2.0880	2.7337	8.1858	7.0485	7.6172	0.0205
8.9	2.0390	2.6636	7.9843	6.8624	7.4234	0.0200
9	1.8995	2.4638	7.4105	6.3328	6.8716	0.0185
9.1	2.0397	2.6645	7.9871	6.8650	7.4260	0.0200
9.2	2.1107	2.7662	8.2792	7.1346	7.7069	0.0207
9.3	1.9367	2.5171	7.5635	6.4740	7.0187	0.0189
9.4	1.6078	2.0463	6.2112	5.2257	5.7185	0.0154
9.5	1.6487	2.1049	6.3795	5.3811	5.8803	0.0158
9.6	1.3893	1.7334	5.3125	4.3961	4.8543	0.0131
9.7	1.1927	1.4520	4.5041	3.6499	4.0770	0.0110
9.8	0.5371	0.5136	1.8085	1.1617	1.4851	0.0040
9.9	0.1406	-0.0540	0.1782	-0.3432	-0.0825	-0.0002
10	-0.1326	-0.4451	-0.9451	-1.3801	-1.1626	-0.0031
10.1	-0.6509	-1.1871	-3.0766	-3.3476	-3.2121	-0.0086
10.2	-1.1458	-1.8955	-5.1113	-5.2258	-5.1686	-0.0139
10.3	-1.5675	-2.4992	-6.8454	-6.8266	-6.8360	-0.0184
10.4	-1.8086	-2.8442	-7.8366	-7.7415	-7.7891	-0.0210
10.5	-1.8831	-2.9510	-8.1432	-8.0244	-8.0838	-0.0218
10.6	-2.3429	-3.6091	-10.0336	-9.7695	-9.9015	-0.0266
10.7	-2.6461	-4.0432	-11.2806	-10.9206	-11.1006	-0.0299
10.8	-2.5110	-3.8498	-10.7251	-10.4078	-10.5665	-0.0284
10.9	-2.1646	-3.3539	-9.3007	-9.0930	-9.1969	-0.0247
11	-2.2810	-3.5205	-9.7791	-9.5346	-9.6568	-0.0260
11.1	-2.4320	-3.7367	-10.4003	-10.1080	-10.2541	-0.0276
11.2	-2.7632	-4.2108	-11.7620	-11.3649	-11.5634	-0.0311
11.3	-2.8563	-4.3441	-12.1448	-11.7183	-11.9316	-0.0321
11.4	-2.7559	-4.2004	-11.7320	-11.3373	-11.5346	-0.0310
11.5	-2.7303	-4.1637	-11.6267	-11.2400	-11.4333	-0.0308
11.6	-2.2771	-3.5150	-9.7632	-9.5199	-9.6416	-0.0259
11.7	-2.2434	-3.4667	-9.6246	-9.3919	-9.5083	-0.0256
11.8	-1.9130	-2.9938	-8.2661	-8.1380	-8.2020	-0.0221
11.9	-1.5226	-2.4348	-6.6607	-6.6560	-6.6583	-0.0179
12	-1.3065	-2.1256	-5.7723	-5.8360	-5.8042	-0.0156
12.1	-0.8897	-1.5289	-4.0584	-4.2539	-4.1561	-0.0112
12.2	-0.6630	-1.2044	-3.1262	-3.3934	-3.2598	-0.0088
12.3	-0.4585	-0.9117	-2.2855	-2.6174	-2.4514	-0.0066
12.4	-0.0458	-0.3208	-0.5883	-1.0507	-0.8195	-0.0022
12.5	0.2855	0.1533	0.7738	0.2066	0.4902	0.0013
12.6	0.3558	0.2541	1.0631	0.4737	0.7684	0.0021
12.7	0.6174	0.6286	2.1388	1.4666	1.8027	0.0049
12.8	0.7985	0.8878	2.8835	2.1540	2.5188	0.0068
12.9	1.1488	1.3892	4.3237	3.4834	3.9036	0.0105

Time (s)	Data from load cell 1	Data from load cell 2	Calibrated Load of load cell 1 (N)	Calibrated Load of load cell 2 (N)	Average Load (N)	Average pressure (kPa)
13	0.8961	1.0274	3.2845	2.5242	2.9044	0.0078
13.1	0.7160	0.7696	2.5441	1.8407	2.1924	0.0059
13.2	0.5708	0.5618	1.9471	1.2896	1.6184	0.0044
13.3	0.7004	0.7473	2.4800	1.7815	2.1308	0.0057
13.4	0.7002	0.7471	2.4793	1.7809	2.1301	0.0057
13.5	0.4375	0.3710	1.3989	0.7836	1.0912	0.0029
13.6	0.4107	0.3327	1.2889	0.6821	0.9855	0.0027
13.7	0.3698	0.2740	1.1205	0.5266	0.8235	0.0022
13.8	0.0788	-0.1425	-0.0761	-0.5779	-0.3270	-0.0009
13.9	-0.2466	-0.6084	-1.4141	-1.8131	-1.6136	-0.0043
14	-0.2617	-0.6299	-1.4760	-1.8702	-1.6731	-0.0045
14.1	-0.2044	-0.5479	-1.2404	-1.6527	-1.4466	-0.0039
14.2	-0.4524	-0.9029	-2.2602	-2.5940	-2.4271	-0.0065
14.3	-0.6424	-1.1749	-3.0416	-3.3153	-3.1784	-0.0086
14.4	-1.0917	-1.8180	-4.8888	-5.0204	-4.9546	-0.0133
14.5	-1.4812	-2.3756	-6.4906	-6.4990	-6.4948	-0.0175
14.6	-1.5844	-2.5234	-6.9150	-6.8908	-6.9029	-0.0186
14.7	-1.8702	-2.9325	-8.0903	-7.9756	-8.0330	-0.0216
14.8	-1.7497	-2.7599	-7.5944	-7.5179	-7.5561	-0.0203
14.9	-1.4099	-2.2735	-6.1972	-6.2282	-6.2127	-0.0167
15	-1.4977	-2.3992	-6.5582	-6.5614	-6.5598	-0.0177
15.1	-1.4249	-2.2951	-6.2592	-6.2854	-6.2723	-0.0169
15.2	-2.1928	-3.3942	-9.4165	-9.1998	-9.3081	-0.0250
15.3	-2.0394	-3.1746	-8.7857	-8.6176	-8.7016	-0.0234
15.4	-1.6853	-2.6678	-7.3298	-7.2736	-7.3017	-0.0196
15.5	-1.4027	-2.2633	-6.1678	-6.2010	-6.1844	-0.0166
15.6	-1.1221	-1.8616	-5.0141	-5.1361	-5.0751	-0.0137
15.7	-1.2717	-2.0757	-5.6290	-5.7037	-5.6663	-0.0152
15.8	-1.0123	-1.7043	-4.5623	-4.7191	-4.6407	-0.0125
15.9	-0.8378	-1.4546	-3.8448	-4.0568	-3.9508	-0.0106
16	-0.6186	-1.1408	-2.9435	-3.2248	-3.0842	-0.0083
16.1	-0.6628	-1.2041	-3.1254	-3.3927	-3.2590	-0.0088
16.2	-0.6517	-1.1883	-3.0799	-3.3507	-3.2153	-0.0087
16.3	-0.9422	-1.6040	-4.2741	-4.4530	-4.3635	-0.0117
16.4	-0.4791	-0.9412	-2.3701	-2.6955	-2.5328	-0.0068
16.5	-0.3375	-0.7384	-1.7878	-2.1580	-1.9729	-0.0053
16.6	-0.4812	-0.9441	-2.3786	-2.7033	-2.5410	-0.0068
16.7	-0.5194	-0.9987	-2.5355	-2.8482	-2.6919	-0.0072
16.8	-0.6104	-1.1291	-2.9098	-3.1937	-3.0518	-0.0082
16.9	-0.7878	-1.3831	-3.6394	-3.8672	-3.7533	-0.0101
17	-0.5982	-1.1116	-2.8597	-3.1475	-3.0036	-0.0081
17.1	-0.5051	-0.9783	-2.4769	-2.7941	-2.6355	-0.0071

Time (s)	Data from load cell 1	Data from load cell 2	Calibrated Load of load cell 1 (N)	Calibrated Load of load cell 2 (N)	Average Load (N)	Average pressure (kPa)
17.2	-0.1948	-0.5342	-1.2010	-1.6163	-1.4087	-0.0038
17.3	-0.2519	-0.6158	-1.4356	-1.8329	-1.6342	-0.0044
17.4	-0.4476	-0.8961	-2.2406	-2.5759	-2.4083	-0.0065
17.5	-0.1370	-0.4515	-0.9635	-1.3971	-1.1803	-0.0032
17.6	-0.1610	-0.4858	-1.0621	-1.4881	-1.2751	-0.0034
17.7	-0.1564	-0.4792	-1.0431	-1.4705	-1.2568	-0.0034
17.8	-0.2203	-0.5706	-1.3057	-1.7130	-1.5093	-0.0041
17.9	-0.0721	-0.3585	-0.6965	-1.1506	-0.9236	-0.0025
18	-0.0737	-0.3607	-0.7029	-1.1565	-0.9297	-0.0025
18.1	0.0314	-0.2104	-0.2710	-0.7579	-0.5144	-0.0014
18.2	-0.0199	-0.2838	-0.4820	-0.9526	-0.7173	-0.0019
18.3	0.0385	-0.2003	-0.2419	-0.7310	-0.4864	-0.0013
18.4	-0.5149	-0.9923	-2.5170	-2.8311	-2.6741	-0.0072
18.5	-0.5285	-1.0119	-2.5733	-2.8830	-2.7281	-0.0073
18.6	-0.7662	-1.3521	-3.5506	-3.7851	-3.6679	-0.0099
18.7	-0.8823	-1.5183	-4.0279	-4.2257	-4.1268	-0.0111
18.8	-0.8383	-1.4553	-3.8470	-4.0588	-3.9529	-0.0106
18.9	-0.6545	-1.1922	-3.0911	-3.3610	-3.2261	-0.0087
19	-0.7496	-1.3284	-3.4824	-3.7223	-3.6024	-0.0097
19.1	-0.8057	-1.4087	-3.7130	-3.9351	-3.8240	-0.0103
19.2	-0.3861	-0.8080	-1.9877	-2.3425	-2.1651	-0.0058
19.3	0.1640	-0.0205	0.2744	-0.2544	0.0100	0.0000
19.4	0.5807	0.5760	1.9878	1.3272	1.6575	0.0045
19.5	0.7073	0.7571	2.5082	1.8075	2.1578	0.0058
19.6	0.8845	1.0109	3.2371	2.4804	2.8588	0.0077
19.7	1.1724	1.4230	4.4208	3.5731	3.9970	0.0108
19.8	1.2699	1.5626	4.8219	3.9433	4.3826	0.0118
19.9	1.8652	2.4147	7.2695	6.2026	6.7360	0.0181
20	1.8997	2.4642	7.4115	6.3337	6.8726	0.0185
20.1	2.4938	3.3145	9.8541	8.5884	9.2213	0.0248
20.2	3.0748	4.1463	12.2434	10.7939	11.5187	0.0310
20.3	3.2329	4.3725	12.8932	11.3937	12.1434	0.0327
20.4	3.6339	4.9466	14.5423	12.9160	13.7291	0.0369
20.5	3.8427	5.2455	15.4008	13.7085	14.5546	0.0392
20.6	3.5673	4.8512	14.2683	12.6630	13.4656	0.0362
20.7	3.5375	4.8086	14.1460	12.5501	13.3480	0.0359
20.8	3.6536	4.9748	14.6232	12.9906	13.8069	0.0372
20.9	2.9657	3.9900	11.7945	10.3796	11.0871	0.0298
21	2.3037	3.0424	9.0724	7.8669	8.4697	0.0228
21.1	2.1769	2.8609	8.5511	7.3857	7.9684	0.0214
21.2	1.3869	1.7300	5.3027	4.3871	4.8449	0.0130
21.3	1.0153	1.1982	3.7750	2.9769	3.3760	0.0091

Time (s)	Data from load cell 1	Data from load cell 2	Calibrated Load of load cell 1 (N)	Calibrated Load of load cell 2 (N)	Average Load (N)	Average pressure (kPa)
21.4	0.2247	0.0663	0.5238	-0.0242	0.2498	0.0007
21.5	-0.2965	-0.6797	-1.6191	-2.0022	-1.8106	-0.0049
21.6	-1.3174	-2.1411	-5.8170	-5.8772	-5.8471	-0.0157
21.7	-2.3903	-3.6770	-10.2288	-9.9496	-10.0892	-0.0271
21.8	-3.1511	-4.7661	-13.3571	-12.8373	-13.0972	-0.0352
21.9	-3.7104	-5.5667	-15.6567	-14.9600	-15.3084	-0.0412
22	-5.0222	-7.4445	-21.0508	-19.9392	-20.4950	-0.0552
22.1	-5.4548	-8.0638	-22.8295	-21.5811	-22.2053	-0.0598
22.2	-5.4511	-8.0585	-22.8143	-21.5671	-22.1907	-0.0597
22.3	-5.8136	-8.5774	-24.3050	-22.9431	-23.6240	-0.0636
22.4	-5.3528	-7.9178	-22.4104	-21.1942	-21.8023	-0.0587
22.5	14.2614	20.1597	58.2412	53.2535	55.7474	0.1500
22.6	16.4337	23.2694	67.1737	61.4988	64.3363	0.1731
22.7	20.8689	29.6184	85.4108	78.3331	81.8719	0.2203
22.8	25.7220	36.5656	105.3664	96.7536	101.0600	0.2720
22.9	29.8453	42.4680	122.3208	112.4038	117.3623	0.3158
23	25.9694	36.9197	106.3838	97.6927	102.0382	0.2746
23.1	44.0336	62.7785	180.6618	166.2571	173.4594	0.4668
23.2	48.7916	69.5894	200.2260	184.3164	192.2712	0.5174
23.3	52.6915	75.1722	216.2623	199.1190	207.6907	0.5589
23.4	55.6128	79.3539	228.2741	210.2069	219.2405	0.5900
23.5	57.5812	82.1717	236.3681	217.6782	227.0232	0.6109
23.6	59.7367	85.2572	245.2312	225.8596	235.5454	0.6338
23.7	56.1910	80.1817	230.6520	212.4018	221.5269	0.5961
23.8	49.7321	70.9358	204.0934	187.8862	195.9898	0.5274
23.9	14.4014	20.3602	58.8172	53.7851	56.3012	0.1515
24	23.7814	33.7876	97.3868	89.3878	93.3873	0.2513
24.1	11.6431	16.4116	47.4751	43.3155	45.3953	0.1222
24.2	5.5199	7.6463	22.2971	20.0743	21.1857	0.0570
24.3	2.8847	3.8741	11.4614	10.0721	10.7668	0.0290
24.4	-4.0581	-6.0645	-17.0866	-16.2799	-16.6832	-0.0449
24.5	-8.2012	-11.9952	-34.1224	-32.0053	-33.0638	-0.0890
24.6	-11.8296	-17.1893	-49.0421	-45.7773	-47.4097	-0.1276
24.7	-6.4139	-9.4368	-26.7735	-25.2217	-25.9976	-0.0700
24.8	-2.1154	-3.2834	-9.0981	-8.9060	-9.0021	-0.0242
24.9	5.3084	7.3436	21.4276	19.2716	20.3496	0.0548
25	13.3533	18.8598	54.5072	49.8067	52.1570	0.1404
25.1	18.5882	26.3535	76.0328	69.6764	72.8546	0.1961
25.2	25.5607	36.3347	104.7032	96.1414	100.4223	0.2702
25.3	33.2010	47.2717	136.1192	125.1408	130.6300	0.3515
25.4	37.9150	54.0197	155.5026	143.0332	149.2679	0.4017
25.5	51.6359	73.6610	211.9215	195.1122	203.5169	0.5477

Time (s)	Data from load cell 1	Data from load cell 2	Calibrated Load of load cell 1 (N)	Calibrated Load of load cell 2 (N)	Average Load (N)	Average pressure (kPa)
25.6	50.5392	72.0912	207.4122	190.9497	199.1809	0.5360
25.7	43.4249	61.9071	178.1589	163.9467	171.0528	0.4603
25.8	30.4255	43.2985	124.7065	114.6060	119.6562	0.3220
25.9	7.5290	10.5224	30.5584	27.7000	29.1292	0.0784
26	-10.3540	-15.0770	-42.9746	-40.1765	-41.5756	-0.1119
26.1	-18.6957	-27.0180	-77.2748	-71.8383	-74.5566	-0.2006
26.2	-22.1339	-31.9399	-91.4126	-84.8885	-88.1505	-0.2372
26.3	-21.9555	-31.6845	-90.6790	-84.2114	-87.4452	-0.2353
26.4	-18.8521	-27.2420	-77.9181	-72.4321	-75.1751	-0.2023
26.5	-11.7837	-17.1235	-48.8532	-45.6030	-47.2281	-0.1271
26.6	-0.4599	-0.9136	-2.2910	-2.6225	-2.4567	-0.0066
26.7	12.0012	16.9243	48.9476	44.6747	46.8112	0.1260
26.8	25.0413	35.5912	102.5675	94.1700	98.3687	0.2647
26.9	36.1416	51.4811	148.2108	136.3023	142.2565	0.3828
27	39.9739	56.9670	163.9687	150.8480	157.4084	0.4236
27.1	49.3572	70.3991	202.5518	186.4632	194.5075	0.5234
27.2	25.0511	35.6051	102.6076	94.2070	98.4073	0.2648
27.3	30.0186	42.7161	123.0335	113.0617	118.0476	0.3177
27.4	23.5748	33.4918	96.5371	88.6034	92.5703	0.2491
27.5	14.3658	20.3093	58.6709	53.6500	56.1604	0.1511
27.6	2.9025	3.8996	11.5347	10.1398	10.8373	0.0292
27.7	4.6490	6.3997	18.7163	16.7688	17.7425	0.0477
27.8	-16.7754	-24.2692	-69.3788	-64.5497	-66.9642	-0.1802
27.9	-17.6494	-25.5203	-72.9727	-67.8671	-70.4199	-0.1895
28	-12.4335	-18.0537	-51.5252	-48.0694	-49.7973	-0.1340
28.1	-17.1501	-24.8056	-70.9196	-65.9720	-68.4458	-0.1842
28.2	-14.9720	-21.6876	-61.9633	-57.7046	-59.8340	-0.1610
28.3	-10.8995	-15.8578	-45.2176	-42.2470	-43.7323	-0.1177
28.4	-5.6527	-8.3471	-23.6433	-22.3322	-22.9878	-0.0619
28.5	2.1289	2.7923	8.3540	7.2037	7.7789	0.0209
28.6	10.3154	14.5112	42.0160	38.2764	40.1462	0.1080
28.7	19.5950	27.7948	80.1726	73.4978	76.8352	0.2068
28.8	24.7292	35.1444	101.2841	92.9853	97.1347	0.2614
28.9	27.0563	38.4755	110.8527	101.8179	106.3353	0.2861
29	29.1229	41.4339	119.3506	109.6621	114.5064	0.3081
29.1	32.4793	46.2385	133.1515	122.4014	127.7765	0.3438
29.2	23.5204	33.4139	96.3134	88.3970	92.3552	0.2485
29.3	14.6517	20.7185	59.8463	54.7350	57.2907	0.1542
29.4	2.9470	3.9634	11.7180	10.3089	11.0134	0.0296
29.5	-8.6755	-12.6742	-36.0728	-33.8056	-34.9392	-0.0940
29.6	-14.6769	-21.2652	-60.7501	-56.5847	-58.6674	-0.1579
29.7	-16.3861	-23.7119	-67.7780	-63.0720	-65.4250	-0.1761

Time (s)	Data from load cell 1	Data from load cell 2	Calibrated Load of load cell 1 (N)	Calibrated Load of load cell 2 (N)	Average Load (N)	Average pressure (kPa)
29.8	-14.5643	-21.1040	-60.2870	-56.1572	-58.2221	-0.1567
29.9	-11.7591	-17.0884	-48.7523	-45.5098	-47.1310	-0.1268
30	-8.1554	-11.9296	-33.9340	-31.8314	-32.8827	-0.0885
30.1	-3.0878	-4.6754	-13.0966	-12.5968	-12.8467	-0.0346
30.2	3.5910	4.8851	14.3657	12.7529	13.5593	0.0365
30.3	11.4398	16.1207	46.6395	42.5441	44.5918	0.1200
30.4	20.8514	29.5933	85.3388	78.2666	81.8027	0.2201
30.5	25.5237	36.2816	104.5508	96.0008	100.2758	0.2698
30.6	29.3913	41.8181	120.4540	110.6806	115.5673	0.3110
30.7	31.2533	44.4836	128.1105	117.7482	122.9294	0.3308
30.8	31.3572	44.6323	128.5376	118.1424	123.3400	0.3319
30.9	29.0091	41.2709	118.8824	109.2299	114.0561	0.3069
31	25.1510	35.7482	103.0185	94.5863	98.8024	0.2659
31.1	17.7932	25.2155	72.7637	66.6588	69.7113	0.1876
31.2	9.3179	13.0831	37.9141	34.4900	36.2020	0.0974
31.3	-0.6067	-1.1238	-2.8948	-3.1798	-3.0373	-0.0082
31.4	-10.6521	-15.5037	-44.2004	-41.3081	-42.7542	-0.1151
31.5	-14.2710	-20.6841	-59.0810	-55.0440	-57.0625	-0.1536
31.6	-14.3596	-20.8109	-59.4451	-55.3801	-57.4126	-0.1545
31.7	-14.7806	-21.4137	-61.1765	-56.9783	-59.0774	-0.1590
31.8	-14.1536	-20.5160	-58.5981	-54.5983	-56.5982	-0.1523
31.9	-12.3871	-17.9874	-51.3347	-47.8935	-49.6141	-0.1335
32	-8.8851	-12.9743	-36.9348	-34.6013	-35.7681	-0.0963
32.1	-3.0374	-4.6033	-12.8895	-12.4057	-12.6476	-0.0340
32.2	5.7737	8.0097	23.3408	21.0377	22.1893	0.0597
32.3	13.4211	18.9569	54.7861	50.0641	52.4251	0.1411
32.4	15.9248	22.5410	65.0813	59.5674	62.3243	0.1677
32.5	18.1157	25.6772	74.0899	67.8830	70.9865	0.1910
32.6	22.0511	31.3106	90.2718	82.8202	86.5460	0.2329
32.7	24.6177	34.9847	100.8254	92.5619	96.6936	0.2602
32.8	24.5881	34.9423	100.7037	92.4496	96.5766	0.2599
32.9	22.5816	32.0701	92.4534	84.8339	88.6436	0.2385
33	16.0587	22.7326	65.6318	60.0755	62.8536	0.1691
33.1	4.5410	6.2451	18.2720	16.3588	17.3154	0.0466
33.2	-8.1944	-11.9855	-34.0944	-31.9795	-33.0370	-0.0889
33.3	-14.6201	-21.1838	-60.5164	-56.3689	-58.4426	-0.1573
33.4	-14.7450	-21.3627	-61.0301	-56.8432	-58.9366	-0.1586
33.5	-11.6364	-16.9128	-48.2479	-45.0442	-46.6461	-0.1255
33.6	-12.7254	-18.4716	-52.7255	-49.1774	-50.9514	-0.1371
33.7	-10.6197	-15.4573	-44.0672	-41.1851	-42.6261	-0.1147
33.8	-6.9474	-10.2005	-28.9671	-27.2465	-28.1068	-0.0756
33.9	-2.3837	-3.6675	-10.2014	-9.9244	-10.0629	-0.0271

Time (s)	Data from load cell 1	Data from load cell 2	Calibrated Load of load cell 1 (N)	Calibrated Load of load cell 2 (N)	Average Load (N)	Average pressure (kPa)
34	2.9359	3.9474	11.6722	10.2666	10.9694	0.0295
34.1	5.4748	7.5818	22.1118	19.9032	21.0075	0.0565
34.2	10.3426	14.5500	42.1277	38.3794	40.2536	0.1083
34.3	13.9221	19.6741	56.8462	51.9658	54.4060	0.1464
34.4	17.6482	25.0080	72.1678	66.1088	69.1383	0.1860
34.5	19.0711	27.0449	78.0186	71.5095	74.7640	0.2012
34.6	22.3831	31.7859	91.6369	84.0802	87.8586	0.2364
34.7	23.9902	34.0864	98.2451	90.1801	94.2126	0.2535
34.8	22.7337	32.2878	93.0787	85.4111	89.2449	0.2402
34.9	16.4625	23.3106	67.2922	61.6082	64.4502	0.1734
35	5.3053	7.3392	21.4148	19.2598	20.3373	0.0547
35.1	-5.9219	-8.7325	-24.7503	-23.3541	-24.0522	-0.0647
35.2	-14.1844	-20.5602	-58.7249	-54.7153	-56.7201	-0.1526
35.3	-16.0524	-23.2342	-66.4059	-61.8055	-64.1057	-0.1725
35.4	-15.0934	-21.8613	-62.4624	-58.1653	-60.3138	-0.1623
35.5	-12.0931	-17.5665	-50.1258	-46.7776	-48.4517	-0.1304
35.6	-7.4740	-10.9542	-31.1322	-29.2451	-30.1886	-0.0812
35.7	0.6187	0.6304	2.1442	1.4716	1.8079	0.0049
35.8	10.8030	15.2091	44.0207	40.1268	42.0738	0.1132
35.9	18.4705	26.1851	75.5489	69.2297	72.3893	0.1948
36	21.2405	30.1503	86.9389	79.7436	83.3413	0.2243
36.1	22.6601	32.1824	92.7759	85.1316	88.9538	0.2394
36.2	20.8788	29.6325	85.4514	78.3705	81.9110	0.2204
36.3	17.2441	24.4295	70.5060	64.5747	67.5404	0.1817
36.4	12.4121	17.5126	50.6375	46.2346	48.4360	0.1303
36.5	4.7044	6.4791	18.9442	16.9793	17.9617	0.0483
36.6	-3.9762	-5.9472	-16.7498	-15.9690	-16.3594	-0.0440
36.7	-9.8445	-14.3476	-40.8796	-38.2428	-39.5612	-0.1065
36.8	-12.0861	-17.5565	-50.0970	-46.7511	-48.4240	-0.1303
36.9	-12.1565	-17.6573	-50.3864	-47.0182	-48.7023	-0.1311
37	-11.0731	-16.1064	-45.9316	-42.9061	-44.4188	-0.1195
37.1	-9.6191	-14.0249	-39.9527	-37.3871	-38.6699	-0.1041
37.2	-7.0769	-10.3858	-29.4994	-27.7379	-28.6187	-0.0770
37.3	-4.0118	-5.9982	-16.8963	-16.1043	-16.5003	-0.0444
37.4	0.7591	0.8314	2.7214	2.0044	2.3629	0.0064
37.5	6.7576	9.4182	27.3867	24.7724	26.0795	0.0702
37.6	12.8757	18.1762	52.5437	47.9942	50.2690	0.1353
37.7	16.6723	23.6109	68.1547	62.4043	65.2795	0.1757
37.8	18.7323	26.5598	76.6252	70.2232	73.4242	0.1976
37.9	20.8003	29.5202	85.1288	78.0727	81.6008	0.2196
38	19.8440	28.1512	81.1966	74.4430	77.8198	0.2094
38.1	17.5040	24.8015	71.5746	65.5612	68.5679	0.1845

Time (s)	Data from load cell 1	Data from load cell 2	Calibrated Load of load cell 1 (N)	Calibrated Load of load cell 2 (N)	Average Load (N)	Average pressure (kPa)
38.2	12.1616	17.1539	49.6071	45.2835	47.4453	0.1277
38.3	4.3463	5.9664	17.4716	15.6199	16.5457	0.0445
38.4	-4.1476	-6.1925	-17.4544	-16.6194	-17.0369	-0.0458
38.5	-10.4045	-15.1493	-43.1823	-40.3683	-41.7753	-0.1124
38.6	-12.4716	-18.1083	-51.6819	-48.2141	-49.9480	-0.1344
38.7	-12.1425	-17.6372	-50.3287	-46.9649	-48.6468	-0.1309
38.8	-11.9448	-17.3541	-49.5157	-46.2145	-47.8651	-0.1288
38.9	-9.8330	-14.3311	-40.8322	-38.1989	-39.5155	-0.1063
39	-7.0856	-10.3983	-29.5354	-27.7712	-28.6533	-0.0771
39.1	-4.7361	-7.0349	-19.8742	-18.8531	-19.3637	-0.0521
39.2	-1.6137	-2.5654	-7.0355	-7.0020	-7.0188	-0.0189
39.3	1.9893	2.5923	7.7797	6.6736	7.2266	0.0194
39.4	5.8873	8.1723	23.8079	21.4688	22.6384	0.0609
39.5	9.0714	12.7303	36.9005	33.5543	35.2274	0.0948
39.6	11.4447	16.1276	46.6593	42.5624	44.6109	0.1200
39.7	12.6899	17.9102	51.7797	47.2889	49.5343	0.1333
39.8	13.2768	18.7503	54.1929	49.5165	51.8547	0.1395
39.9	13.0492	18.4246	53.2572	48.6528	50.9550	0.1371
40	9.4359	13.2521	38.3994	34.9379	36.6687	0.0987
40.1	9.4822	13.3184	38.5897	35.1136	36.8517	0.0992
40.2	9.4503	13.2727	38.4585	34.9925	36.7255	0.0988
40.3	8.3492	11.6964	33.9309	30.8131	32.3720	0.0871
40.4	6.7617	9.4240	27.4035	24.7878	26.0957	0.0702
40.5	4.8494	6.6865	19.5401	17.5294	18.5347	0.0499
40.6	1.3890	1.7330	5.3112	4.3950	4.8531	0.0131
40.7	-1.6875	-2.6710	-7.3390	-7.2821	-7.3105	-0.0197
40.8	-5.0260	-7.4499	-21.0663	-19.9535	-20.5099	-0.0552
40.9	-6.8714	-10.0917	-28.6547	-26.9582	-27.8065	-0.0748
41	-7.3107	-10.7205	-30.4608	-28.6254	-29.5431	-0.0795
41.1	-6.8999	-10.1325	-28.7718	-27.0663	-27.9190	-0.0751
41.2	-6.2988	-9.2720	-26.3001	-24.7847	-25.5424	-0.0687
41.3	-5.5847	-8.2497	-23.3636	-22.0741	-22.7189	-0.0611
41.4	-4.8937	-7.2606	-20.5226	-19.4516	-19.9871	-0.0538
41.5	-3.1186	-4.7196	-13.2235	-12.7140	-12.9687	-0.0349
41.6	-1.0004	-1.6874	-4.5137	-4.6741	-4.5939	-0.0124
41.7	0.7746	0.8535	2.7850	2.0631	2.4240	0.0065
41.8	2.0841	2.7280	8.1694	7.0333	7.6014	0.0205
41.9	4.0428	5.5320	16.2237	14.4680	15.3459	0.0413
42	5.8595	8.1325	23.6936	21.3633	22.5285	0.0606
42.1	6.9761	9.7310	28.2852	25.6017	26.9435	0.0725
42.2	6.6941	9.3272	27.1254	24.5311	25.8282	0.0695
42.3	6.5282	9.0898	26.4433	23.9015	25.1724	0.0677

Time (s)	Data from load cell 1	Data from load cell 2	Calibrated Load of load cell 1 (N)	Calibrated Load of load cell 2 (N)	Average Load (N)	Average pressure (kPa)
42.4	6.3500	8.8347	25.7105	23.2251	24.4678	0.0658
42.5	7.2366	10.1038	29.3562	26.5903	27.9733	0.0753
42.6	8.3313	11.6709	33.8574	30.7453	32.3014	0.0869
42.7	8.9083	12.4969	36.2301	32.9355	34.5828	0.0931
42.8	8.6453	12.1204	35.1487	31.9373	33.5430	0.0903
42.9	8.4172	11.7938	34.2106	31.0713	32.6409	0.0878
43	8.1330	11.3871	33.0422	29.9928	31.5175	0.0848
43.1	5.8614	8.1353	23.7017	21.3708	22.5362	0.0606
43.2	2.1111	2.7668	8.2808	7.1362	7.7085	0.0207
43.3	-2.4991	-3.8328	-10.6761	-10.3626	-10.5194	-0.0283
43.4	-6.0922	-8.9763	-25.4507	-24.0006	-24.7256	-0.0665
43.5	-6.1187	-9.0141	-25.5593	-24.1009	-24.8301	-0.0668
43.6	-6.5015	-9.5622	-27.1337	-25.5541	-26.3439	-0.0709
43.7	-8.2016	-11.9958	-34.1240	-32.0068	-33.0654	-0.0890
43.8	-7.0306	-10.3196	-29.3092	-27.5623	-28.4358	-0.0765
43.9	-5.0844	-7.5335	-21.3064	-20.1751	-20.7408	-0.0558
44	-0.5100	-0.9854	-2.4971	-2.8127	-2.6549	-0.0071
44.1	3.4515	4.6855	13.7921	12.2235	13.0078	0.0350
44.2	7.1121	9.9257	28.8444	26.1179	27.4811	0.0740
44.3	8.2348	11.5327	33.4606	30.3790	31.9198	0.0859
44.4	8.9141	12.5051	36.2538	32.9574	34.6056	0.0931
44.5	9.7073	13.6406	39.5155	35.9682	37.7419	0.1016
44.6	9.5329	13.3910	38.7983	35.3061	37.0522	0.0997
44.7	9.0273	12.6672	36.7194	33.3871	35.0532	0.0943
44.8	7.5586	10.5648	30.6803	27.8126	29.2464	0.0787
44.9	5.7121	7.9216	23.0877	20.8040	21.9459	0.0591
45	3.1933	4.3158	12.7304	11.2434	11.9869	0.0323
45.1	1.5018	1.8945	5.7751	4.8232	5.2991	0.0143
45.2	-1.4918	-2.3908	-6.5340	-6.5391	-6.5366	-0.0176
45.3	-4.8900	-7.2553	-20.5071	-19.4373	-19.9722	-0.0537
45.4	-6.5230	-9.5929	-27.2217	-25.6355	-26.4286	-0.0711
45.5	-7.0875	-10.4011	-29.5433	-27.7784	-28.6608	-0.0771
45.6	-7.4176	-10.8735	-30.9004	-29.0312	-29.9658	-0.0806
45.7	-7.1688	-10.5174	-29.8774	-28.0868	-28.9821	-0.0780
45.8	-6.9330	-10.1798	-28.9077	-27.1917	-28.0497	-0.0755
45.9	-5.8494	-8.6287	-24.4521	-23.0789	-23.7655	-0.0640
46	-3.9224	-5.8702	-16.5286	-15.7648	-16.1467	-0.0435
46.1	-1.8185	-2.8585	-7.8775	-7.7792	-7.8283	-0.0211
46.2	-0.4064	-0.8371	-2.0712	-2.4195	-2.2453	-0.0060
46.3	1.4122	1.7662	5.4068	4.4832	4.9450	0.0133
46.4	2.3820	3.1546	9.3947	8.1643	8.7795	0.0236
46.5	2.8878	3.8785	11.4743	10.0840	10.7791	0.0290

Time (s)	Data from load cell 1	Data from load cell 2	Calibrated Load of load cell 1 (N)	Calibrated Load of load cell 2 (N)	Average Load (N)	Average pressure (kPa)
46.6	3.0216	4.0701	12.0245	10.5918	11.3082	0.0304
46.7	3.2241	4.3600	12.8573	11.3606	12.1090	0.0326
46.8	2.9414	3.9554	11.6949	10.2876	10.9913	0.0296
46.9	2.7318	3.6552	10.8328	9.4918	10.1623	0.0273
47	2.1099	2.7650	8.2756	7.1314	7.7035	0.0207
47.1	1.4060	1.7574	5.3814	4.4597	4.9206	0.0132
47.2	0.1728	-0.0080	0.3104	-0.2212	0.0446	0.0001
47.3	-1.1501	-1.9017	-5.1292	-5.2423	-5.1858	-0.0140
47.4	-2.3975	-3.6874	-10.2584	-9.9770	-10.1177	-0.0272
47.5	-3.5388	-5.3211	-14.9513	-14.3089	-14.6301	-0.0394
47.6	-4.7591	-7.0679	-19.9690	-18.9406	-19.4548	-0.0524
47.7	-4.9191	-7.2970	-20.6269	-19.5479	-20.0874	-0.0541
47.8	-4.6881	-6.9663	-19.6771	-18.6712	-19.1741	-0.0516
47.9	-4.6847	-6.9614	-19.6630	-18.6582	-19.1606	-0.0516
48	-4.2246	-6.3028	-17.7713	-16.9119	-17.3416	-0.0467
48.1	-3.7323	-5.5981	-15.7470	-15.0434	-15.3952	-0.0414
48.2	-2.9294	-4.4487	-12.4453	-11.9956	-12.2205	-0.0329
48.3	-1.8014	-2.8340	-7.8071	-7.7142	-7.7607	-0.0209
48.4	-0.6981	-1.2546	-3.2705	-3.5266	-3.3986	-0.0091
48.5	0.6327	0.6504	2.2017	1.5246	1.8631	0.0050
48.6	1.7469	2.2454	6.7831	5.7537	6.2684	0.0169
48.7	1.9015	2.4667	7.4189	6.3405	6.8797	0.0185
48.8	2.4805	3.2955	9.7996	8.5381	9.1689	0.0247
48.9	3.0275	4.0785	12.0486	10.6141	11.3314	0.0305
49	3.4199	4.6403	13.6625	12.1038	12.8832	0.0347
49.1	3.5965	4.8931	14.3886	12.7741	13.5814	0.0365
49.2	3.0938	4.1735	12.3215	10.8660	11.5937	0.0312
49.3	2.7382	3.6644	10.8593	9.5162	10.1877	0.0274
49.4	1.4657	1.8428	5.6266	4.6861	5.1564	0.0139
49.5	-0.2371	-0.5947	-1.3750	-1.7769	-1.5760	-0.0042
49.6	-2.2009	-3.4059	-9.4498	-9.2306	-9.3402	-0.0251
49.7	-3.7985	-5.6929	-16.0192	-15.2946	-15.6569	-0.0421
49.8	-4.7705	-7.0842	-20.0157	-18.9837	-19.4997	-0.0525
49.9	-4.9297	-7.3121	-20.6704	-19.5880	-20.1292	-0.0542
50	-4.5500	-6.7686	-19.1091	-18.1469	-18.6280	-0.0501
50.1	-8.8186	-12.8790	-36.6612	-34.3488	-35.5050	-0.0955
50.2	-7.4093	-10.8617	-30.8664	-28.9997	-29.9330	-0.0805
50.3	-6.4875	-9.5421	-27.0759	-25.5008	-26.2883	-0.0707
50.4	-5.4492	-8.0558	-22.8067	-21.5601	-22.1834	-0.0597
50.5	-4.0346	-6.0307	-16.9897	-16.1905	-16.5901	-0.0446
50.6	-2.8662	-4.3583	-12.1856	-11.7560	-11.9708	-0.0322
50.7	-1.9642	-3.0670	-8.4765	-8.3321	-8.4043	-0.0226

Time (s)	Data from load cell 1	Data from load cell 2	Calibrated Load of load cell 1 (N)	Calibrated Load of load cell 2 (N)	Average Load (N)	Average pressure (kPa)
50.8	-1.1455	-1.8951	-5.1103	-5.2249	-5.1676	-0.0139
50.9	-0.0865	-0.3791	-0.7557	-1.2052	-0.9805	-0.0026
51	0.9410	1.0918	3.4694	2.6949	3.0821	0.0083
51.1	1.9613	2.5523	7.6647	6.5674	7.1161	0.0191
51.2	2.4443	3.2437	9.6507	8.4006	9.0257	0.0243
51.3	2.9040	3.9018	11.5410	10.1455	10.8432	0.0292
51.4	3.6539	4.9753	14.6246	12.9919	13.8083	0.0372
51.5	3.9699	5.4275	15.9237	14.1911	15.0574	0.0405
51.6	4.5374	6.2399	18.2572	16.3451	17.3012	0.0466
51.7	4.1889	5.7411	16.8244	15.0225	15.9235	0.0428
51.8	3.5527	4.8304	14.2085	12.6079	13.4082	0.0361
51.9	2.9697	3.9958	11.8110	10.3948	11.1029	0.0299
52	1.4142	1.7691	5.4150	4.4907	4.9528	0.0133
52.1	-0.0453	-0.3201	-0.5861	-1.0487	-0.8174	-0.0022
52.2	-1.0747	-1.7938	-4.8192	-4.9562	-4.8877	-0.0132
52.3	-2.2352	-3.4550	-9.5909	-9.3608	-9.4758	-0.0255
52.4	-3.2889	-4.9633	-13.9234	-13.3601	-13.6418	-0.0367
52.5	-3.7326	-5.5985	-15.7481	-15.0444	-15.3962	-0.0414
52.6	-3.7461	-5.6178	-15.8035	-15.0955	-15.4495	-0.0416
52.7	-4.0858	-6.1041	-17.2005	-16.3850	-16.7928	-0.0452
52.8	-3.4287	-5.1634	-14.4984	-13.8908	-14.1946	-0.0382
52.9	-3.0795	-4.6636	-13.0625	-12.5654	-12.8140	-0.0345
53	-3.0999	-4.6928	-13.1465	-12.6429	-12.8947	-0.0347
53.1	-3.2715	-4.9384	-13.8519	-13.2941	-13.5730	-0.0365
53.2	-3.5647	-5.3581	-15.0576	-14.4071	-14.7324	-0.0396
53.3	-3.4604	-5.2089	-14.6289	-14.0113	-14.3201	-0.0385
53.4	-3.4986	-5.2636	-14.7860	-14.1564	-14.4712	-0.0389
53.5	-3.2974	-4.9754	-13.9584	-13.3924	-13.6754	-0.0368
53.6	-3.0971	-4.6888	-13.1349	-12.6322	-12.8836	-0.0347
53.7	-3.0932	-4.6831	-13.1188	-12.6174	-12.8681	-0.0346
53.8	-2.8896	-4.3918	-12.2818	-11.8447	-12.0633	-0.0325
53.9	-2.8945	-4.3988	-12.3019	-11.8633	-12.0826	-0.0325
54	-3.3345	-5.0286	-14.1110	-13.5332	-13.8221	-0.0372
54.1	-3.3934	-5.1129	-14.3532	-13.7568	-14.0550	-0.0378
54.2	-3.1813	-4.8093	-13.4811	-12.9518	-13.2164	-0.0356
54.3	-3.0490	-4.6199	-12.9372	-12.4497	-12.6935	-0.0342
54.4	-2.7769	-4.2304	-11.8184	-11.4170	-11.6177	-0.0313
54.5	-1.9780	-3.0868	-8.5333	-8.3845	-8.4589	-0.0228
54.6	-1.2626	-2.0627	-5.5916	-5.6692	-5.6304	-0.0152
54.7	-0.5038	-0.9765	-2.4715	-2.7891	-2.6303	-0.0071
54.8	0.8416	0.9494	3.0606	2.3174	2.6890	0.0072
54.9	0.9199	1.0615	3.3823	2.6145	2.9984	0.0081

Time (s)	Data from load cell 1	Data from load cell 2	Calibrated Load of load cell 1 (N)	Calibrated Load of load cell 2 (N)	Average Load (N)	Average pressure (kPa)
55	0.9526	1.1084	3.5171	2.7389	3.1280	0.0084
55.1	1.1604	1.4058	4.3713	3.5274	3.9494	0.0106
55.2	1.1602	1.4055	4.3707	3.5268	3.9487	0.0106
55.3	1.0877	1.3017	4.0725	3.2515	3.6620	0.0099
55.4	0.8869	1.0142	3.2467	2.4892	2.8679	0.0077
55.5	1.0479	1.2448	3.9090	3.1007	3.5048	0.0094
55.6	1.0228	1.2088	3.8056	3.0051	3.4054	0.0092
55.7	1.2432	1.5243	4.7117	3.8416	4.2767	0.0115
55.8	1.1182	1.3454	4.1978	3.3672	3.7825	0.0102
55.9	1.1543	1.3971	4.3465	3.5045	3.9255	0.0106
56	1.0209	1.2062	3.7980	2.9981	3.3981	0.0091
56.1	0.9821	1.1505	3.6382	2.8507	3.2444	0.0087
56.2	0.7525	0.8219	2.6942	1.9793	2.3367	0.0063
56.3	0.3341	0.2230	0.9738	0.3912	0.6825	0.0018
56.4	-0.0992	-0.3973	-0.8079	-1.2535	-1.0307	-0.0028
56.5	-0.7971	-1.3963	-3.6774	-3.9022	-3.7898	-0.0102
56.6	-1.2191	-2.0004	-5.4129	-5.5042	-5.4585	-0.0147
56.7	-1.6771	-2.6561	-7.2961	-7.2425	-7.2693	-0.0196
56.8	-2.3086	-3.5600	-9.8925	-9.6393	-9.7659	-0.0263
56.9	-2.4648	-3.7836	-10.5348	-10.2322	-10.3835	-0.0279
57	-2.5175	-3.8591	-10.7518	-10.4324	-10.5921	-0.0285
57.1	-2.6895	-4.1053	-11.4591	-11.0853	-11.2722	-0.0303
57.2	-2.7807	-4.2358	-11.8338	-11.4312	-11.6325	-0.0313
57.3	-2.7399	-4.1775	-11.6663	-11.2766	-11.4714	-0.0309
57.4	-2.5785	-3.9464	-11.0025	-10.6639	-10.8332	-0.0292
57.5	-2.3186	-3.5744	-9.9339	-9.6775	-9.8057	-0.0264
57.6	-2.1795	-3.3752	-9.3619	-9.1495	-9.2557	-0.0249
57.7	-1.6855	-2.6680	-7.3305	-7.2743	-7.3024	-0.0197
57.8	-1.1488	-1.8998	-5.1239	-5.2374	-5.1807	-0.0139
57.9	-0.4079	-0.8392	-2.0771	-2.4250	-2.2511	-0.0061
58	0.0735	-0.1501	-0.0979	-0.5980	-0.3480	-0.0009
58.1	0.4118	0.3342	1.2934	0.6862	0.9898	0.0027
58.2	0.5719	0.5634	1.9516	1.2938	1.6227	0.0044
58.3	0.7634	0.8374	2.7388	2.0205	2.3797	0.0064
58.4	0.9268	1.0715	3.4111	2.6410	3.0261	0.0081
58.5	1.3922	1.7376	5.3245	4.4073	4.8659	0.0131
58.6	1.6678	2.1321	6.4577	5.4532	5.9555	0.0160
58.7	1.7431	2.2399	6.7675	5.7392	6.2534	0.0168
58.8	1.8257	2.3581	7.1069	6.0525	6.5797	0.0177
58.9	1.5664	1.9870	6.0410	5.0686	5.5548	0.0149
59	1.5104	1.9068	5.8104	4.8558	5.3331	0.0144
59.1	1.2328	1.5094	4.6690	3.8021	4.2355	0.0114

Time (s)	Data from load cell 1	Data from load cell 2	Calibrated Load of load cell 1 (N)	Calibrated Load of load cell 2 (N)	Average Load (N)	Average pressure (kPa)
59.2	0.9858	1.1559	3.6537	2.8650	3.2593	0.0088
59.3	0.4495	0.3882	1.4484	0.8293	1.1388	0.0031
59.4	-0.0223	-0.2872	-0.4918	-0.9616	-0.7267	-0.0020
59.5	-0.6611	-1.2016	-3.1182	-3.3860	-3.2521	-0.0088
59.6	-1.3619	-2.2048	-5.9998	-6.0460	-6.0229	-0.0162
59.7	-1.8882	-2.9582	-8.1640	-8.0437	-8.1039	-0.0218
59.8	-2.4356	-3.7418	-10.4148	-10.1214	-10.2681	-0.0276
59.9	-2.5457	-3.8994	-10.8676	-10.5393	-10.7035	-0.0288
60	-2.6043	-3.9834	-11.1088	-10.7620	-10.9354	-0.0294
60.1	-2.8056	-4.2714	-11.9362	-11.5257	-11.7310	-0.0316
60.2	-2.7087	-4.1328	-11.5379	-11.1581	-11.3480	-0.0305
60.3	-2.7560	-4.2005	-11.7325	-11.3377	-11.5351	-0.0310
60.4	-2.6606	-4.0639	-11.3401	-10.9755	-11.1578	-0.0300
60.5	-2.5414	-3.8933	-10.8501	-10.5232	-10.6866	-0.0288
60.6	-2.3332	-3.5953	-9.9939	-9.7328	-9.8634	-0.0265
60.7	-1.9470	-3.0424	-8.4058	-8.2669	-8.3364	-0.0224
60.8	-1.5697	-2.5024	-6.8546	-6.8350	-6.8448	-0.0184
60.9	-0.9575	-1.6259	-4.3371	-4.5111	-4.4241	-0.0119
61	-0.6346	-1.1638	-3.0096	-3.2858	-3.1477	-0.0085
61.1	-0.3337	-0.7330	-1.7723	-2.1437	-1.9580	-0.0053
61.2	0.0617	-0.1670	-0.1463	-0.6427	-0.3945	-0.0011
61.3	0.5338	0.5089	1.7951	1.1493	1.4722	0.0040
61.4	0.6572	0.6855	2.3024	1.6176	1.9600	0.0053
61.5	0.6710	0.7052	2.3591	1.6699	2.0145	0.0054
61.6	0.9334	1.0809	3.4381	2.6660	3.0521	0.0082
61.7	1.1607	1.4062	4.3726	3.5286	3.9506	0.0106
61.8	1.3446	1.6695	5.1290	4.2268	4.6779	0.0126
61.9	1.5209	1.9219	5.8539	4.8959	5.3749	0.0145
62	1.6030	2.0394	6.1915	5.2076	5.6996	0.0153
62.1	1.6360	2.0867	6.3272	5.3328	5.8300	0.0157
62.2	1.5277	1.9315	5.8816	4.9214	5.4015	0.0145
62.3	1.1423	1.3799	4.2972	3.4589	3.8780	0.0104
62.4	0.6189	0.6307	2.1450	1.4723	1.8086	0.0049
62.5	0.1893	0.0156	0.3783	-0.1585	0.1099	0.0003
62.6	-0.3788	-0.7975	-1.9574	-2.3146	-2.1360	-0.0057
62.7	-0.8061	-1.4092	-3.7144	-3.9364	-3.8254	-0.0103
62.8	-1.6513	-2.6191	-7.1899	-7.1445	-7.1672	-0.0193
62.9	-2.3275	-3.5871	-9.9706	-9.7113	-9.8410	-0.0265
63	-2.7452	-4.1851	-11.6881	-11.2967	-11.4924	-0.0309
63.1	-2.8723	-4.3670	-12.2108	-11.7792	-11.9950	-0.0323
63.2	-2.6613	-4.0649	-11.3430	-10.9781	-11.1605	-0.0300
63.3	-2.5466	-3.9007	-10.8712	-10.5427	-10.7070	-0.0288
63.4	-2.4488	-3.7608	-10.4693	-10.1716	-10.3205	-0.0278
63.5	-2.4350	-3.7409	-10.4124	-10.1191	-10.2657	-0.0276

Time (s)	Data from load cell 1	Data from load cell 2	Calibrated Load of load cell 1 (N)	Calibrated Load of load cell 2 (N)	Average Load (N)	Average pressure (kPa)
63.6	-2.1530	-3.3373	-9.2529	-9.0488	-9.1509	-0.0246
63.7	-2.0118	-3.1351	-8.6722	-8.5128	-8.5925	-0.0231
63.8	-1.8149	-2.8533	-7.8627	-7.7656	-7.8141	-0.0210
63.9	-1.6275	-2.5851	-7.0923	-7.0544	-7.0734	-0.0190
64	-1.1688	-1.9284	-5.2059	-5.3131	-5.2595	-0.0142
64.1	-0.5190	-0.9983	-2.5342	-2.8470	-2.6906	-0.0072
64.2	-0.0917	-0.3866	-0.7770	-1.2249	-1.0010	-0.0027
64.3	0.3754	0.2821	1.1436	0.5479	0.8458	0.0023
64.4	0.9281	1.0732	3.4161	2.6456	3.0308	0.0082
64.5	1.2013	1.4643	4.5395	3.6826	4.1111	0.0111
64.6	1.5895	2.0201	6.1360	5.1563	5.6461	0.0152
64.7	1.5787	2.0047	6.0916	5.1153	5.6035	0.0151
64.8	1.7929	2.3112	6.9722	5.9282	6.4502	0.0174
64.9	1.7537	2.2552	6.8112	5.7796	6.2954	0.0169
65	1.8921	2.4532	7.3800	6.3046	6.8423	0.0184
65.1	1.5675	1.9886	6.0456	5.0729	5.5592	0.0150
65.2	1.3943	1.7406	5.3331	4.4152	4.8741	0.0131
65.3	0.9694	1.1324	3.5862	2.8027	3.1945	0.0086
65.4	0.5016	0.4628	1.6626	1.0270	1.3448	0.0036
65.5	-0.1551	-0.4774	-1.0380	-1.4658	-1.2519	-0.0034
65.6	-0.9246	-1.5789	-4.2021	-4.3865	-4.2943	-0.0116
65.7	-1.7585	-2.7726	-7.6308	-7.5515	-7.5912	-0.0204
65.8	-2.5914	-3.9648	-11.0554	-10.7127	-10.8840	-0.0293
65.9	-2.8641	-4.3552	-12.1767	-11.7477	-11.9622	-0.0322
66	-2.7692	-4.2194	-11.7868	-11.3878	-11.5873	-0.0312

Figure B.2: Experimental Pressure time-history for B60S10

B.3 Temperature profile:

Table B.2 depicts the total time required and the increase in temperature throughout the test.

Table B.2: Temperature profile of all boiler specimens

Time (min)	Temperature (K)								
	B40S8	B50S8	B60S8	B40S10	B50S10	B60S10	B40S12	B50S12	B60S12
0	308	308	307	306	306	306	307	306	305
1	309	311	313	308	311	309	307	310	311
2	311	313	315	311	313	315	310	312	315
3	315	317	319	314	318	319	313	316	319
4	319	321	323	315	321	323	314	320	323
5	320	322	324	318	328	324	317	321	325
6	322	324	326	322	333	326	321	323	328
7	324	326	328	325	335	328	324	325	330
8	327	329	331	328	338	331	327	328	335
9	329	331	333	331	340	333	330	330	340
10	333	335	337	333	343	337	332	334	343
11	336	338	340	338	345	340	337	337	348
12	338	343	342	341	348	345	340	342	350
13	341	348	345	343	350	350	342	347	354
14	342	350	348	346	351	353	345	349	356
15	343	354	350	349	356	355	348	353	358

Time (min)	Temperature (K)								
	B40S8	B50S8	B60S8	B40S10	B50S10	B60S10	B40S12	B50S12	B60S12
16	343	356	353	350	359	357	350	355	361
17	344	362	356	352	362	359	353	361	363
18	344	364	358	353	365	365	355	363	367
19	347	367	361	355	369	370	359	366	369
20	350	370	364	356	370	377	362	369	373
21	351	373	367	358	371	379	364	372	376
22	352	377	369	360	371	382	364	376	379
23	354	379	372	362	372	384	365	378	382
24	355	380	373	363	373	387	366	379	385
25	356	380	374	365	373	388	367	381	386
26	357	383	375	368	374	389	368	382	387
27	359	386	377	368	375	390	370	384	388
28	360	387	378	370	376	392	372	387	389
29	361	389	379	370	375	393	372	388	390
30	362	394	380	373	376	394	373	388	392
31	363	395	381	374	378	395	374	390	394
32	364	396	382	375	379	396	374	391	395
33	365	396	383	376	380	397	375	391	396
34	366	396	384	378	381	398	376	392	396
35	367	397	385	379	382	401	377	393	397
36	369	398	387	380	383	401	379	395	397
37	371	398	389	381	384	402	380		398
38	372	398	390	382	385	403	381		
39	373	399	391	383	385	403	382		
40	373	400	391	384	386	403	383		
41	374	400	392	385	387	404	384		
42	374	401	392	386		403	385		
43	374	402	392	388		404	386		
44	375	402	393	390		404	387		
45	377	402	395	391			389		
46	379	402	396	392			389		
47	381		397	392					
48	384		397	393					
49	385		398	393					
50	387		399	393					
51				394.15					
52				396.15					
53				397.15					
54				398.15					